Photobiomodulation of the response to exercise-induced damage in murine skeletal muscle

vorgelegt von
Fabiola Arpino

aus
San Vito die Normanni, Italien
2019

Dekan: Prof. Dr. med. Sergij Goerdt
Referent: Prof. Dr. med. Norbert Gretz

TABLE OF CONTENTS

ABBREVIATION

ATP	Adenosine tri-phosphate
BF	Bright field
β-ME	B-mercaptoethanol
C-RP	C-reactive protein
CK	Creatine kinase
Cox	Cytochrome c oxidase
CW	Cold water
DMEM	Dulbecco's modified eagle medium
DMSO	Dimethylsulfoxid
DOMS	Delayed onset muscle soreness
ECM	Exstracellular matrix
EDTA	Ethylenediaminetetraacetic acid
ELISA	Enzyme-linked Immunosorbent Assay
FBS	Fetal bovine serum
FDR	False discovery rate
GO	Gene Ontology
H&E	Hematoxylin and eosin
HS	Horse serum
IgG	Immunglobulin G
IF	Immunofluorescence
IHF	Immunohistofluorescence
LAS X	Leica Application Suite X
LDH	Lactate dehydrogenase
LEDs	Light emitting diodes
MAPK	Mitogen-activated protein kinase
MRFs	Myogenic regulatory factors
NES	Normalized enrichment score
NF-kappa B	Nuclear factor 'kappa-light-chain-enhancer' of activated B-cells
NO	Nitric oxide
PBS	Phosphate buffered saline
PBM	Photobiomodulation
PFA	Paraformaldehyde
RNA	Ethylenediaminetetraacetic acid
ROS	Reactive oxidative species

RT	Room temperature
TGF-β	Transforming growth factor beta
TNF-α	Tumor necrosis factor alpha
SD	Standard deviation
WGA	Wheat germ agglutinin
XTT	2,3-Bis-(2-methoxy-4-nitro5-sulfophenyl)-2H-tetrazolium-5-carboxanilide salt
ZEN	ZEISS Efficient Navigation

1   INTRODUCTION

1.1   Skeletal muscle tissue: structure and contraction mechanism

Skeletal muscle is the largest cellular compartment in the body, comprising circa 40% of all body weight. Muscle is composed of 75% of water, 20% of proteins and 5% of carbohydrates, fat and salts[1].

The skeletal muscle fulfils mechanical and metabolic functions. The most known function is the capability of skeletal muscle to generate force and power, in order to produce movement and maintain the posture. The metabolic role involves its contribution to the basal metabolism, the production of heat for the thermo-homeostasis and the conversion of oxygen and substrates into energy needed for movement. Moreover, it functions as a storage of amino acids, carbohydrates and fat.

The architecture of muscle fibers is well organized and redundant (Figure 1). It consists of multiple fascicles of muscle fibers bound together by connective tissue, called epimysium. The muscle fibers are kept together in each fascicle by the perimysium. Inside each fascicle, each muscle fiber is covered by a thin connective tissue, the endomysium. Nutrients are supplied by blood vessels and capillaries placed among the fascicles and fibers. A single fiber can be centimeters long (up to 30cm in humans) and is a multinucleated cell, derived from the fusion of several activated satellite cells, and the nuclei are decentralized. Satellite cells are the adult stem cells of skeletal muscles, placed between the sarcolemma (the muscle cell membrane) and the basal lamina. When they are activated by myogenic factors, they proliferate, differentiate and fuse info new muscle fibers, contributing to muscle growth, repair and turnover[2].

Each muscle fiber is made of long protein bundles of myofibrils, containing myofilaments. The most abundant myofilaments proteins are actin and myosin, which are the responsible for muscle contraction. Those proteins are arranged in a repeating unit called sarcomere, which is the contractile basic unit of skeletal muscle. The repetition of sarcomeres along the myofibril, gives to the skeletal muscle the typical striated pattern. A sarcomere is included between two Z-lines (or disks) that contain a part from the actin, titin, nebulin and α-actinin. The mechanism of muscle contraction was introduced in the 1954, with the sliding filament theory, and over the years was updated with additional information of the cross-bridge cycle[3].
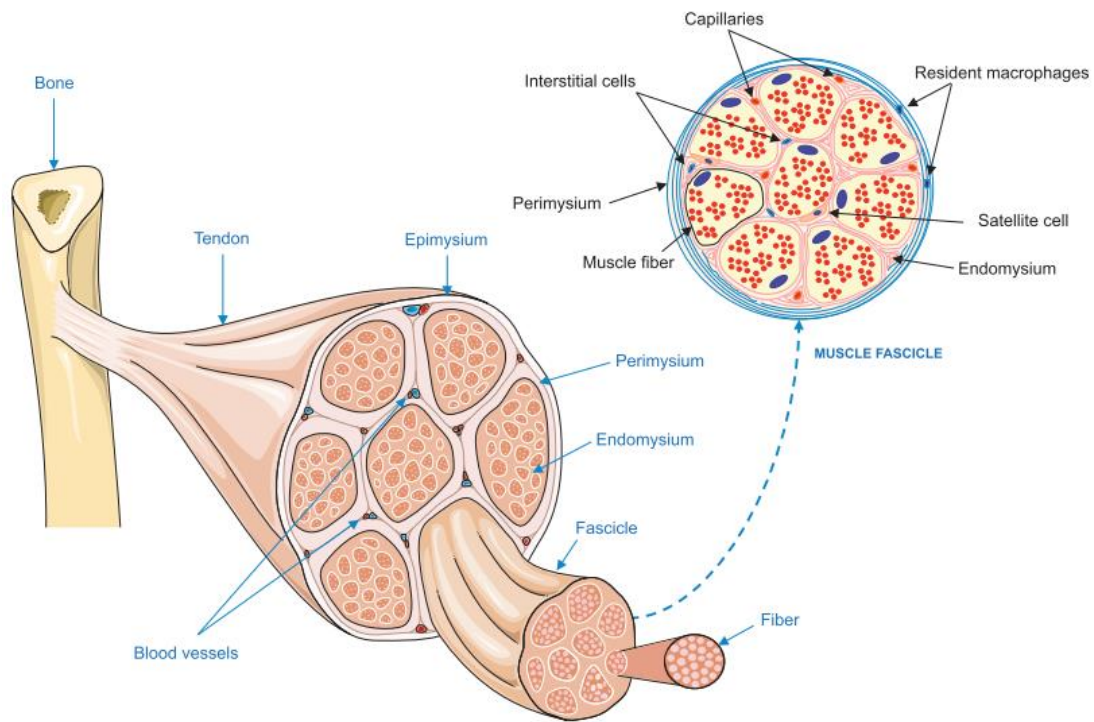
Figure 1: Structure of skeletal muscle [4].

The theory states that the actin and myosin form a protein complex by attachment of a myosin head on the actin filament, thereby forming a sort of cross-bridge between the two filaments. When the bridge is stable, myosin filaments of muscle fibers slide past the actin filaments, provoking the shortening of the sarcomeres and, therefore, the contraction of the fiber (Figure 2).
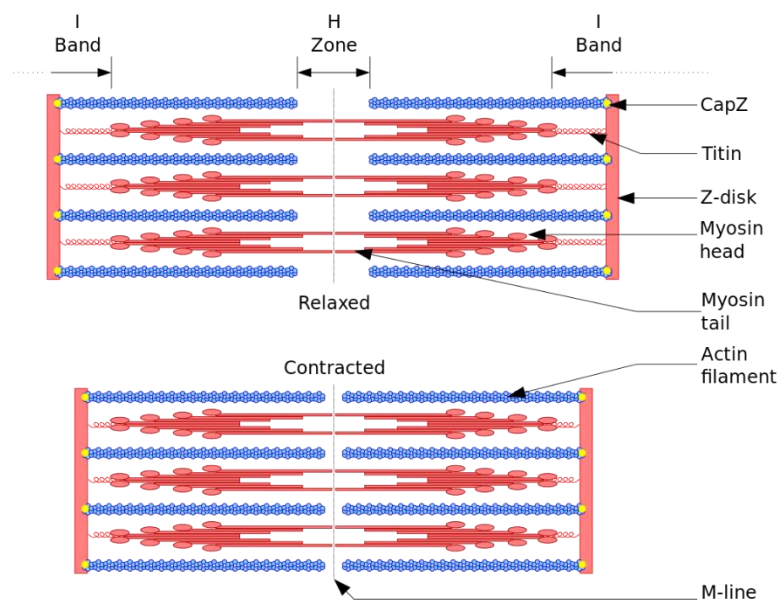
Figure 2: Schematic configuration of relaxed and contracted sarcomere [5].

The transmission of force produced by individual actin-myosin cross-bridges is transmitted longitudinally and laterally through structural proteins of the cytoskeleton within the fiber, and the movement is produced when the force reaches tendons.

The extracellular matrix (ECM) provides structurally a biochemical support to the skeletal tissue during its functions. The contractile apparatus is connected to the ECM by protein complexes (i.e. dystroglycans and integrins[6]) called costameres and by intermediate filament proteins, such as desmin. According to Ramaswamy et al.[7], more than 80% of muscle force is transferred via this lateral way.

Other organelles are in the sarcoplasm of muscle fibers, like the transverse tubular system (T tubule), the sarcoplasmic reticulum and the mitochondrial network. The T tubule system functions as the conductor of the nerve action potential in order to activate the muscle contraction. The sarcoplasmic reticulum is responsible for the storage, release and reuptake of the calcium after activation. The mitochondria generate the energy needed for the muscle action, and many of them are located close to the sarcolemma in order to reduce the distance from the capillaries that provide the oxygen supply[1].

1.2 Muscular response to a damage induced by a damaging contraction

Muscle contractions are classified into three basic types: isometric, concentric and eccentric. The isometric contraction occurs when the force generated without the movement of the limbs or joints, i.e. while sustaining a load in a static way. An action is concentric when the muscle contracts while shortening, like in flexing the elbow. An eccentric contraction, the production of force is accompanied with the lengthening of the muscle, i.e. lowering a load from a bent elbow position[8]. In the '50, it was observed for the first time that the symptoms of the delayed onset muscle soreness (DOMS) appeared mainly in subjects who performed eccentric exercised[9]. In the last years, DOMS is associated with the damage induced by exercise. It has been widely proven that muscles that contract eccentrically during an uncustomized action undergo more or less severe damage, depending on the dynamic of the movement[10, 11]. However, the eccentrically training of muscles induces an adaptation of the tissue that will be able to sustain the same exercise suffering less damage. This phenomenon is known as repeated-bout effect[12] and reflects mainly a structural reinforcement of contractile materials[13].

1.2.1   Initial events after muscular damage

The initial events that characterize an uncustomized eccentric contraction is a mechanical damage to the sarcomere structure and to the extracellular matrix. The prominent theory[14] about the structural disruption of sarcomeres finds the cause in the fact that during the eccentric action, the muscles is lengthening while the actin and myosin filaments are contracting the sarcomere in the opposite direction; hence the two myofilaments are forced to stretch beyond the optimum overlap. Moreover, according to this theory, the sarcomere is not uniform and the majority of length change is taken from the weakest part, leading to its failure. Overstretching sarcomeres leads to the disruption of other weak points, like ECM structures and costameres, since they are involved in the lateral transmission of force. The overstretching of sarcomeres results in the overload of the sarcolemma, leading to the disruption of phospholipidic layer or to the opening of the stretch-activated channels. The increased membrane permeability, leads to the influx of plasma proteins (like albumin and immunoglobulins) and external ions, like calcium. The latter activates the degradation of damaged contractile proteins by means of calcium-activated calpains. The injury to cell structures, provokes the leakage of intracellular proteins like myoglobin and creatine kinase (CK) that can be detected in the blood stream in the days following the exercise and are considered markers of muscular damage[15].

1.2.2   Pro-inflammation phase, anti-inflammation phase and regeneration

The immune system plays a relevant role in the event following a muscle injury: in the first moment, it promotes the degradation of damaged proteins, and subsequently, it favors the muscle regeneration.

The immune response is triggered by cell debris and content leakage from the muscle lesion site. The complement system is activated immediately within seconds after the injury and induces the migration of neutrophils and macrophages to the injured site. Moreover, the resident mast cells in skeletal muscle are activated, degranulates and release pro-inflammation cytokines, like TNF-α, and histamine to recruit more mast cells and other immune cells.

Neutrophils appear in the tissue already 1 hour after the injury[16], their number peaks in 6-24h, and start to decrease after 24h[17]. Neutrophils worsen the degradation status of the injured tissue by producing reactive oxygen species (ROS) that activates a series of pathways, like NF-

kappa B signaling pathways, attract myocytes to the injured site and enhance degradation process. Within 24h, neutrophils are substituted by macrophages mainly with a pro-inflammatory phenotype (M1)[17]. M1 macrophages remove cellular debris by producing cytotoxic levels of nitric oxide that induces apoptosis of the damaged cells; moreover, they enhance the inflammatory response releasing pro-inflammatory cytokines like TNF-α and chemokines, like ccl2. The tumor necrosis factor activates the ubiquitin-proteasome pathway, which is one of the main mechanism for proteolysis of damaged proteins in eukaryotic cells.

T cells are recruited at the injured site in the second wave of immune cell infiltration, around the third day. They secrete growth factor and cytokine to modulate the microenvironment of the area[18]. Their role is not fully understood. However, there is evidence about their contribution to muscle regeneration[19].

The resolution of the inflammation phase corresponds with the shift of the macrophages from the pro-inflammation to the anti-inflammation phenotype (M2). M2 macrophages regulate the termination of inflammation and promote the late stage of myogenesis and regeneration[20]. In Figure 3 are resumed the succession of events following the muscular damage.
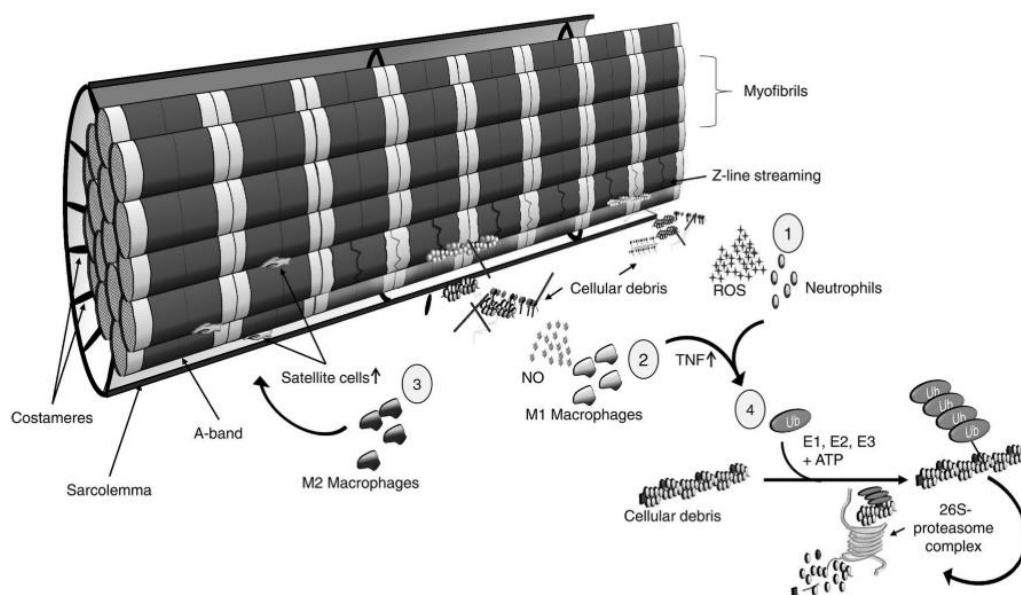
Figure 3: Representation of the succession of events following a muscular damage induced by exercise. (1) Neutrophils arrive and increase the level of ROS and cytokines that attract M1 macrophages (2). TNF released by M1 macrophages and neutrophils activates the ubiquitin-proteasome proteolysis (4). In the meantime, the inflammation goes towards resolution and M1 macrophages start to shift to the M2 phenotype (3). Satellite cells were activated and attracted by M1 macrophages, and, once on the injured site, they start to differentiate, stimulated by M2 macrophages[21].

Skeletal muscle regeneration is a process mediated by satellite cells, the adult muscle stem cells that remain quiescent in the niche between the sarcoplasm and the basal laminal until they received appropriate stimuli. The activation of satellite cells is triggered by several

sources. Immune cells are able to orchestrate the activation, expansion and differentiation of muscle cells during regeneration. Indeed, the macrophages M1 release factors that promote the proliferation and migration of stem cells towards the injured sites. M2 macrophages instead, stimulate the differentiation of myoblasts that fuse with other myogenic cells in order to create new myotubes that will repair the damages fibers. Figure 4 summarizes the time course of immune response in parallel to muscle regeneration.
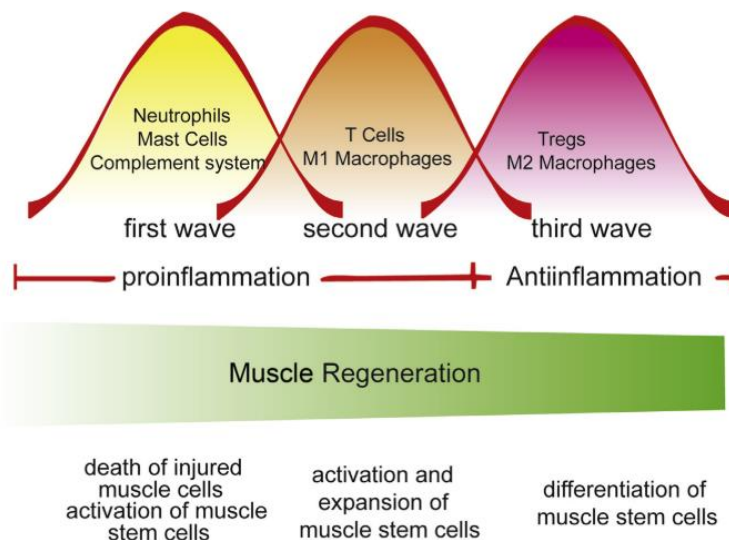
Figure 4: Representation of the three waves of immune cells in parallel to muscle regeneration process, involving the activation, expansion and differentiation of stem cells[18].

1.3   Exercise-induced damage models

To understand the mechanisms and prevention of muscular injury, or to evaluate treatments for improving muscular recovery, an experimental model of muscle damage is needed.

In humans, injury models are limited for ethical reasons; hence, experimental models have focused on inducing a moderate damage through exercise, in particular exercise that involves eccentric contractions. The most common models are the ones that are aiming to injure the elbow flexor[22] and the knee extensor muscle[23] by means of machines, usually isokinetic dynamometers that allow the control of the movement while the muscle of interest is eccentrically contracting to lower the weight. Other models induce injury to a group of muscles during whole-body exercise. The most commonly used exercises are the downward-stepping model, where the subject steps down stairs with one leg, and the downhill running model[24]. In both, eccentric contractions occurs in the hip and knee extensor muscle groups as they lower the body down the slope against gravity.

For the animal experimentation, rodents are commonly used, and the models can be categorized in the ones that induce muscular injury through contraction, and the models that induce muscular trauma by injection of a toxin[20], crushing[25], ischemia[26] or low temperature[27]. Focusing on the damage contraction-induced models on rodents, in literature models are described where the animal are conscious and forced to exercise, or kept under anesthesia and the contraction is induced into a selected muscle with proper machines[28]. Conscious *in vivo* models involve the animals in performing a whole-body exercise for a prolonged period or until exhaustion. Downhill running or walking are widely used, and they induce damage in the antigravity muscles. For rats, a decline of -16° to -18° with a maximum speed of 25 m/min has been used. For mice, a slope of -20° with a maximum speed of 21 m/min and of -14° with a maximum speed of 40 m/min has been applied[8]. However, these numbers depend on the strain of the rodents. It has been shown that there are strains of mice with higher learning skills in performing physical tasks than others[29]. Swimming[30] and climbing[31] a ladder are other activities used for inducing a muscular damage. However, the application of these exercises requires more training and practice effort; therefore, they are less common in experimental studies with animals.

1.3.1   Signs of muscular damage

The easiest practice to monitor the functional status of muscles after an exercise is throw blood analysis of specific markers.

Creatine kinase (CK) is one of the most common marker of structural damage in the skeletal muscle and myocardium. The CK is an enzyme that catalysis the conversion of creatine into phosphocreatine that serves as energy reservoir for ATP regeneration. When structural damage to muscle cells occurs, the CK leaks into blood stream and its level peak between 24h and 5 days, according to the entity of the damage [32].

Other enzymes, the levels of which increase after an intense eccentric exercise, are the lactate dehydrogenase (LDH), aspartate transferase (AST) and myoglobin (MB)[32]. However, their plasma levels are checked with less frequency.

The inflammation status is often monitored with the plasma level of c-reactive protein (C-RP). The C-RP is released by the liver in response to factors secreted by macrophages. Its role is to label the surface of dying cells in order to promote the phagocytosis by the macrophages.

Hence, C-RP levels tend to increase 48h after the activation of macrophages in the injured tissue. [33]

Another sign of damage is the delayed onset muscle soreness (DOMS), that refers to the pain and muscular stiffness felt several hours up to days after a damaging exercise. The quantification consists in rating the intensity of pain by the subjects that performed the physical activity[23]. Therefore, the quantification of DOMS is qualitative and subjective, and cannot be performed in animal studies.

Histological samples of muscles are often analyzed in animal studies that involved muscular damage. The standard hematoxylin-eosin staining is most common, and allows the visualization of swollen[34] and necrotic fibers[35, 36], the infiltration of immune cells[36, 37] and the presence of regenerative fibers[34]. Another easy possibility to detect the damaged fibers is the staining with a secondary antibody for immunoglobulins (IgG)[38]. Immunoglobulins are big plasma proteins that exudate into the interstitial fluid after the injury, and from the interstitial fluid, penetrate into the muscle fibers that lost the continuity of the sarcolemma. Hence, the number of positive IgG fibers is correlated with the number of fibers with membrane damage. More fined techniques of immunostaining aim to detect different populations of immune cells with specific antibodies[17].

1.4   Photobiomodulation (PBM) as a novel treatment for muscle recovery

PBM refers to the use of photons at a non-thermal intensity to modulate biological activity. Its application occur by means of coherent light sources (lasers) or non-coherent light sources with consisting in light-emitting diodes (LEDs). The phenomenon involves the absorption of light at a certain wavelength by chromophores resident in biological tissues. The most common "optical window" used in PBM are the red (600-700 nm) and near infrared (780-1110 nm) wavelengths, because of the higher tissue penetration and low scattering in tissues compared to other wavelengths[39].

Among the therapeutic interventions for treatment of muscle injury, PBM has been widely investigated[40, 41]. Indeed, clinical studies reported that red and infrared light have a protective effect when applied before or during exercise, reducing pain, plasma markers of damage, and increasing the performance of the subjects. In clinical studies, the application of light occurred via lasers, in multiple point of the exercised muscles, or using flexible LEDs sheets applied to the skin (Figure 5).

Investigations in animals confirmed the benefits reported in humans, and, additionally documented a decreased of myonecrosis, infiltration of inflammatory cells and oxidative stress[31, 42]. On in vitro studies, PMB promoted the energy production in myocytes, the proliferation of myoblasts[43] and their differentiation into myotubes[44], the cell cycle entry of satellite cells[45], displaying the potential of PBM to enhance muscle regeneration. In the case of animals, the application of the light therapy occurred pointing the lasers on few spots of the exercise muscles, or placing the animal under a LEDs lamp at a certain distance, like shown as example in Figure 6.
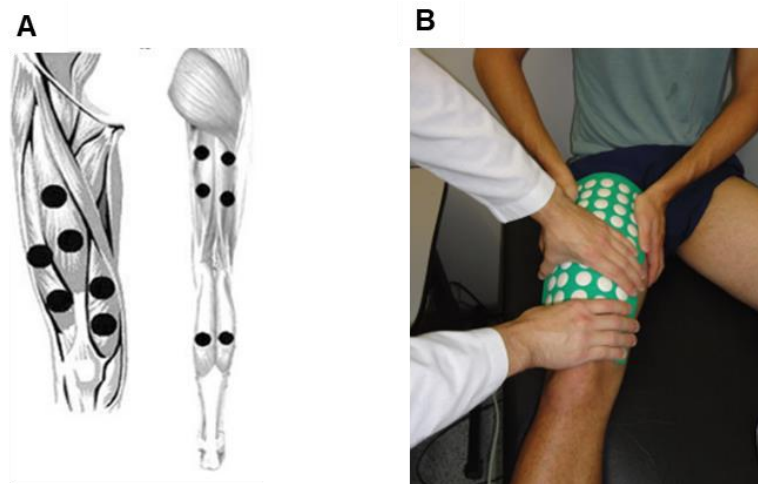
Figure 5: Application of light therapy by means of: (A) lasers pointed to multiple sports of the muscles[46], (B) a flexible board of LEDs distributed homogenously on the muscle skin surface[23].
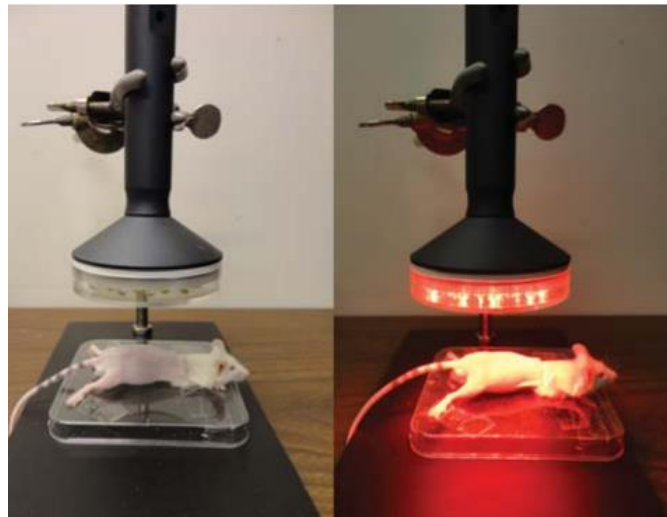

Figure 6: An example of light therapy application by means of a LEDs lamp placed at a certain distance from the animal[31].

All these beneficial effects lead to the consideration of the PBM as a therapy to improve muscular recovery post exercise.

1.4.1 Mechanism of BPM

PBM has an effect in living systems only when photons are absorbed by chromophores. Examples of chromophores are chlorophyll, hemoglobin, cytochrome C oxidase (Cox), myoglobin, flavins and flavoproteins[39].

Four possible mechanisms of action were proposed for the first time by Karu[47]: first, the light absorbed by Cox changes its redox state enhancing the biochemical activity, hence the performance of the electron transport chain; second, the excitation energy is converted to heat, which causes a local increase in the temperature of the absorbing chromophores, causing a conformational change that triggers biochemical activity; third, the increased mitochondrial activity is associated to an increase in cellular superoxide ($^-O_2$), that can be reabsorbed by mitochondria as a source of electrons, accelerating the respiratory chain; fourth, photoabsorbing chromophores can directly be converted into photosensitizers which can transmit energy to adjacent molecules, triggering biochemical reactions.

Moreover, the red and infrared light induces the photodisociation of NO from Cox. Under stress conditions, like hypoxia or necrosis, NO is abundant and has a high affinity to Cox, inhibiting its activity. Hence, the release of NO by light, enhance the Cox activity. The cellular level of NO might increase also in no stress condition because of its photodissociation from other intracellular stores, like myoglobin or hemoglobin[39].

1.4.2 PBM dosage

The main parameters to describe PBM are the wavelength (nm), energy (J), energy density (J/cm^2), power (W) and power density (W/cm^2). Energy and power are linked by the irradiation time ((Energy (J) = Power (W) × Time (s)). Even if these three parameters are linked by a physical low, each of them seems to influence on the response of a biological system. Hence, for instance, if the energy delivered is constant but the power and the irradiation time are changed, the biological outcome may be different.

Moreover, in PBM the effect of biphasic dose response must be taken into account. This phenomenon is described by the Arndt-Schulz model: if insufficient stimuli are applied there will be no response (because the minimum threshold has not been met), if the intensity of the stimuli increases, a threshold will be crossed and a biological response is achieved. However, if the intensity of the stimuli increased too much, the stimulation disappears and is replaced by an inhibition instead[48, 49]. Since the intensity of the stimuli in PBM can be changed varying

the energy, power and irradiation time, defining an effective dose for a clinical use of PBM is a critical point.

1.5 Cryotherapy as conventional method to mitigate the post-exercise damage

Cryotherapy refers to a cooling strategy in order to mitigate the biological response in tissues that suffered a stress. Cryotherapy includes whole-body immersion in dry air, ice cold pack application or ice massage. It is a common practice to accelerate the recovery from an intense exercise.

There are no fixed guidelines for this practice. The clinical studies describe application of 3min up to 20min with temperatures between 3°C to 15°C. The application time is reduced, as the temperature is lowered down, in order to avoid damage to the tissues. An extreme case is the full immersion of the body in dry air at -110°C for 3-4min. The main reported benefit of the cryotherapy is the reduction of DOMS in humans at 24h, 48h, 72h and 96h after the high intense exercise, but there a no consistent evidences of speeding up the post-exercise recovery. In animals, the main finding reported is the reduction of the intensity of the inflammation response after muscular injury.

The mechanism of action of the cryotherapy are not fully understood yet. Probably, the main active factor is the low temperature that reduces the blood flow decreasing the permeability to immune cells in the injured muscle. The reduction of inflammation is associated with a reduction of pain caused by decreasing the osmotic pressure of the exudate, which pressurizes nociceptors.   Another effect of the cooling of tissue is the reduction of the metabolic rate of muscular cells, protecting the tissue from the secondary hypoxic damage[50, 51].

1.6 Aim of the study

In the last years, the PBM has been proposed as a treatment to speed up the recovery of muscles, which underwent a damaging exercise, characterized by eccentric contraction. A common practice as a post-exercise treatment is cryotherapy, its benefit, however, in terms of functional recovery is questionable.

Although, several studies report the effectiveness of the PBM in improving the status of injured skeletal muscles, little is known about the mechanisms of cellular signaling behind it.

Moreover, most of the studies focus either on histological evaluation or on gene expression of specific factors.

The main aim of the present work, is to evaluate the effect of the infra-/red light on exercised muscles during the inflammation, which is a crucial phase that affects the regeneration, and therefore the functional recovery of the muscles.

The project was structured as follows:

- Preliminary studies on a cell line of muscular cells (C2C12) in order to confirm the main findings reported in literature and to support the following *in vivo* study.
- Assessment of the protocol for the exercise-induced damage model through the evaluation of histological samples of muscles at different time points.
- Application of the two treatments, light therapy and cryotherapy to the animals, after performing the exercise-induced damage.
- Analysis and comparison of the plasma concentration of CK and C-RP
- Qualitative and quantitative comparison of the morphology of histological samples, after a standard hematoxylin-eosin staining and anti-IgG staining.
- Comprehensive gene expression profiling and comparison among the experimental groups in order to detect marker genes involved in process of inflammation, repair and regeneration, and identify signaling pathways regulated by the different treatments.

2 MATERIAL AND METHODS

2.1 Material

2.1.1 Devices

Description	Manufacterer
Autostainer	Leica
Autotechnikon	Leica
Axio Scan.Z1	Zeiss
Bench centrifuge	Biozymt
Centrifuge	Eppendof
Cobas ®	Roche
Corning® 96 well plates, clear bottom	Sigma Aldrich
Confocal Microscope DM 6000 CFS	Leica
Cover slips	Roth
Cook steamer	Braun
Cryovials	Thermo Scientific
DMM230 Industrial Multimeter	Multimetrix
GeneChip Scanner 3000	Affymetrix
Glass capillaries	Hirschmann Hematokrit kapillaren
Eppis 1.5 mL, 2mL, 5mL	Eppendof
Eppis heating plate	HCL
Forceps	Jeweler's forceps
Heparin – Litium eppis	Starstedt
Heat bead sterilizer	Fine Science Tools
Incubator Heraeus	Thermo Scientific
Microscope DFF 3000G	Leica
Fluidics station 450	Affymetrix

Laminar Flow	Kendro Laboratory Products
LEDs board	Enmech
Lumileds LUXEON Rebel LXML-PR01-0275	Philips
Luna cell counter	Byozimt
Microplate Reader Infinite® 200 PRO	Tecan
Microtome RM 2245	Leica
Multichannel pipette	Eppendorf
Pet shaver	Isis - Aesculap
Pipettes	Gilson/Eppendorf
Pipette boy	Eppendorf
Pipette tips	Starlab
Scale for rodents	Satorius U 4100
Scalpel	B-Braun - Aesculap
Serological pipettes	Starstedt
TECAN ®	Tecan Group
Tissue embedding system Histocore Arcadia	Leica
Tissue homogenizer	Kinematica AG
Treadmills	Panlab Harvard Apparatus
Vacum Pump	Eppendof
Vacum Pump Handler	Vacuumbrand®
Vortexer Reax top	Heidolph
Water bath	Memmert
96-well white plate with opaque bottom	Brand®

2.1.2   Chemicals, kits and consumables

Antifate diamont mouting	Invitrogen

B-mercaptoethanol (β-ME)	Aldrich
CellTiter-Glo® Luminescent Cell Viability	Promega
Chicken anti-mouse IgG Alexa Fluor ® 647	ThermoFisher Scientific
Chicken serum	Jackson ImmunoResearch Laboratories, Inc.
Citrate	Merck
Colorimetric Cell Viability Kit III (XTT)	PromoKine
Mouse Creatine Kinase Activity Assay Kit	Abcam
Mouse C Reactive Protein ELISA Kit	Abcam
Depilatory cream	Veet®
Dulbecco's Modified Eagle Medium (DMEM)	Gibco
Dimethylsulfoxid (DMSO)	Sigma Aldrich
Ethanol	Emsure Merck
Fetal Bovine Serum (FBS)	Gibco
Goat anti-rat IgG Alexa Fluor ® 647	ThermoFisher Scientific
Goat serum	ThermoFisher Scientific
Horse serum	Life Technologies
Type F immersion liquid	Leica
Isofluorane	CP-Pharma
Isopropanol	Sigma Aldrich
Parafolmaldehyde (PFA)	Merk
Phosphate buffered saline (PBS)	Gibco
Protease K	Abcam
Rat anti-mouse F4/80	eBioscience
Rat anti-mouse Ly6G	Biolegend
RNAase fibrous tissue mini kit	QIAGEN
RNAase free water	Sigma-Adrich
Sytox Orange	Invitrogen

Trypan blue	Gibco
Trypsin 0.25% EDTA	Gibco
WGA 488 conjugated	Biotium

2.1.3 Software

JMP Genomics 7	SAS
JMP 11	SAS
Ilastik	Free source software
ImageJ	Free source software
LAS X Life Science	Leica
ZEN	Zeiss

2.2 *In vitro* study

2.2.1 Cell culture

C2C12 cells (immortal murine myoblasts) from ATCC® CRL-1772™ (Manassas, USA) were cultured in Dulbecco´s modified Eagle´s medium (DMEM, high glucose, L-glutamine, pyruvate) containing 10% fetal bovine serum (FBS), under standard conditions at 37°C and 5% CO_2.

A seeding density of 18×10^3 /cm² and 9×10^3 /cm² for a culturing period of 2 days and 3 days respectively, guaranteed a confluence <60% with the consequent preservation of the myoblast phenotype. 0.25% Trypsin-EDTA (1x) phenol red from Gibco® was used to detach the cells with 2min incubation time at 37°C.

Sub-cultures of C2C12 myoblasts were differentiated into myotubes when a confluence of 100% was achieved. At that point, the medium was switched to Dulbecco´s modified Eagle´s medium (DMEM, high glucose, L-glutamine, pyruvate) containing 5% heat inactivated horse serum. The differentiation medium was replaced once a day and full cell differentiation was reached in 4-5 days.

The morphological changes due to the differentiation process were evaluated using a LEICA inverted bright field (BF) microscope (Mannheim, DE).

2.2.2 Irradiation with red and infrared light

The irradiation experiments were conducted on C2C12 at two different phenotypes: at the state of proliferative cells called myoblasts; at the state of fully differentiated myocytes developed from myoblasts, referred to as myotubes.

Myoblasts were kept in proliferative state with a density of 3000 cells/well and 1500 cells/well for experiments lasting from 0 to 24h, and from 24h to 72h respectively. After seeding, cells were incubated at least 24h at 37°C at 5% CO_2 before the irradiation procedure.

For the differentiation, myoblasts were seeded at 3000 cells/well. Following the differentiation protocol, mature myotubes fully developed at the 7-8 day after the plating.

In all cases, the wells of the plate H line were filled with medium as a chemical blank. Medium was renewed 30 min before the irradiation and the cells were illuminated with infrared light. The right half of the plate was taped with black foil as negative light control. The infrared lamp was a Lumileds LUXEON Rebel LXML-PR01-0275 (Koninklijke Philips N.V., Eindhoven, Netherlands) with the following specifications (Table 1).

Lumileds LUXEON Rebel LXML-PR01-0275 specifics	
Number of diodes	128
Wavelength peak	834nm or 656nm
Beam divergence	±15°
Frequency	Continuous
Power density	23 mW/cm^2
Application mode	55 mm distance

Table 1: Specifications of the infrared lamp Lumileds LUXEON Rebel LXML-PR01-0275 released by Philips (Eindhoven, Netherlands), used for the irradiation of myoblasts, and differentiated myocytes developed from myoblasts, which will be simply referred to as myotubes.

In the experiments are tested different values of the energy density, harvesting time from the irradiation and consecutive irradiation days, keeping fixed one or two parameters per time, as summarized in Table 2.

The experiments were done in three replicates (plates) and, at least in three repetitions for each parameter.

Cell type	Energy density [J/cm²]	Irradiation time [s]	N° irradiation day	Harvesting time [h]
Myoblasts	1.25	55	1	24
	2.5	110	1	24
	5	220	1	24
	2.5	110	1	3
	2.5	110	1	6
Myoblasts	2.5	110	1	12
Myotubes	2.5	110	1	24
	2.5	110	1	48
Myoblasts	2.5	110	3	24

Table 2: Overview of the tested parameters regarding the infrared light experiments on myoblasts (C2C12 cell line) and myotubes differentiated from the C2C12.

2.2.3 Cell metabolism (XTT) and ATP production

The Colorimetric Cell Viability Kit III (XTT) from PromoKine (PromoCell GmbH, Heidelberg, Germany) and CellTiter-Glo® Luminescent Cell Viability Assay (Promega, Mannheim,) were used for testing the effect of infrared light on metabolism/proliferation and ATP production respectively.

The XTT assay is based on the cleavage of the tetrazolium salt to a soluble orange dye, formazan, by metabolically active cells in culture. The enzymes involved in the metabolism of the tetrazolium salt are inactivated right after the cell death; therefore, the amount of the formed formazan directly correlates to the viable cells. Following the protocol of the company, myoblasts and myotubes were incubated with the kit reagents for 1h and 30min respectively. Then, the absorbance of the formazan was measured at 450nm and 640nm reference through the spectrophotometric microplate reader Infinite® 200 PRO (Tecan Group AG, Männedorf, Switzerland).

The CellTiter-Glo® Luminescent Cell Viability uses the firefly luciferase to convert luciferine and ATP to oxyluciferin and light. Therefore, the emitted light is proportional to the ATP amount in the cell. According to the company protocol, the kit reagents are mixed and added to the wells containing the cells. The plate was shaken for 2min to facilitate the cell to lyse. After 10min, the content of each well was transferred from the black plate to the wells of a

96-well white plate with opaque bottom. This kind of plate optimizes the luminescence signal since the photons can be transmitted only upward. The luminescence was detected by the microplate reader Infinite® 200 PRO (Tecan Group AG, Männedorf, Switzerland).

The upper half of each 96-well black plate was used for the XTT measurements, while the lower half of the same plate was used for measuring the ATP. In this way, the viability and the ATP production were tested under the same conditions for each replicate.

The raw optical values, both absorbance and luminescence, were normalized with the respective no light control, obtaining a so called fold change. The distribution of the normalized data was displayed by box-and-whisker plots. Both means ±standard deviation (SD) and median ±range of the fold changes were reported.

Based on the nonparametric Wilcoxon test, differential fold changes were analyzed using a commercial software package JMP 11 from SAS. A p-value ≤0.05 was considered as significant.

2.3 *In vivo* study

2.3.1 Animal groups

All experiments were conducted in accordance with the German Animal Protection Law and approved by the local authority (Regierungspräsidium Nordbaden, Karlsruhe Germany in agreement with EU guideline 2010/63/EU).

For the purpose of the study, CD-1 male mice (10 weeks old, body weight 33±2 g) were purchased from Charles River Laboratories (Sulzfeld, DE) and kept under standard conditions at 20-23°C, fed ad libitum for ca. 1 week before the start of the experiment.

The animals were randomly assigned to six groups: control mice (Control) kept at rest and without any treatment (n=5), running mice involved in a pilot study for the assessment of the exercise protocol (n=8), running mice (Run) performing the established exercise protocol (n=9), running mice receiving the light therapy (Run+LEDs) or the cryotherapy (Run+CW) after the established exercise protocol (n=9 for Run+LEDs, n=9 for Run+CW). In total, 40 mice were included in the study.

The animals were housed individually in cages to avoid conflict behavior that could interfere with the exercise performance and/or the applied therapy.

2.3.2 Development of an exercise-induced damage model

The running on treadmills was chosen as exercise to stress the muscle limbs of the mice. Treadmills were purchased from Panlab Harvard Apparatus (Barcelona, ES) and had 5 lines for training 5 mice simultaneously, a shocking grid at the bottom of each line, and an adjustable slope. A control unit touchscreen allows control of the speed of the belt, the intensity of the electrical shock and the running time Figure 7. The specifics of the treadmills are summarized in Table 3.
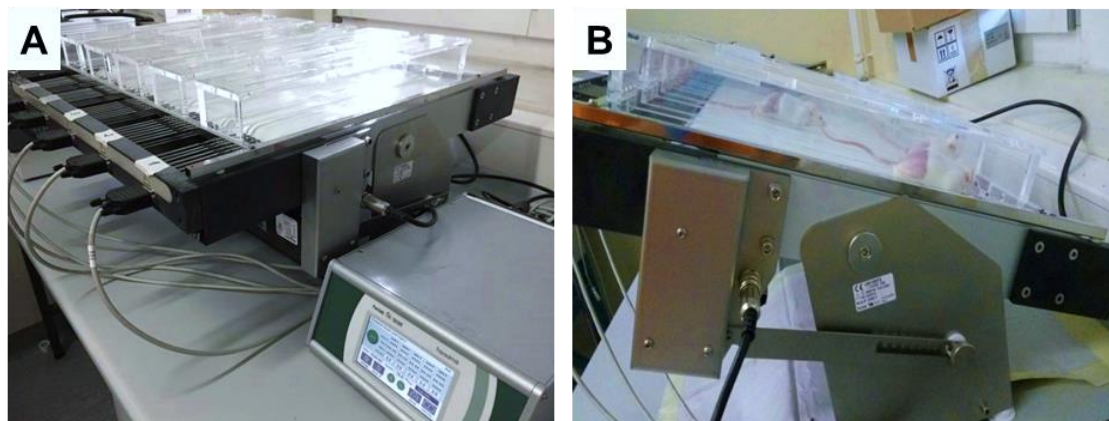

Figure 7: (A) The treadmills purchased from Panlab Harvard Apparatus (Barcellona, Spain) had five lines with a shocking grid at the bottom of each line. The slope of the running surface could be adjusted manually. A control unit allowed to adapt the speed and the intensity of the shocks, and to record the running distance and time, and the number of shocks. (B) Mice placed inside the channels of the treadmills and running at a negative slope of 25°.

Treadmills specifics - Panlab Harvard Apparatus	
Belt speed	From 0.4 to 150cm/s
Electrical shock intensity	From 0 to 2mA
Slope	From −25° to +25°
Running lines	5
Running line dimension	45 cm

Table 3: Specifics of the treadmills purchased by Panlab Harvard Apparatus (Barcellona, ES) and used for the exercise-induced damage model.

Three modalities of exercise were tested to establish the protocol that causes the most pronounced stress in the limb muscles:

1) Long-term uphill running: Two mice were trained for 9 days, with a weekend as a break in between the 5° and the 8° day. In the first 5 days, the mice ran 1h/day at 10° upslope, and the training consisted in a warm-up phase of 5 min at 12cm/s, followed by an increasing of 2 cm/s every minute, until a maximum speed of 25cm/s was reached. On day 8°, 9°, and 10°, the training was repeated, with a maximum speed of

30 cm/s and +10° inclination. On the 11° day, the mice were forced to run at +20° slope until exhaustion, keeping 30cm/s as maximum speed. At 24h after the exhausting run, the animals were sacrificed for the harvesting of the organs.

2) Long-term downhill running: Two mice were trained for 9 days, with the same protocol described for the long term uphill running at 1). The only difference was the slope of the running band: a decline of -10° was used for the running that occurred between the 5° and the 10° day; on the 11th day the mice were force to run downhill at -20° slope and 30 cm/s as maximum speed. The necropsy occurred 24h after the exhaustion exercise.

3) Short-term downhill running: Six mice underwent a single day of three bouts of intensive running at -25° slope, separated by 15min rest. For every bout, the animals were started on the treadmills with a warm-up phase of 5min at 12 cm/s. Then, a progressive ramping speed was applied (2 cm/s every minute) til the mice were still able to keep the pace of the treadmills. At that point, the speed was kept constant until the exhaustion of the animals. During the 15min break, the mice were placed in the own cage. In the previous two days, the mice were adapted for 10min to the type of exercise, starting with a speed of 7 cm/s and reaching a maximum speed of 18 cm/s at the second day.

The six mice were divided in three groups (2 mice per group) according to the day of sacrifice: at 48h (2 days), 72h (3 days), 168h (7 days).

Blood samples were collected before the adaptation phase for baseline value, and at 24h, at 48h, 72h and 168h after the exhaustive run. A typical experimental schedule is shown in Figure 8.
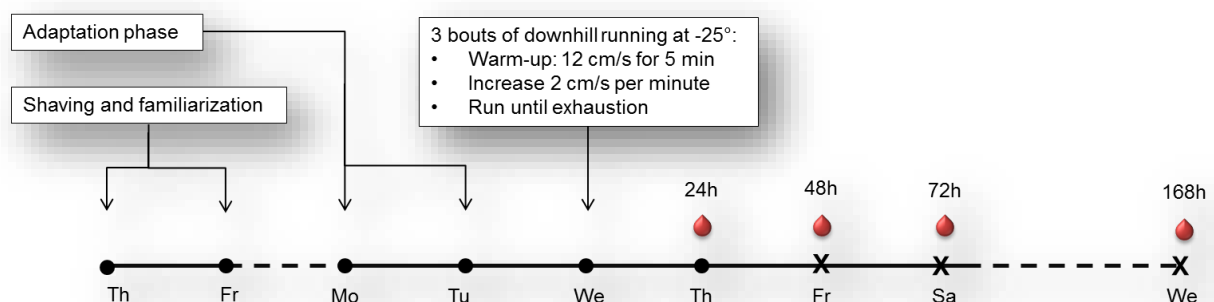
Figure 8: Example of the experimental schedule for the short-term downhill running exercise. At the days before the exercise week, the mice were depilated and familiarized with the treadmills. An adaptation phase of two days preceded the exercise day and consisted in 10min train at 7cm/s. On the day of the damaging exercise, the mice underwent three bouts of intensive running at -25° slope, separated by 15 min rest. According to the scarifying day, blood samples (red drop symbol) were taken

at 24h, 48h, 72h, 168h and before the exercise week for baseline values. According to the group, the necropsy occurred at 48h, 72h and 168h.

In all cases (except the control group), 2 days of low speed walk (7 cm/s) for 5min followed by 2 days at rest were planned to allow mice to familiarize themselves with the treadmills. Moreover, the mice were placed in stationary conditions for 5min before every exercising session. All the animals were also shaved on the limbs to minimize the difference among the experimental groups.

2.3.3 Application of the treatment after the exercise: light therapy and cryotherapy

On the base of the results reported in the chapter 3, the treatments post-exercise were combined with the short-term downhill protocol, previously described in 2.3.2.

<u>Light therapy</u>

A non-commercial cluster of LEDs produced by ENMECH (Berlin, DE) was used for the light therapy. The tool consisted in a board of 84 infrared (850nm) and 84 red (656nm) LEDs positioned on a grid as a support, at 12cm from the platform where the mouse was placed for the irradiation (Figure 9).
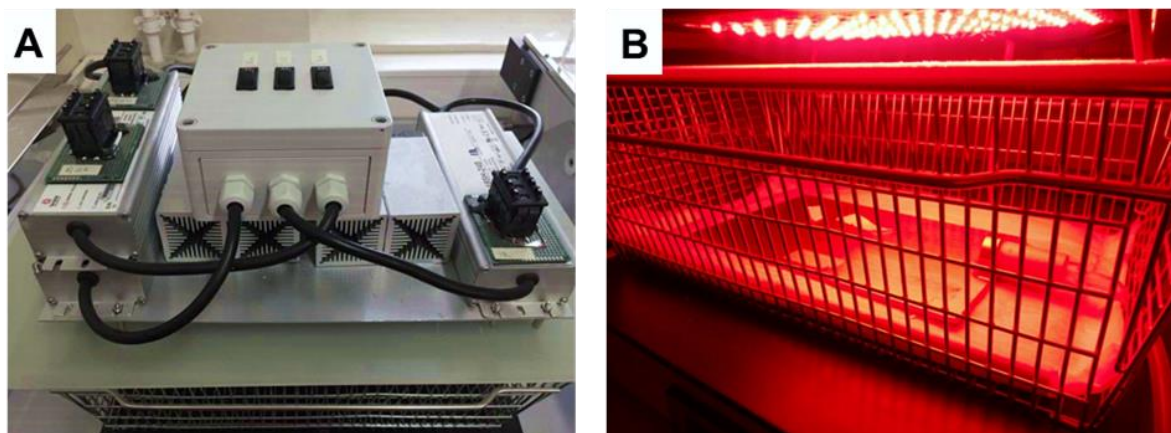
Figure 9: (A) Board of 84 infrared (850nm) and 84 red (656nm) LEDs from ENMECH (Berlin,DE).A control unit allowed to adjust the power density for each wavelength. A diffusor positioned under the LEDs cluster provided an homogenous distribution of the light. (B)The LEDs board was sustained by a metal grid at 12cm from the platform where the mouse was placed for the irradiation.

The optical power density reaching the mouse skin was measured with an optical energy meter from Newport® (Irvine, USA) and was 32mW/cm^2 for infrared and 14 mW/cm^2 for the red light. The specifics of the LEDs board and the optical parameters used for the light therapy are summarized in Table 4: Optical parameters of the light-emitting diodes therapy applied to the Run+LEDs group at the end of the exercise and at 24 h after the first irradiation.

The mice were depilated with Veet® cream on the half lower body part during the familiarization phase. At the end of the three bouts of downhill running, Run+LEDs mice were anesthetized by isofluorane inhalation and placed with the belly down under the LEDs (Figure 10 (A)) . The limbs were slightly stretched and fixed with a tape, and the upper body part was covered with aluminum foil (Figure 10 (B)).

The irradiation lasted 3 minutes for a total dosage of 5.8 J/cm^2 and 2.5 J/cm^2 for infrared and red light respectively. After the irradiation the mice were put back inside their own cages. The light treatment was repeated at 24h from the first irradiation.

ENMECH LEDs board specifics	
Number of LEDs	84 (850nm), 84 (656nm)
Wavelength peak	850nm (infrared), 656 nm (red)
Frequency	Continuous
Power density (at skin surface)	32 mW/cm^2 (850nm), 14 mW/cm^2 (656nm)
Irradiation time	3 min
Energy density (at skin surface)	5.8 J/cm^2 (infrared), 2.5 J/cm^2 (red)
Application mode	12 cm distance

Table 4: Optical parameters of the light-emitting diodes therapy applied to the Run+LEDs group at the end of the exercise and at 24 h after the first irradiation.
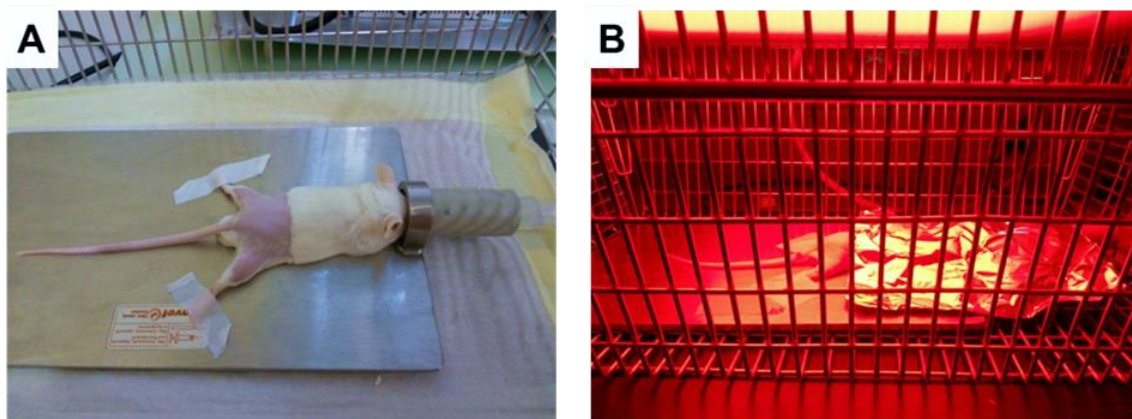
Figure 10: Application of the light therapy to the exercise legs. (A) The mouse were depilated on the lower half body, placed with the belly down and the limbs slightly stretched and fixed with a surgical tape. The mouse was rapidly induced to dormant conditions by isofluorane inhalation. (B) The mouse was irradiated for 3min and the upper body, including the head, was covered by aluminum foil.

Cryotherapy

The cryotherapy consisted in the application of cold water at 4±1°C to the lower limbs of the Run+CW mice for 5min.

The mice were depilated with Veet® cream on the half lower body part during the familiarization phase (described in 2.3.2). At the end of the three bouts of downhill running,

the animals were anesthetized by isofluorane inhalation and the cryotherapy was applied. The treatment with cold water was repeated at 24h after the first application.

Three of the Run+CW mice were immersed half body in cold water (Figure 11 (A)), and they are referred as Run+CW Imm. Subsequent considerations that will be discussed in the chapter 3, led to change the application modality. Hence, in the case of the six remaining mice of the Run+CW group, the cryotherapy consisted in the application of ice cold water packs to the legs (Figure 11(B)). In both cases, the water temperature was monitored by a thermometer. The change in the application modality occurred after observations that will be shown and discussed in the next chapters.
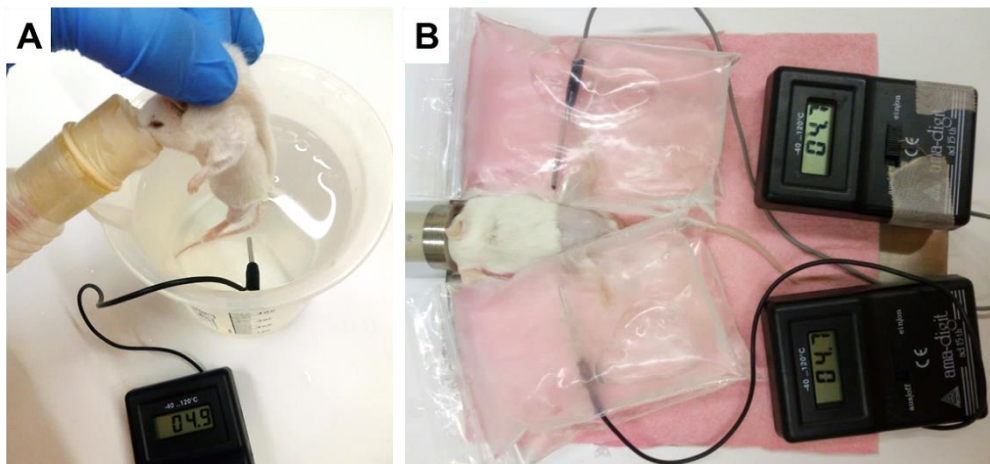

Figure 11: Two different application modalities of the cryotherapy: (A) The mouse was held half body in the cold water for 5 min. (B) Cold water packs were applied for 5min to the exercise muscles, avoiding a direct contact with the internal organs. In both cases, the temperature was monitored and kept at 4±1°C.

On the basis of the results reported in the next chapter, the experimental schedule for the application of the post exercise treatments (red/infrared therapy or cryotherapy) is shown in Figure 12.
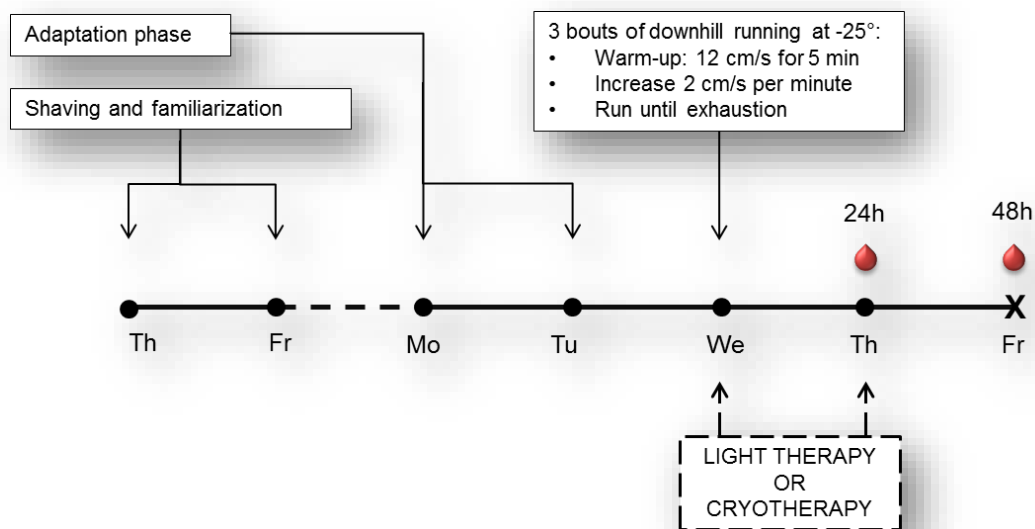
Figure 12: Example of an experimental schedule when the light or cryotherapy was applied in combination with a short-term downhill running. In the days before the exercise week, the mice were depilated and familiarized with the treadmills. An adaptation phase of two days preceded the exercise day and consisted in 10min train at 7cm/s. On the day of the damaging exercise, the mice underwent three bouts of intensive running at -25° slope, separated by 15 min rest. The treatment was applied within the 15min that followed the last bout and at 24h post-exercise. 15 min rest. Blood samples (red drop symbol) were taken at 24h, 48h. The necropsy was scheduled at 48h after the downhill running.

2.3.4   Blood collection and analysis

According to the time point of the exercise protocol (section 2.3.2), blood samples (≈150μL) were collected via ophthalmic venous plexus (orbital sinus) in lithi-um-heparinized tubes (Microvette 200 LH Sarstedt, Nümbrecht, DE) using glass capillaries (Micropipettes 20μl Blaubrand, Wertheim, DE). After centrifugation (5 minutes at 3000 g, 4°C) plasma was separated in 1.5 ml tubes (Eppendorf, Dreieich, DE) and stored at -20°C and later.

The plasma Creatine Kinase (CK) activity was determined by a colorimetric kit (Abcam, Cambridge, UK). Each plasma sample was mixed with reagents in a ratio of 1:15. A standard curve was prepared following the manufacturer protocol. The CK in the samples converted the creatine provided by the kit reagents, into phosphocreatine and ADP with the production of NADH. The newly generated products reacted with an enzyme mix to form an intermediate, which reduced the transparent reagents solution to a colored product with strong absorbance at 450 nm. The absorbance was measured kinetically every 2min, for 30min.

The plasma C-reactive protein (C-RP) was measured by a sandwich ELISA kit (Abcam, Cambridge, UK). Each plasma was diluted 1:200 and incubated in the wells with an antibody mix. A standard curve was also generated according to the manufacturer protocol. After the incubation, several washing steps followed. The addition of TMB substrate and a stop solution

turned the well content into a yellow dye, where the intensity was proportional to the amount of bound analyte. The intensity was measured at 450 nm with a spectrophotometer.

Every sample was measured in duplicates for both parameters.

The calibration curves were used to verify the linearity of the optical signal detected from the samples and to calculate the absolute value of the plasma parameters.

For selected samples, the lactate dehydrogenase (LDH) was measured in addition, through the Cobas c311 analyzer (Roche Diagnostics GmbH, Mannheim, DE).

To take in account the individual animal variability, the absolute values of CK and C-RP per time point of each mouse were divided on the respective baseline values. The ratio, so called fold change, express the variation over time of that parameter in relation to the individual baseline.

The absolute values and the fold changes of CK and C-RP were reported as means ±SD. The distribution over time of the normalized data was displayed by box-and-whisker plots.

 Based on the nonparametric Wilcoxon test, differential fold changes were analyzed using a commercial software package JMP 11 from SAS. A p-value ≤0.05 was considered significant.

2.4   Histology and microscopy

On the day of necropsy, the mice were sacrificed by cervical dislocation. The skin was removed, and quadriceps, gastrocnemius, soleus, tibialis muscle from the left leg were dissected and snap frozen in liquid nitrogen; while, the right leg was removed at the level of the hip joint and fixed in 4% PFA for 24h or 2% PFA all over the weekend. Other organs, like heart, liver, kidney, skin and testes, were also harvested to be available for further analysis. All the tools and the surfaces were properly sterilized before the start of the procedure and between one animal and the next one.

2.4.1   H&E and IF staining procedure

Fixed tissues were processed routinely, embedded in paraffin, cut (7µm thickness) and:
- Stained with hematoxylin and eosin (H&E) in all cases;
- Processed for immunofluorescence (IF) staining only for the animals following the established exercise protocol.

H&E slides were used to detect morphological change induced by the exercise and the whole muscle sections were acquired using Axio Scan Z1 Zeiss with a 20x objective.

For the IF staining, the quadriceps sections were left overnight at 37°C and processed for deparaffinization in Xylene and rehydration decreasing alcohol gradient solution from 100% to 70%. Afterwards, the slides were washed three times (5min each) in PBS and incubated in citrate buffer at 98°C in a steam cooker for 10min, followed by 20min of cooling at RT. After three washing steps in PBS, the sections were permeabilized with 0.25% Triton X-100 in PBS for 10min and then blocked in 5% chicken serum for 2h. Thereafter, samples were incubated overnight at 4°C with an anti-mouse IgG secondary antibody Alexa Fluor ® 647 (Invitrogen, DE), diluted in PBS (1:200) for the identification of the damaged muscle fibers. After incubation with the secondary antibody, slides were washed again (3 times, 5min) and counterstained with WGA Alexa Fluor® 488 conjugate (1:400 dilution in PBS) for cell membrane staining, and with SYTOX Orange (1:10 in 10mM EDTA and 1mM Tris-HCl solution) for nuclei identification.

The IF muscle sections were analyzed with a confocal microscope Leica TCS SP8 (LEICA, Mannheim, DE) and a full scan of the section was realized using the overview tile scan option, with a resolution of 1045x1045 pixel, 200ms acquisition time, and 20x oil immersion objective.

2.4.2 Evaluation of the histological changes due to the exercise and therapies applied

The IF full scan of the muscle sections that showed morphological evidence of the damage were processed for a quantification analysis of the damaged muscular fibers and infiltration of cell populations.

Ilastik was used as software for imaging segmentation in order to separate in three images the muscle fibers edges (Figure 13(A)), inner fibers areas (Figure 13(B)) and the background (Figure 13(C)).
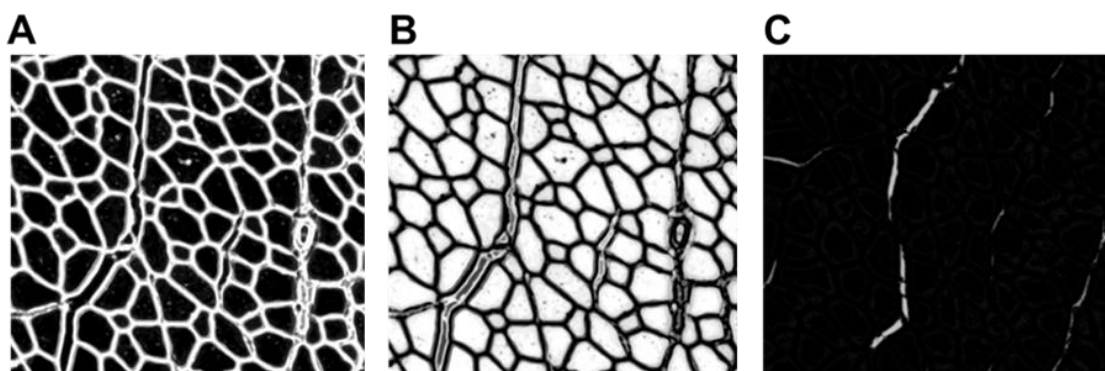

Figure 13: Results of the segmentation procedure of muscle sections in fluorescence executed by Ilastik software. The procedure involved the detection and separation of three areas of the muscle section: the muscle fibers edges (A), the inner fibers areas (B), the background (C).

Through a customized macro in ImageJ, the segmented images were evaluated in order to identify and count the muscle fibers of individual tissue sections. The final image containing the counted muscle cells was overlapped with the corresponding original IF picture in order to verify the counting results and add, if necessary, the missing cells manually (Figure 14). Inaccuracies in automatic counting were due to the quality of the stained tissue section. The error in the automatic counting ranged from 2% to 18%.
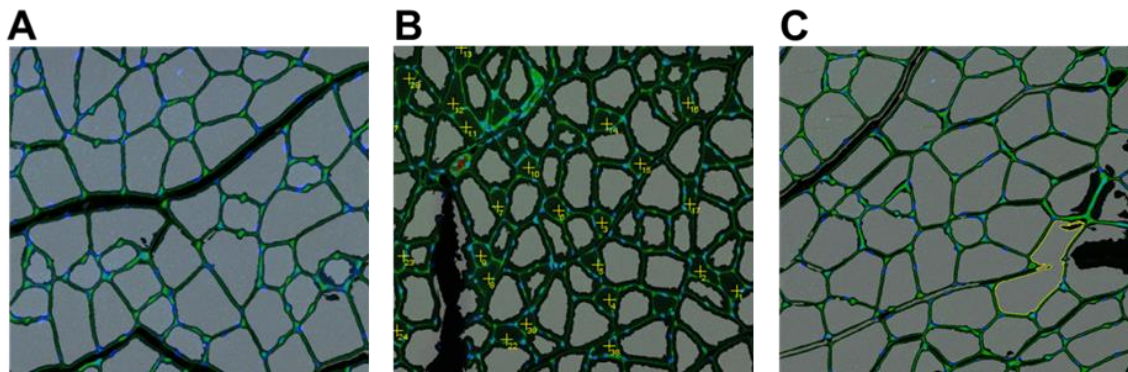
Figure 14: Overlapping of the original IF muscle section and the corresponding segmented image with the counted fibers. Each gray area is a muscle fiber that was counted by a macro in ImageJ. (A) An example of a good segmentation and counting procedure with an univocal matching between the gray areas and the muscle cells. (B) An example of miscounting result due to the limitation of the software in detecting the smaller fibers. In this case, the missing fibers were added manually (yellow crosses). (C)An example of miscounting results due to the limitation of the software in detecting the fibers edges, so two or more fibers were counted automatically as one. In the specific case, a singular gray area (yellow contour) was counted manually as two fibers.

The total section area and the areas with cell infiltration were calculated with ImageJ selecting manually the boundary of the zone of interest.

The fiber density was calculated as the total counted fibers on the total section area (total fibers/mm^2). The fiber density, total counted fibers and total section area were reported as mean±SD for each experimental group.

The fibers which were altered, with respect to the normal morphology, were counted manually and normalized on the total fibers number of the corresponding section. The normalized values were expressed in percentage for each experimental group.

The total area with cell infiltration was normalized on the total area of the corresponding tissue slide (infiltrated area). The normalized infiltrated area for each experimental group was reported in means±SD and percentages.

Based on the nonparametric Wilcoxon test, differential normalized values were analyzed using a commercial software package JMP 11 from SAS. A p-value ≤0.05 was considered significant.

2.5 Gene expression

2.5.1 RNA isolation from cell culture

For RNA isolation and subsequent gene expression analysis, cells were harvested from the 96-well plate with TRIzol (32 µL/well) and stored at -80°C in a freezing container (Mr. Frosty™, Thermo Scientific™, DE). The RNA isolation procedure consisted in adding 200 µL chloroform per 1 mL TRIzol, followed by 3min incubation time at RT. Afterwards the samples were centrifuged at 12000 xg for 15min at 4°C obtaining three phases: the organic phase (lower phase) containing lipids and proteins, the interphase containing DNA and the upper aqueous phase containing the RNA. The upper phase was transferred into a new tube and precipitated by the addition of 500 µL isopropanol for 1 mL TRIzol. The samples were inverted, incubated for 10min at RT and further centrifuged at 12000 xg for 10min at 4°C.

Two washing step followed adding 1mL 80 % ethanol and centrifugation at 12000 xg for 5min at 4 °C. At the end, the RNA pellet was air dried for 20min and dissolved in 20-30µL RNase-free water.

2.5.2 RNA isolation from muscle tissue biopsy

The RNA was isolated from the snap-frozen quadriceps using the RNAse fibrous tissue minikit (QIAGEN, Hilden, DE). According to the manufacturer protocol, 30 mg of frozen tissue for each mouse were homogenized using a tissue homogenizer (Kinematica AG, Luzern, CH) and successively incubated for 10min with Protease K at 55°C. After the enzymatic digestion, the homogenate was centrifuged for 3min at 10000xg and the transparent phase was separated into a new eppis. Ethanol 100% was added to the phase and the solution was centrifuged through a silica-membrane spin column with a binding capacity of 100mg RNA. Digestion of genomic DNA was performed and, after several washing steps, the RNA was released from the silica membrane and dissolved in 30µL RNA-free water.

The RNA samples of six mice for each experimental group were selected for the complete gene expression analysis.

2.5.3 Gene expression and bioinformatics analysis

The purity of the isolated RNA was measured with a spectrophotometer (TECAN, Männedorf, CH) at the absorbance ratio of 260/280 and 260/230. Furthermore, the RNA integrity was verified through the calculation of the RNA Integrity Number (RIN), obtained by an electrophoresis process of the RNA sample with Agilent 2100 Bioanalyzer. Samples with RIN > 7.0 and 260/280 > 2.0 were considered for the gene expression profiling.

cDNA was synthesized using the SuperScript Choice System and according to the manufacturer instructions. It followed the cRNA production using the ENZO BioArray HighYield RNA Transcript Labeling Kit biotin-labeled. A standard protocol from Affymetrix was used for the in vitro transcription (IVT). Fragmentation of the cRNA was obtained using Affymetrix defined protocol. For gene expression profiling, labeled and fragmented cRNA was hybridized to Affymetrix Mogene-2_0-st microarrays with an Incubation of 16h at 45° C. The Affymetrix fluidics station 450 was used to wash the microarrays, while the scanning was performed with Affymetrix Genechip scanner 3000.

The Custom CDF Version 22 with Entrez based gene definitions was used for annotation. The raw fluorescence intensity values were normalized applying quantile normalization. Based on OneWay-ANOVA, differential gene expression was analyzed using a commercial software package JMP Genomics 7 from SAS. Singular gene expression was considered significant for a nominal p-value≤0.05 (or 5%). For pathways analysis, a false positive rate of a=0.1 with FDR correction was considered as the level of significance (p-adjusted ≤0.1 or 10%). Gene Set Enrichment Analysis (GSEA) was applied to determine whether defined lists (or sets) of genes exhibit a statistically significant bias in their distribution within a ranked gene list (see http://www.broadinstitute.org/gsea/ for details).

The significant list of genes was processed by the DAVID Bioinformatics Resources 6.8 tool (https://david.ncifcrf.gov/home.jsp) in order to identify biological domains according to the Gene Ontology (GO) annotation (see http://www.geneontology.org/ for details) and UniProtKB (UP) keywords. The identified domains related to membrane and cytoskeleton structures, myogenesis and immunity system were taken into account and further clustered under customized names to facilitate the representation of the results. The Table 5 reports the GO identification (ID) number, the original domain name, and the customized name of the domains were from the analysis, while the Table 6 reports the UP keyword and the customized name.

GO ID	GO domain	Customized name
0016020	Membrane	Membrane/cytoskeleton
0016021	Integral component of membrane	Membrane/cytoskeleton
0032233	Positive regulation of actin filament bundle assemble	Membrane/cytoskeleton
0005856	Cytoskeleton	Membrane/cytoskeleton
0007517	Muscle organ development	Myogenesis
0035914	Skeletal muscle cell differentiation	Myogenesis
0002376	Immune system process	Immunity
0007159	Leukocyte cell-cell adhesion	Immunity
0048245	Eosinophil chemotaxis	Immunity
0002523	Leukocyte migration involved in inflammatory response	Immunity
0071347	Cellular response to interleukin-1	Immunity
0050853	B cell receptor signaling pathway	Immunity
0042110	T cell activation	Immunity
0002548	Monocyte chemotaxis	Immunity
0002250	Adaptive immune response	Immunity
0007159	Leukocyte cell-cell adhesion	Immunity
0045087	Innate immune response	Immunity

Table 5: List of the GO domains and the respective ID that were identified from the clustering of significant genes operated by the DAVID Bioinformatics Resources 6.8 tool. In the third column is reported the name used to classify the domains.

UP keyword	Customized name
Membrane	Membrane/cytoskeleton
Transmembrane	Membrane/cytoskeleton
Cytoskeleton	Membrane/cytoskeleton
Myogenesis	Myogenesis
Immunity	Immunity
Adaptive immunity	Immunity
Innate immunity	Immunity

Table 6: UP keywords that were identified from the clustering of significant genes operated by the DAVID Bioinformatics Resources 6.8 tool. In the second column is reported the name used to classify the domains.

The expression of a singular gene is reported in fold change compared to the reference group.

Control or Run was taken as reference group.

The fold change of one gene compared to the reference is obtained raising the differential gene expression (expressed in log_2) on the basis of two:

$$Differential\ gene\ A_x\ expression = \ log_2(A_x) - log_2(A_r) = \ log_2\left(\frac{A_x}{A_r}\right)$$

$$Fold\ change = \frac{A_x}{A_r} = 2^{log_2(A_x) - log_2(A_r)}$$

Where:

A_x is the fluorescence intensity of the expressed gene A for x group (Run or Run+LEDs Run+CW);

A_r is the fluorescence intensity of the expressed gene A for the reference group.

Pathways concerning cell functions were obtained from the public database Kyoto Encyclopedia of Genes and Genomes (KEGG) combining the expression pattern of the genes. Pathways are clustered in 6 main categories: metabolism, genetic information processing, environmental information processing, cellular processes, organismal system, human diseases. In each category, pathways are further classified into sub-categories (see https://www.genome.jp/kegg/pathway.html for details). For the purpose of this study, the main category of human diseases was ignored. Each KEGG pathway is associated with a normalized enrichment score (NES), the nominal p-value, and the p-adjusted. Pathways overall up-regulated and down-regulated in comparison to the reference group have been characterized by NES positive and negative values, respectively. A p-adjusted ≤ 0.1 was considered significant.

3 RESULTS

3.1.1 Development of the *in vitro* skeletal muscle model

C2C12 are murine myoblasts derived from satellite cells with the capacity of differentiation in mature skeletal muscle myotubes. This cell line is widely characterized and used as skeletal muscle model in vitro.

The Figure 15 illustrates the general monolayer architecture during proliferation and differentiation. Undifferentiated cells had a fusiform star-shape at 24h after the seeding (Figure 15 (A)). The C2C12 proliferated, stretching towards the nearby cells (Figure 15(B)), and reached the 100% confluence within 3 days (Figure 15(C)). At this time point, it was possible to differentiate the myoblasts into myotubes by serum starvation. The cells started to fuse (Figure 15(D)) and, progressively, more and more elongated shapes appeared (Figure 15(E)). After 4 days from the differentiation induction, the cells looked differentiated: fusiform thin structures aligned in a defined direction, are the features of mature skeletal muscle myotubes (Figure 15(F)).
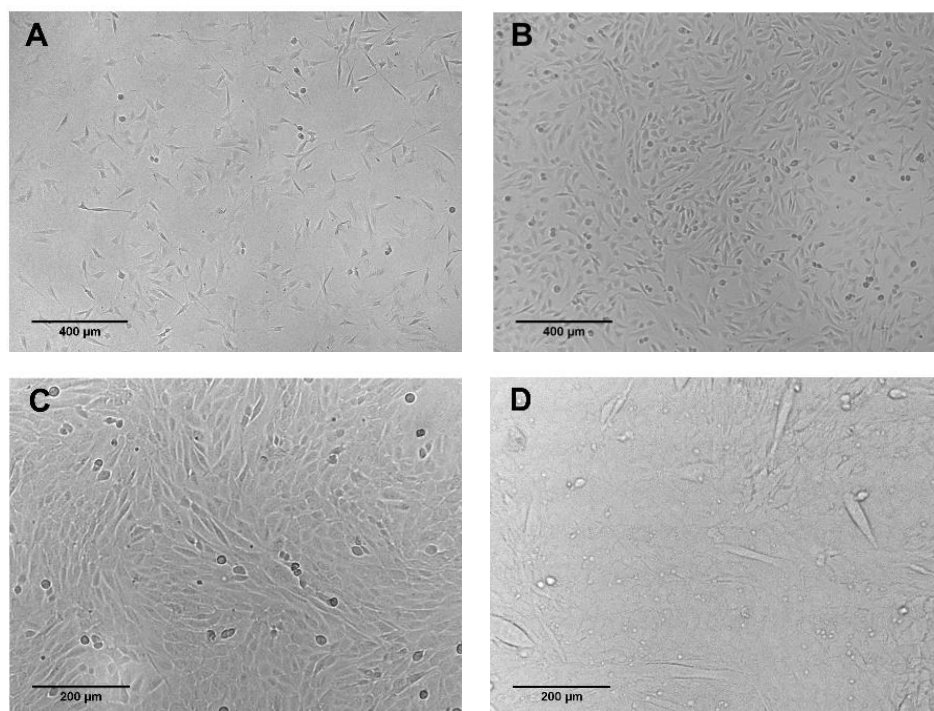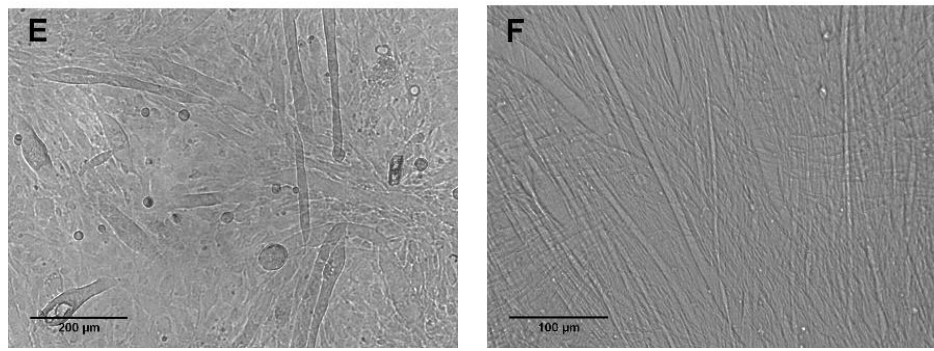
Figure 15: (A) C2C12 at 24h after seeding showed a fusiform star-shape; (B) C2C12 at 2 days after seeding; (C) C2C12 100% confluent at 3 days after seeding were; (D) C2C12 start to fuse after 24h in serum starvation condition; (E) cells at the intermediate differentiation stage; (F) fully differentiated myotubes after 4 days from the beginning of the differentiation.

3.2 The effect of infrared and red light on metabolism and ATP production

As a preliminary study before the in vivo experimentation, the proliferative (XTT) and energy production (ATP) effect of red and infrared light was tested on the in vitro skeletal muscle model. The Figure 16 displays the order followed to test different irradiation parameters. The red and green colors are used to indicate negative and positive responses, respectively.

The first parameter tested was the energy density applied to myoblasts at 656nm and 830nm. As a consequence of negative response at 656nm, no further parameters were tested. Instead, positive results were achieved with 2.5 J/cm^2 of infrared light and, subsequently, different harvesting times were tested for that energy density on myoblasts and myotubes.
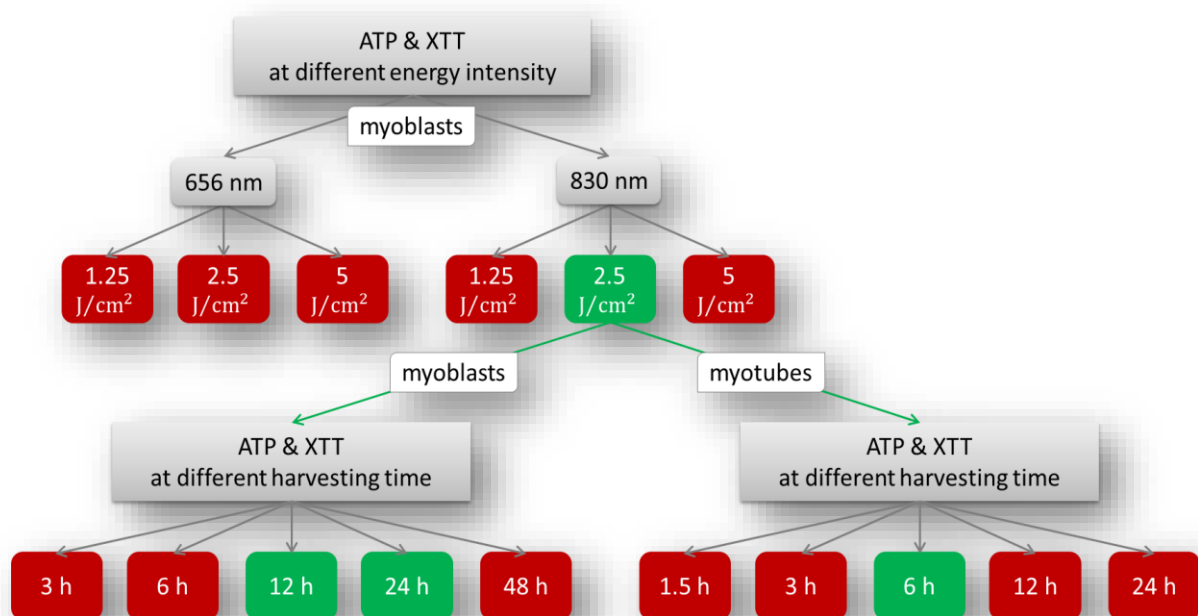
Figure 16: Scheme of the in vitro experiments for testing the red and infrared light on C2C12 myoblasts and myotubes.

34

3.2.1 Proliferative effect on myoblasts of infrared light at 24h after 2.5 J/cm^2 irradiation

To define the energy density that leads to the highest proliferative and energetic effect, XTT and ATP test were conducted on myoblasts for 1.25 J/cm^2 (55s), 2.5 J/cm^2 (110s), 5 J/cm^2 (220s) at 24h after the irradiation.

Comparing the distribution of the data in Figure 17 and in Figure 18, it was evident that the changes for the infrared light were more pronounced. Indeed, at 24h after the irradiation of 2.5 J/cm^2, the ATP and XTT signals were significantly (p-value<0.0001) increased by about 4% and 6% compared to the control (Table 7). For the red light, a decrease of 2.5% in ATP production for 1.25 J/cm^2 was the highest significant (p-value<0.0001) change observed.
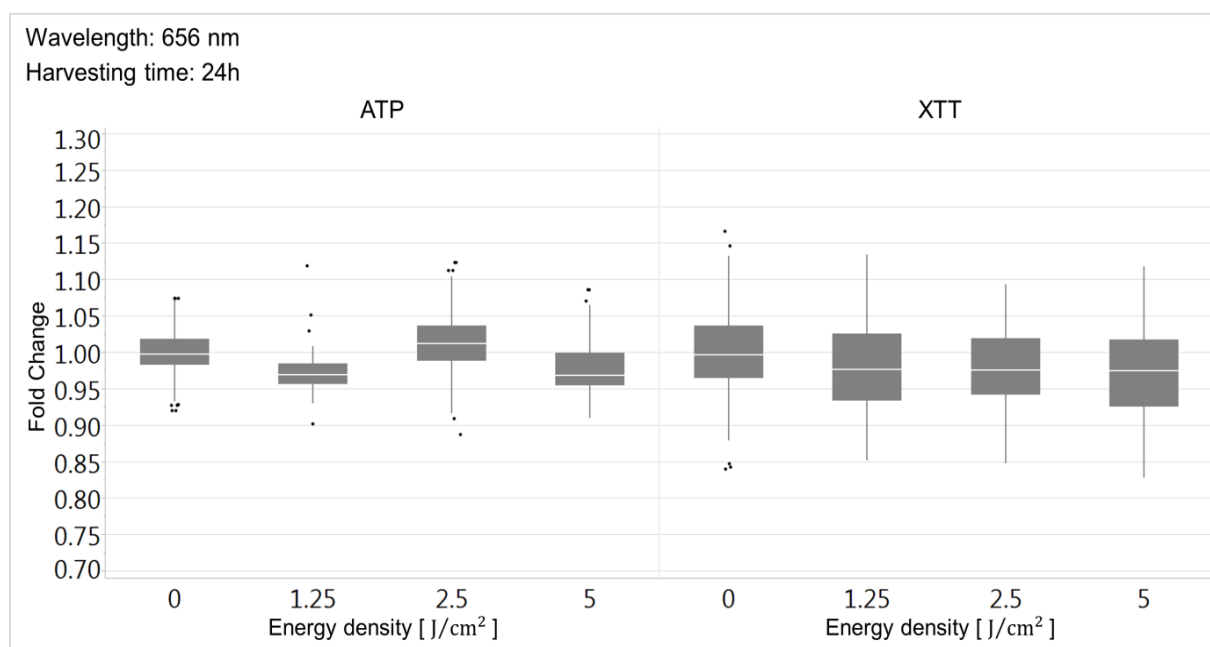
Figure 17: Box-and-whisker plots represents the distribution of XTT and ATP fold change for different energy density of red light on myoblasts. The band inside the box reflects the median. The whiskers extend for values calculated as: 3rd quartile+1.5*(interquartile range) and 1st quartile-1.5*(interquartile range). The dots are the outlier values.
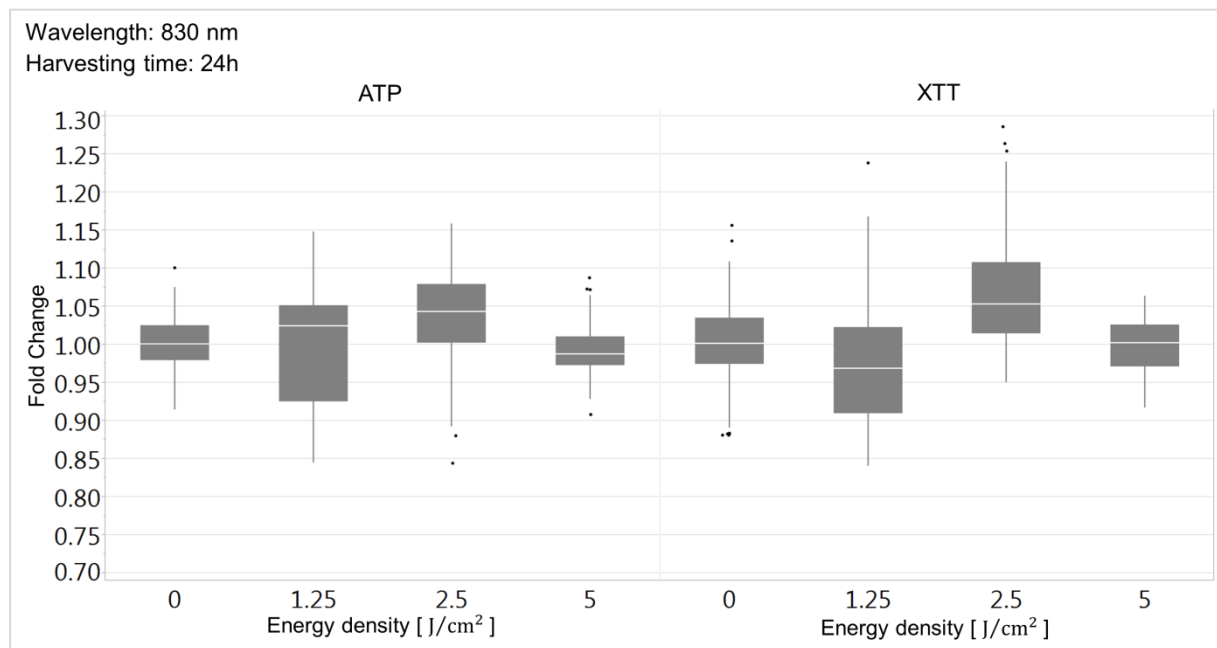
Figure 18: Box-and-whisker plots represents the distribution of XTT and ATP fold change for different energy density of infrared light on myoblasts. The band inside the box reflects the median. The whiskers extend for values calculated as: 3rd quartile+1.5*(interquartile range) and 1st quartile-1.5*(interquartile range). The dots are the outlier values.

Mean values for wavelength: 830nm

Energy density	ATP	XTT
J/cm^2	Mean±SD	Mean±SD
0	0.99±0.03	1.00±0.004
1.25	0.99±0.07	0.98±0.007
2.5	1.04±0.06	1.06±0.005
5	0.99±0.04	0.99±0.01

Table 7: Mean values of ATP and XTT fold changes for 830 nm tested at different energy density on myoblasts

3.2.2 ATP production and proliferation of infrared light on myoblasts at different harvesting time from the irradiation

As a consequence of the results shown previously, the infrared light with a fixed energy density of 2.5 J/cm^2 was chosen for the following experiments.

To examine the time course of the proliferative effect, the XTT and ATP tests were performed at different time points after the irradiation.

At 12h after the irradiation, the ATP production were significantly (p-value<0.0001) 7% higher than the control, while the XTT fold change remained at the no light control level. At 48h after irradiation, both ATP and XTT signals returned to the control values (Figure 19).

Figure 19: Box-and-whisker plots represents the distribution of XTT and ATP fold change for different harvesting time of 2.5 J/cm² infrared light on myoblasts. The band inside the box reflects the median. The whiskers extend for values calculated as: 3rd quartile+1.5*(interquartile range) and 1st quartile-1.5*(interquartile range). The dots are the outlier values.

3.2.3 ATP production in myotubes at 6h after infrared light irradiation

Infrared light at 2.5 J/cm² was applied to differentiated myotubes and the ATP and XTT test were performed at different harvesting times. XTT did not show any change over time compared to the no light control. The only increase (q<0.0001) observed was a 2.5% in the fold change at 6h after the infrared irradiation (Figure 20).

In the case of myotubes, a 1.5h harvesting time was tested to detect a potential intermediate response before 6h. It was not possible to test the ATP production for a harvesting time of 48h because of the difficulty to culture myotubes in 96-well plates for longer than 1 week.
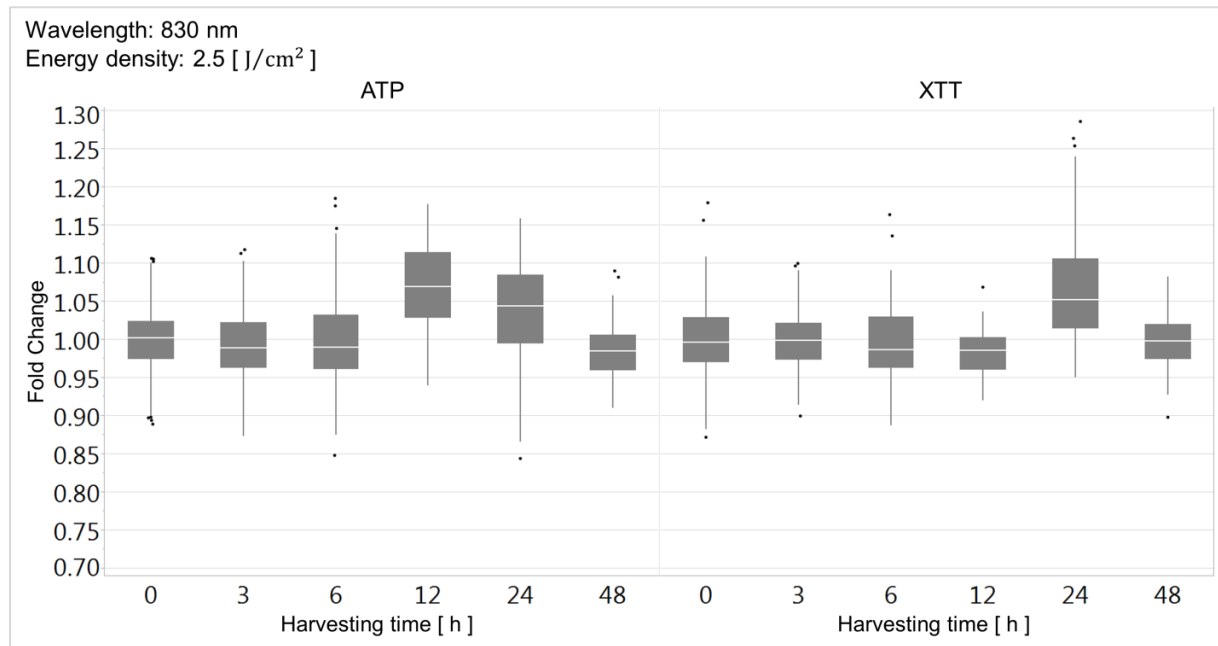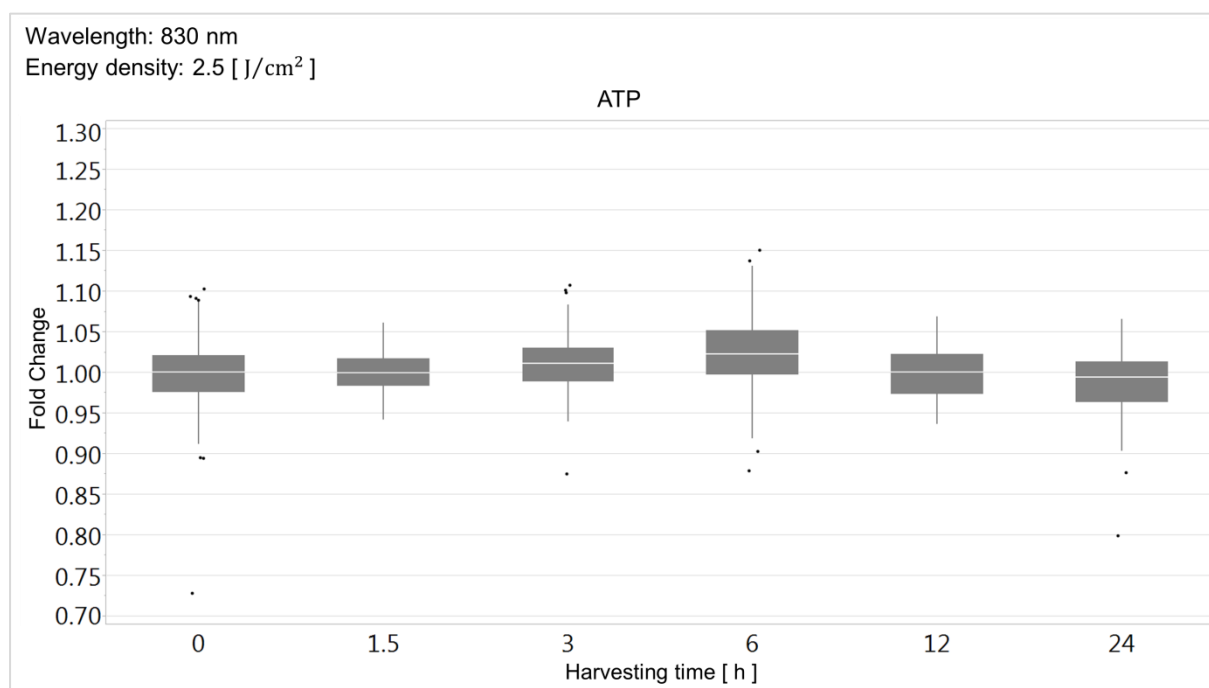
*Figure 20: Box-and-whisker plots represents the distribution of ATP fold change for different harvesting time of 2.5 J/cm²
infrared light on myotubes. The band inside the box reflects the median. The whiskers extend for values calculated as: 3rd
quartile+1.5*(interquartile range) and 1st quartile-1.5*(interquartile range). The dots are the outlier values.*

3.2.4 Modulation of inflammatory and metabolic pathways by infrared light

RNA was extracted for myoblasts and myotubes at 12h and 24h after 2.5 J/cm² irradiation,
and for the corresponding no light control cells. Affymetrix chips were run for the gene
expression and gene set enrichment analysis (GSEA) was performed using Kyoto Encyclopedia
of Genes and Genomes (KEGG) database (see 2.5.1).

An overview of the significantly modified (p-adjusted <5%) genes and pathways (p-value ≤5%)
containing the highest number of regulated genes in comparison to the no light control for
myoblasts and myotubes is reported in Table 8. Pathways included in the category of human
diseases were excluded.

The expression of regulated genes in irradiated myoblasts triplicates from 12h to 24h
compared to the no light control. The regulated pathways do not differ much between the
two time points: 7 pathways at 12h and 11 pathways at 24h.

In spite of the fact that the amount of genes regulated by the infrared light in cultured
myotubes at 12h and 24h is similar, only 7 pathways were overall significant at 24h, against
the 16 pathways at 12h.

Energy density Harvesting time	2.5 J/cm² 12h	2.5 J/cm² 24h	Cell type
Significant differentially (p-adjusted <5%) expressed genes	548	1542	Myoblasts
Significant pathways containing upregulated genes with nominal p-value ≤5%	1	8	
Significant pathways containing downregulated genes with nominal p-value ≤5%	6	3	
Significant differentially (p-adjusted <5%) expressed genes	675	765	Myotubes
Significant upregulated pathways containing with nominal p-value ≤5%	9	5	
Significant downregulated pathways with nominal p-value ≤5%	7	2	

Table 8: Overview of significantly regulated genes and pathways in myoblasts and myotubes at different harvesting time (12h and 24h) from the irradiation of 2.5 J/cm² infrared light. The significant up and down regulation is meant in comparison to the gene expression of the no light control cells.

Table 9 and Table 10 report a selection of pathways activated by infrared light in myoblasts and myotubes, in comparison to the no light control. Each pathway is associated with a main category, a sub-category and a NES. Positive NES corresponded to upregulated pathways, while negative values of NES indicated downregulated pathways.

Most of the pathways regulated in myoblasts are related to metabolic processes (Table 9). In particular, a switch from 12h to 24h was observed. At 12h, all the significant metabolic pathways were downregulated, instead, at 24h there was a push to the metabolism, like lipids, carbohydrates and amino acids, in line with the increase of the signal measured by the XTT test (see 3.2.2).

For what concerns the pathways activation in myotubes, in Table 10 is listed a selection of pathways modulated after 24h of 2.5 J/cm² infrared light. Differently from the effect of the light on myoblasts, in myotubes the light seemed to activate pathways related to the immune system, like TNF and chemokine signaling pathways.

Cell type: myoblasts
Energy density: 2.5 J/cm^2

Pathway	Main Category	Sub Category	Harvesting time	NES
Glycolysis / Gluconeogenesis	1. Metabolism	1.1 Carbohydrate metabolism	12	-1.77
Other types of O-glycan biosynthesis	1. Metabolism	1.7 Glycan biosynthesis and metabolism	12	-1.81
Fatty acid elongation	1. Metabolism	1.3 Lipid metabolism	12	-1.48
Carbon metabolism	1. Metabolism	1.0 Global and overview maps	12	-1.3
N-Glycan biosynthesis	1. Metabolism	1.7 Glycan biosynthesis and metabolism	12	-1.38
Galactose metabolism	1. Metabolism	1.1 Carbohydrate metabolism	24	1.86
Glycerophospholipid metabolism	1. Metabolism	1.3 Lipid metabolism	24	1.68
2-Oxocarboxylic acid metabolism	1. Metabolism	1.0 Global and overview maps	24	1.62
Biosynthesis of amino acids	1. Metabolism	1.0 Global and overview maps	24	1.47
Fatty acid elongation	1. Metabolism	1.3 Lipid metabolism	24	1.57
Tryptophan metabolism	1. Metabolism	1.5 Amino acid metabolism	24	1.48
Glycosphingolipid biosynthesis - globo series	1. Metabolism	1.7 Glycan biosynthesis and metabolism	24	1.54
Metabolism of xenobiotics by cytochrome P450	1. Metabolism	1.11 Xenobiotics biodegradation and metabolism	24	1.38

Table 9: Selected KEGG pathways deriving from the gene expression in myoblasts at 12h and 24h after2.5 J/cm² infrared light irradiation. Each pathway is classified in a main category and sub-category, according to KEGG database, and associated with a Normalized Enrichment Score (NES). A positive NES indicates an up regulation in comparison to the no light control. A negative NES indicates a down regulation in comparison to the no light control.

Cell type: myotubes
Energy density: 2.5 J/cm^2

Pathway	Main Category	Sub Category	Harvesting time	NES
TNF signaling pathway	3. Environmental Info Processing	3.2 Signal transduction	12	1.8
NOD-like receptor signaling pathway	5. Organismal Systems	5.1 Immune system	12	1.79
Chemokine signaling pathway	5. Organismal Systems	5.1 Immune system	12	1.78
Cytokine-cytokine receptor interaction	3. Environmental Info Processing	3.3 Signaling molecules and interaction	12	1.74
Cytosolic DNA-sensing pathway	5. Organismal Systems	5.1 Immune system	12	1.54
Lysosome	4. Cellular Processes	4.1 Transport and catabolism	12	1.46

Table 10: Selected KEGG pathways deriving from the gene expression in myoblasts at 12h after2.5 J/cm² infrared light irradiation. Each pathway is classified in a main category and sub-category, according to KEGG database, and associated with a Normalized Enrichment Score (NES). A positive NES indicates an up regulation in comparison to the no light control. A negative NES indicates a down regulation in comparison to the no light control.

3.3 Selection of the exercise modality for the *in vivo* model

The selection of the exercise protocol for inducing muscular damage in the mice lower limbs occurred on the base of morphological changes in the histology. For this purpose, a comparison of H&E stained sections of quadriceps, triceps surae and tibialis was carried out. The three muscles had different shapes, as it is shown in Figure 21. From the total section of the quadriceps (Figure 21(A)), the vastus medialis, vastus lateralis and the rectus femoris can be distinguish. In Figure 21(B), it is possible to recognize the two heads of the grastrocnemius and the soleus muscle. The tibialis, in Figure 21(C), is the smallest isolated muscle.
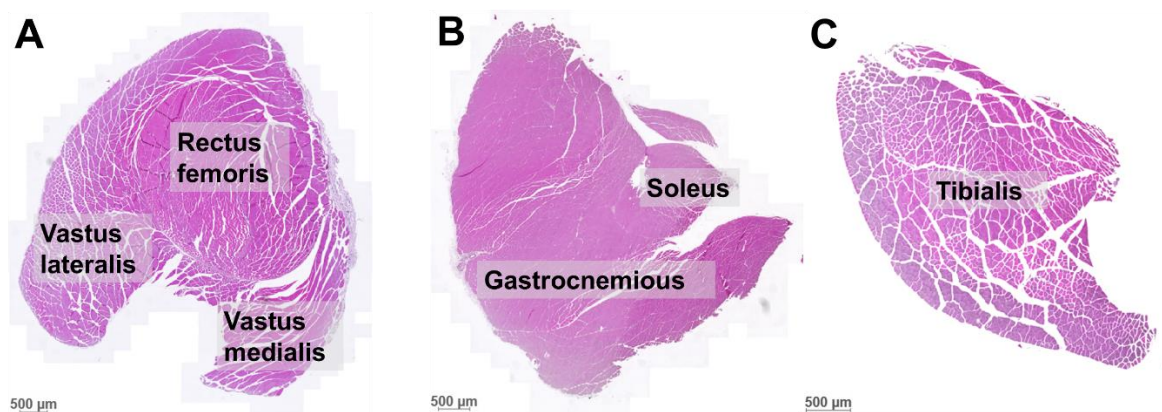
Figure 21: H&E stained full sections of quadriceps (A), triceps surae (B), tibialis (C) from a control mouse.

The histology of control mice showed common features among the three types of muscles, and an example is illustrated in Figure 22. In a healthy tissue, muscle fibers on a cross section were characterized by a polygonal shape, with cell nuclei located at the periphery. Fewer than 3% of myofibers had central nuclei, due to the physiological turnover (Figure 22 (A)). Veins, arteries, nerves were clearly visible, as well as muscle spindles (Figure 22(B)) because the muscles were cut at the middle of the full length. At the interface between the rectus femoris and the vastii, in the central part of the rectus femoris and the soleus, a bundle of flat-nuclei cells was observed. A Masson-Goldner trichrome staining confirmed that it was a collagen bundle and the cells were probably fibroblasts. Moreover, the flat shape of the nuclei led to the conclusion that it was not a newly deposited tissue and the presence in all the mice, further by confirmed that it was a physiological feature.

The histology for the three different modalities of exercise (described in 2.3.2) revealed that only the short-term downhill running mice experienced evident morphological changes. In particular, signs of stress and structural alterations were detected only in the short-term

downhill running at 48h and 72h after the exhaustive exercise. Moreover, this evidence was found only in quadriceps muscles.
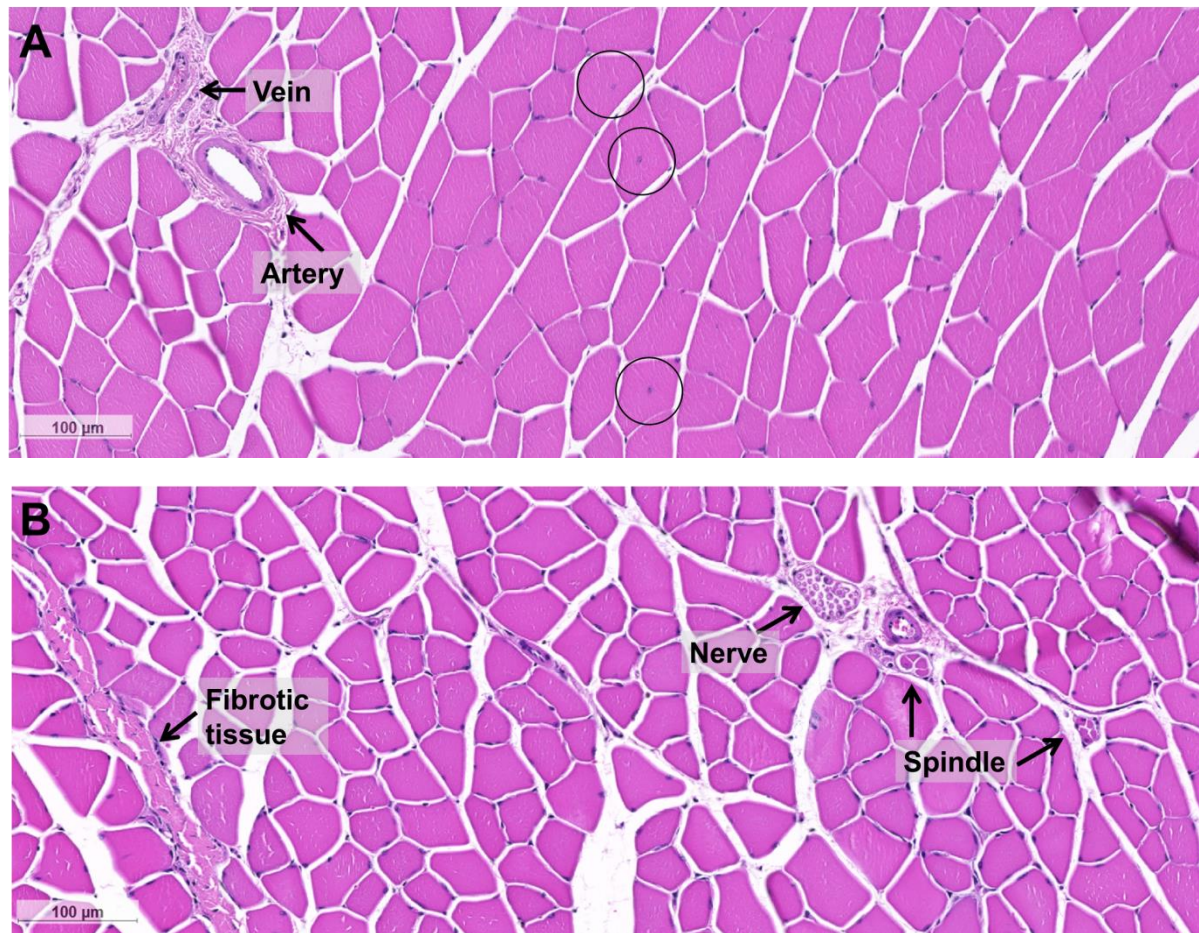
Figure 22: Detail of quadriceps H&E section from a control mouse showing the polygonal cross section of muscle fibers, centralized nuclei, vessels (A), nerves, muscle spindles and fibrotic bundle (B).

The histology of mice processed at 48h after exercise revealed multiple sites of focal degeneration and fiber necrosis (Figure 23), characterized by a pale cytoplasm, by infiltration of mononucleated cells in the interstitial spaces and by evidence of phagocytosis for cellular debris removal in necrotic fibers. Among the population of infiltrated cells, macrophages and leucocytes could be distinguished. Moreover, activated stem cells could also be part of it. Fibers in proximity or surrounded by infiltrated cells, presented a round shape, affected by the inflammatory activity.

The analysis of the downhill running mice scarified at 72h after the exercise, did not display the same level of damage. Indeed, only hypereosinophilic round fibers and swollen fibers were observed (Figure 24). Swollen fibers (Figure 24(B)) are featured like cells with smoother angles and hypereosinophilic fibers, characterized by the loss of angulated shape and a homogenous sarcoplasm.

The quadriceps of mice scarified at 168h were supposed to show evidence of muscle regeneration, characterized by an amount of central nucleated myotubes >3%. However, at 168h after the downhill running, the number of fibers with central nuclei was ca. 1% of the
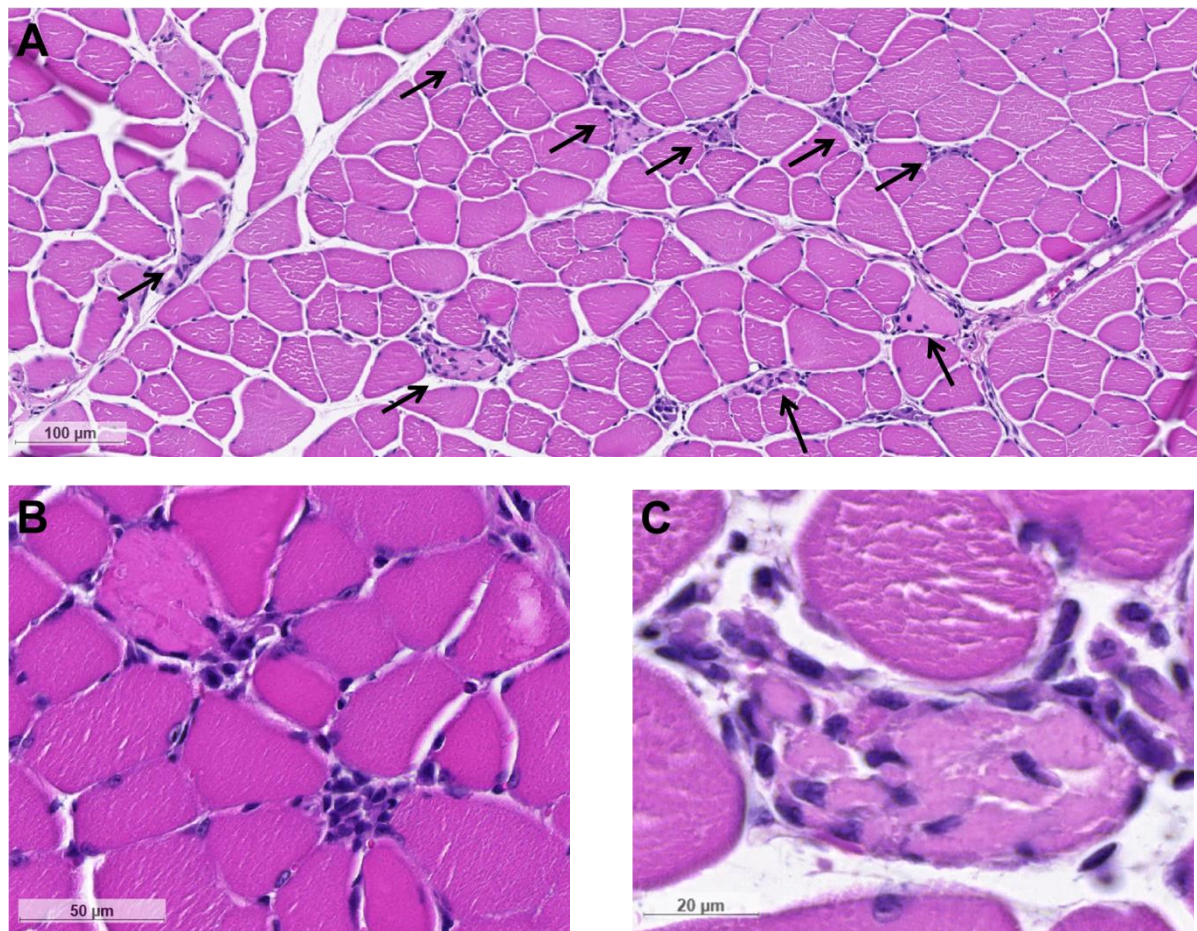
Figure 23: Details of quadriceps H&E section from the two mice running downhill and scarified at 48h after the exercise.(A)Multiple sites of focal degeneration an fibers necrosis. Necrotic fibers are paler than healthy ones. Different population of nucleated cells is infiltrated in the interstitial spaces (B) and macrophages work on necrotic fibers to remove cell debris(C). In (C) is also shown a muscle cell that lost the typical angulated shape and assumed a round one.

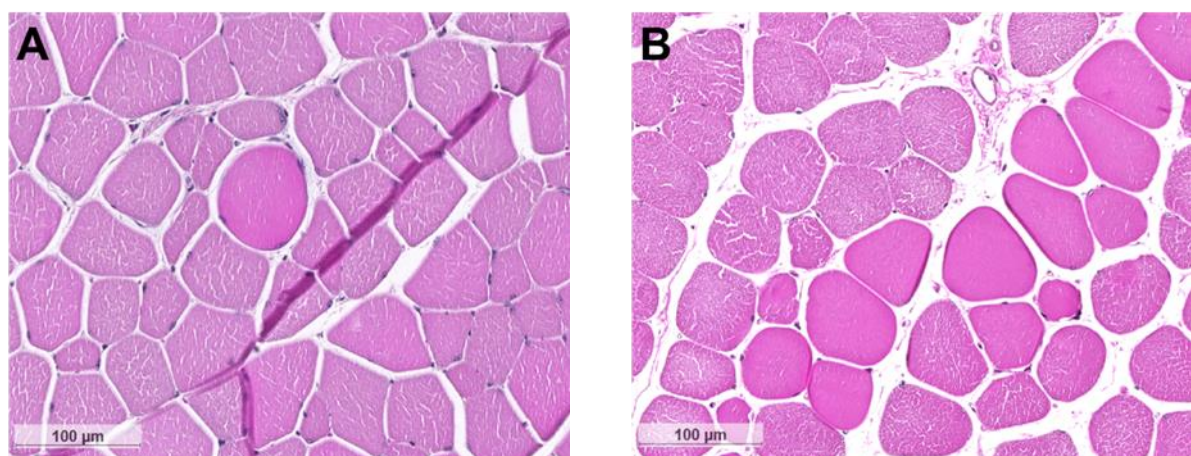*Figure 24: Details of quadriceps H&E section from the two mice running downhill and necropsy at 72h after the exercise. Hypereosinophilic round fibers (A)(B) are an early sign of necrosis and are called hyaline fibers. Swollen fibers (B) have smoother angles and are a sign of stress due to an unbalance of electrolytes.*

total number of fibers. This percentage was similar to the one of the control and the histology at 48h and 72h.

For the short downhill running protocol, the blood sampling was scheduled and the fold change of the CK per each mouse was calculated. The values of CK for the mice scarified at 48h from the exercise were 5.7 fold higher than the individual baseline, while, for the mice with necropsy at 72h, the CK fold change was 3.8. At 168h after the damaging exercise, the animals had the CK value back to the baseline. The leakage of the CK into the blood stream is caused both by integrity loss of the cellular membrane and by an increase of sarcolemma permeability. Hence, it is not necessary to have a mechanical damage for the raise of this marker.

3.4   The exercise and the post-exercise therapies affected the plasma markers

On the basis of the results reported in the 3.3 paragraph, the selected exercise protocol consisted in the short term downhill running, with the harvesting of the tissue at 48h after the exercise.

The selected exercise protocol was repeated for other 6 mice, in order to have in total 9 animals for the Run group without post-exercise therapy. Afterwards, the experiments for the Run+LEDs group were performed, and, at the end, the Run+CW mice followed.

An overview of a typical experimental schedule is illustrated in Figure 12.

3.4.1   Exclusion of three mice of the cryotherapy group from the study

As described in the section 2.3.3, the first three mice of the Run+CW group received the cryotherapy by immersion into ice-cold water. The C-RP of the these animals, increased from 15% at 24h to 33% at 48h post-exercise, with the cryotherapy applied within 15min after the running and at 24h after the exercise. Instead, the CK slightly changed compared to the baseline. In despite of the rapid C-RP increment, the H&E histology of the all harvested muscles (quadriceps, triceps surae and tibialis) were without any sign of damage, where compare to control tissue.

The post-hoc comparison of CK, LDH and C-RP distributions (Figure 25) between the water immersed mice (Run+CW Imm) and the 6 mice with water packs (Run+CW), displayed that the modality of application influenced the trend of C-RP and LDH. These biomarkers increased

significantly (p-value≈0.05) in the Run-CW Imm mice compared to the baseline and to the Run+CW. Instead, there was no significant difference in the CK levels.

In the following paragraphs, only the results of the Run+CW animals will be reported and compared to the other experimental groups.
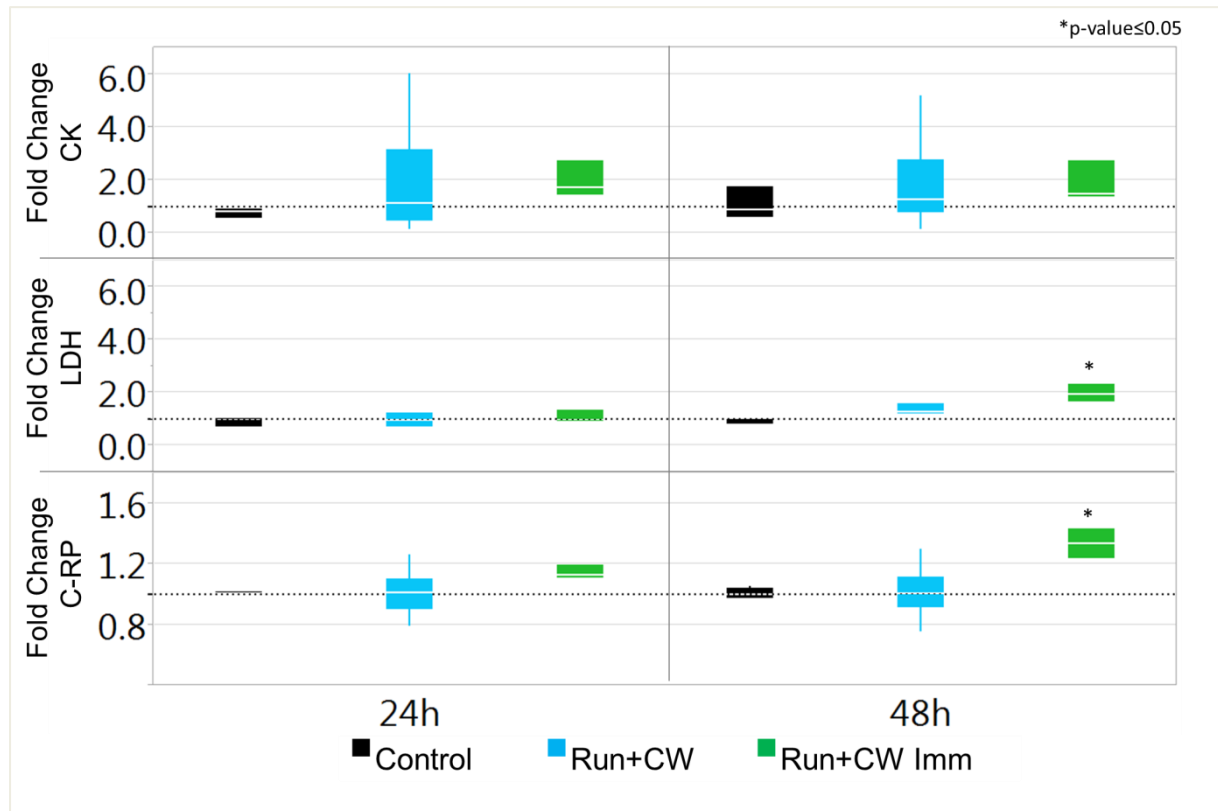
Figure 25: Fold change of C-RP, LDH and CK distribution over time of the Control, Run+CW and Run+CW Imm. The dashed line is placed at fold change equal to 1, meaning no change compared to the baseline. The fold change of the control mice ensures that the measurement of that parameter is true positive, remaining stable around 1. Only in the Run+CW Imm mice there was a significant increase of the C-RP and LDH (p-value≈0.05) compared to the baseline.

3.4.2 Observations on the behavior of animals in response to the exercise

At the placement into the treadmill channel, the animal looked disoriented and did not move. After few seconds, they became more and more confident, moving, sniffing the walls and the floor to find a way out.

When the treadmill was activated at low speed for the first time (at the first day of the familiarization phase), the animal reacted with a gasp and, in most of the cases, did not move by themselves until the rolling band drove them against the bottom of the channel. At that point, the mouse began to walk in the opposite versus of the rolling floor and the shocking grid was turned on. Frequently, the mice emitted a complaining sound at the first shocks; however, they learnt immediately to stay away from the shocking area. Already at the second day of the familiarization phase, the mouse learned to walk as soon as the treadmills band

moved, and they showed memory of the shocking area at the bottom of the channel. After the 2 day break, the behavior in relation to the treadmill looked more confident and the animals seemed to be adapted to the type of exercise.

At the day of the exhausting exercise, the highest performance (in terms of running time) was reached at the end of the first bout, and the worst at the third bout (Table 11). Between one bout and the subsequent one, the mice were placed into their home cage, and their behavior was observed. After the last bout of running, the mice looked visibly tired: they do not drink, or climb or walk in the cage for the first minutes.

Some mice revealed better runners than others were, and, by chance, they were concentrated in the Run+LEDs group, as the total running time displays in the Table 11. However, comparing the means±SD and median of total running time among the different experimental group, no significant difference was detected (Figure 26).

Mouse N°	Experimental group	Running time [min]			
		1°bout	2°bout	3°bout	Total
26	Run	33	27	30	90
27	Run	33	32	30	95.37
28	Run	30	32	30	92
29	Run + LEDs	39	28	29	96
30	Run + LEDs	42	39	36	117
31	Run + LEDs	32	26	26	84
32	Run	29	26	24	79
33	Run	32	28	23	83
34	Run	28	23	20	71
35	Run	27	22	22	71
36	Run	20	18	17	55
37	Run	28	25	25	78
39	Run + LEDs	33	23	18	74
40	Run + LEDs	30	23	21	74
41	Run + LEDs	49	33	28	110
42	Run + LEDs	59	41	36	136
43	Run + LEDs	36	25	21	82
48	Run + LEDs	37	29	31	97
49	Run + CW	24	19	18	61

50	Run + CW	37	27	25	89
51	Run + CW	37	27	26	90
52	Run + CW	25	22	18	65
53	Run + CW	28	27	24	79
54	Run + CW	27	28	24	79

Table 11: List of mice that were exercised for the purpose of the current study. The respective experimental group, the running time per bout, and the total running time is reported. The control mice are missing, since they did not perform any exercise.
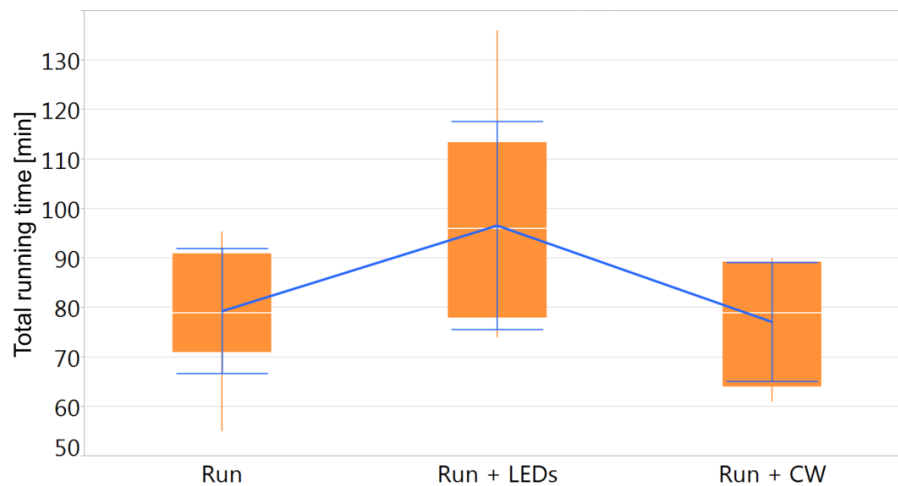
Figure 26: The Box-and-whisker plots in orange represents the distribution of the total running time per each experimental The whiskers extend for values calculated as: 3rd quartile+1.5*(interquartile range) and 1st quartile-1.5*(interquartile range). The overlapping blu line shows the trend of the means±SD of the the total running time per each experimental group. No significant difference was detected.

3.4.3 CK and C-RP changes due to exercise, light therapy and cryotherapy

Blood sampling was scheduled before the beginning of the experiments for baseline values, and at 24h and 48h post-exercise. The absolute values and SD are summarized in Table 12 for the CK, and Table 13 for the C-RP. An increasing trend over time of the mean levels of CK and C-RP was observed in the case of the Run and Run+LEDs mice. However, the CK measures for all the time points had a high SD among the animals of the same experimental cluster. In addition, the CK means at the baseline differed among the experimental sets. Instead, for the C-RP measures, the baseline means are at the same level, except for the Run group. The Run+LEDs animals displayed an increased in the C-RP level in the plasma already at 24h after the exercise. However, as expected from the high variability of the data, none of the changes in the plasma parameters was significant.

	Mean CK[U/L] ±SD		
	Baseline	24h	48h
Control	1833 ±1234	1460 ±1094	1842 ±1364
Run	1377 ±772	3049 ±2680	3333 ±3030
Run + LEDs	1583 ±829	2143 ±1575	2638 ±1810
Run + CW	1777 ±2274	1625 ±1517	1542 ±940

Table 12: Mean values and SD of the CK [U/L] for each experimental group at each time point. All the parameters are characterized by a high standard deviation. Nerveless, there is an increasing trend for the Run and Run+LEDs group.

	Mean C-RP[mg/L] ±SD		
	Baseline	24h	48h
Control	10.6 ±3.9	10.7 ±3.9	10.6 ±3.9
Run	8.7 ±1.5	8.8 ±1.5	9.9 ±1.1
Run + LEDs	10.5 ±2.0	11.2 ±1.9	11.2 ±1.6
Run + CW	10.2 ±1.8	10.4 ±2.8	10.4 ±2.5

Table 13: Mean values and SD of the C-RP [mg/L] for each experimental group at each time point. The baselines are at the same level in all cases, except for the animals of the Run group. It is observed an increasing trend of the C-RP value for the Run and Run+LEDs group, while the C-RP remained unchanged for the Control and Run+CW.

Because of the fluctuation in the baseline values, it was more convenient to display the plasma parameters in terms of fold changes (stated as in section 2.3.4) 24h and 48h from the individual baseline. Anyhow, the normalization of the absolute value did not reduce the SD for the CK (Table 12), and the data were distributed along wide ranges in the case of Run at 24h and Run+CW for 24h and 48h (Figure 27).

The CK fold change of the Run group gradually raised from 24h (p-value≈0.04 compared to the matched-time control) to 48h (p-value≈0.0035 compared to the matched-time control). The median CK of the Run+LEDs reached the same level of Run animals at 48h, and a p-value≈0.054 was found for this time point in comparison to matched time control (Figure 27). The C-RP (Figure 28) increase of 10% at 24h for the Run+LEDs mice and the shift was constant at 48h (with p-value≈0.04 compared to the matched-time control). A significant (p-value≈0.017) arise was measured also from 24h to 48h for the Run mouse. The C-RP fold change for the Run+CW were widely spread around the 1 value. As expected, the fold change of the control mice were tightly distributed around 1, indicating the stability of the measurements.

The fold changes of CK suggested that the exercise succeeded in inducing damage in the muscle. The changes in C-RP suggested that the light therapy induced an earlier increase of this parameter, while the cryotherapy prevented the arise.
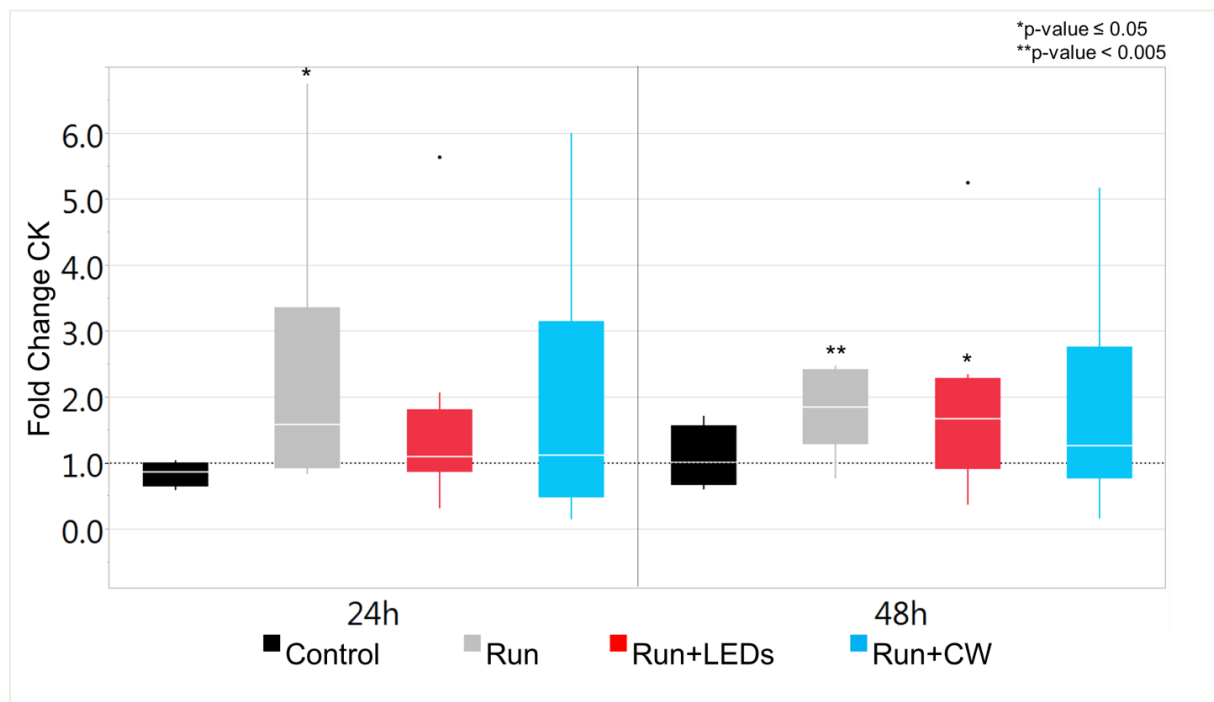
Figure 27: Comparative representation of the CK fold change in plasma among the experimental groups. The baseline as time point is omitted since all the values at the baseline are 1. The dashed line is placed at fold change equal to 1 that means no change compared to the baseline. The CK increased for all the groups and remained unchanged for the Control group. The band inside the box reflects the median. The whiskers extend for values calculated as: 3rd quartile+1.5*(interquartile range) and 1st quartile-1.5*(interquartile range). The dots are the outlier values.

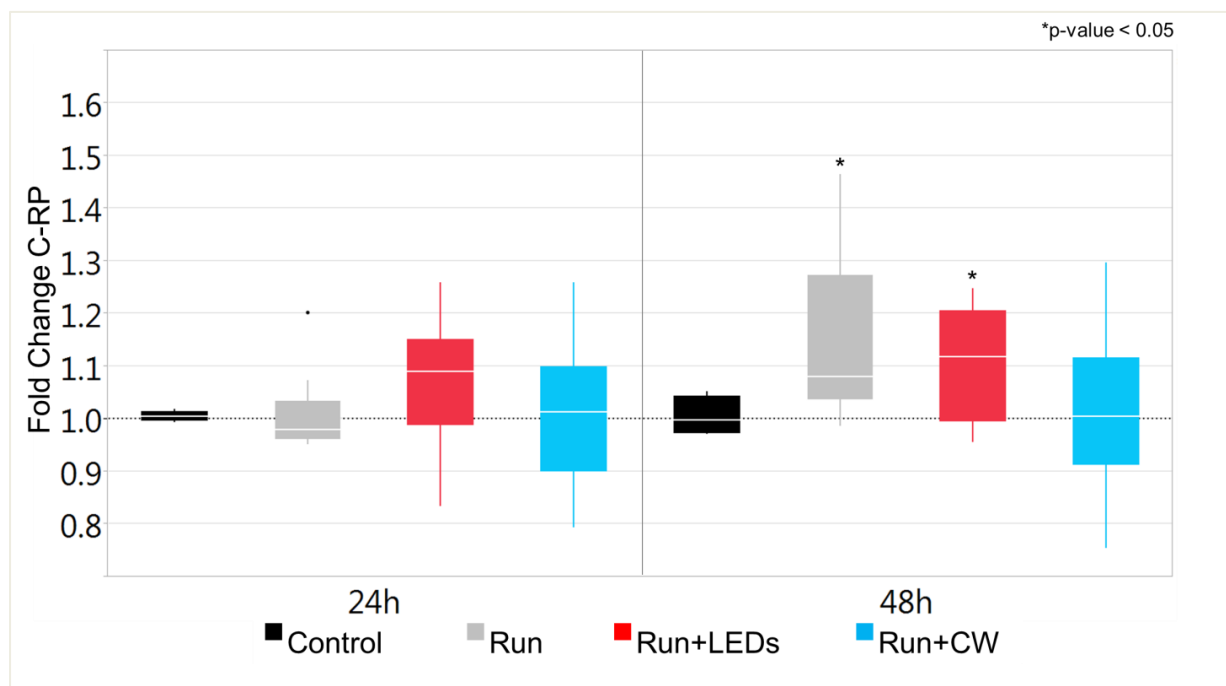*Figure 28: Comparative distribution of the C-RP fold change in plasma among the experimental groups at 24h and 48h. The time point of the baseline is omitted since all the values are exactly 1. The dashed line is placed at fold change equal to 1 that means no change compared to the baseline. The Run+LEDs mice had the plasma C-RP increase already at 24 , and the change*

remained constant ad 48h. Run mice had an increment only at 48h, while for the Run+CW measures remained distributed around a fold change equal to 1. The band inside the box reflects the median. The whiskers extend for values calculated as: 3rd quartile+1.5*(interquartile range) and 1st quartile-1.5*(interquartile range). The dots are the outlier values.

3.5 Histological changes caused by exercise and the post-exercise therapies

As described in section 2.4.2, the total amount of fibers and the total area of tissue sections were obtained in a semi-automated manner. The results in terms of means±SD for the quadriceps muscles are summarized in Table 14. The fibers density was close to the Control for the Run group, while, the Run+LEDs and Run+CW, had means values 26% (p-value≈0.04) and 37% (p-value≈0.03) lower than the Control respectively. The difference in Total fibers/mm^2 between the Run and the Run+CW was also found significant (p-value≈0.03).

	Total fibers	Total area [mm^2]	Total fibers/mm^2
Control	7694.3±913	18.7±1.5	411±31
Run	7253.7±2347.9	18.1±3.6	394.6±85.7
Run + LEDs	6562.5±1507.8	20.4±5	325.9±52.2
Run + CW	7167±1703.8	23.7±3.3	300.6±45.7

Table 14: Means±SD of total fibers, total area and total fibers//mm2 for Control, Run, Run+LEDs and Run+CW quadriceps. The difference in Total fibers/mm2 are significant for Run+LEDs and Run+CW compared to the Control, with a p-value of 0.04 and 0.03 respectively. The fibers density of Run+CW differed also significantly (p-value≈0.03) from the Run.

The signs of damage, like cell infiltration, necrotic, swollen and hyaline fibers (paragraph 2.4.2) were detected on the quadriceps sections of all the experimental groups, and, involved mainly the vastus lateralis and medialis muscles. However, these features were distributed in a different manner and intensity according to the experimental set.

In particular, foci of degradation and necrotic fibers covered a wider area and higher number of mice in the Run+LEDs group than the others. Only 4 Run animals and 4 Run+CW mice had these features, compared to the 7 mice belonging to the Run+LEDs group. In Figure 29 a qualitative comparison of a same extension of tissue area in H&E made clear that the focal degradation occurred more frequently in the red/infrared treated animals (Figure 29B)).

A mean value of 1.7% of the total area was occupied by infiltrated cells in the Run+LEDs mice. This percentage goes down to 0.6% for the running mice and to 0.1% for the cryotherapy treatment. The distribution of the infiltrated area percentages (Figure 30) demonstrated a high variance for the Run+LEDs group, and a no significant difference with the other groups.
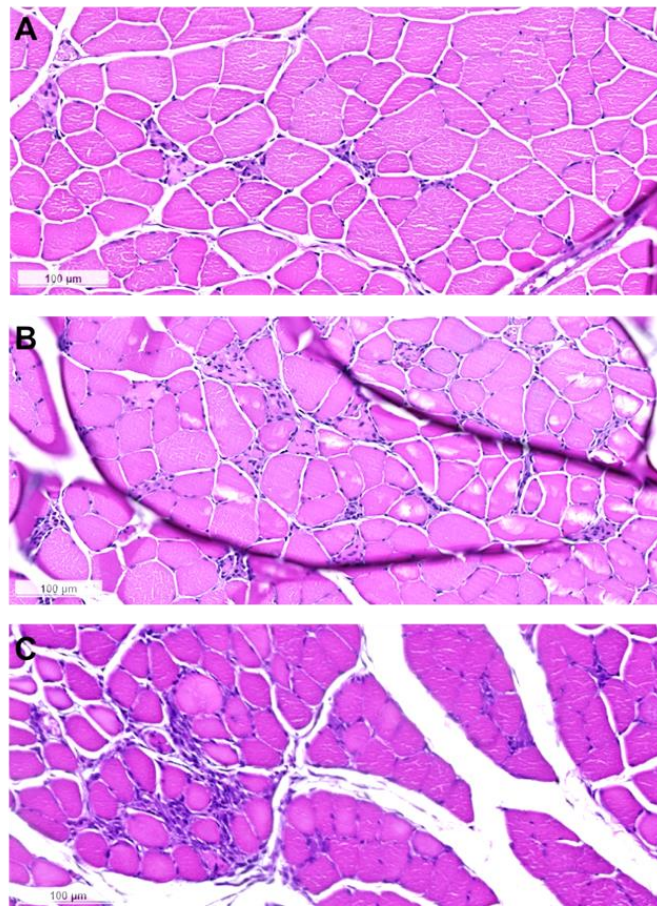
Figure 29: Details of quadriceps section in H&E staining of three mice belonging to the Run group (A), Run+LEDs (B), Run+Cw (C). The same area of vastus medialis showed more necrotic fibers and degradation foci in the mouse receiving the LEDs therapy post-exercise, than the other groups.
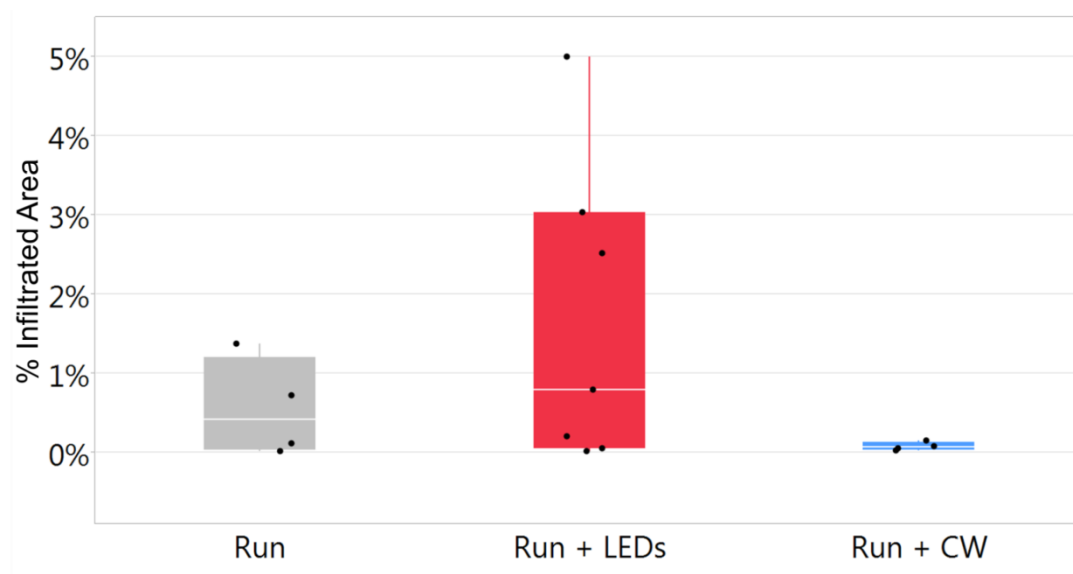
Figure 30: Comparative distribution of the infiltrated areas expressed as percentage on the total area of the quadriceps section. The dots are the percentage for the individual animal that presented foci of infiltrated cells: 4 mice for the Run, 7 mice for the Run+LEDs and 4 mice for the Run+CW. The Control group is not reported since the percentage is equal to 0. The band inside the box reflects the median. The whiskers extend for values calculated as: 3rd quartile+1.5*(interquartile range) and 1st quartile-1.5*(interquartile range). The dots are the outlier values.

As reported in section 2.4.2, the IHF with a secondary antibody against mouse IgG (AlexaFluor®647 conjugated) was performed in order to detect the fibers with a severe damage to the cell membrane. Indeed, immunoglobulin size (≈150000 Da) does not allow the penetration through the sarcolemma, unless the membrane continuity is compromised. In line with the number of animals per group affected by foci of infiltration, the same was found in the case of fibers infiltrated by IgG. Interestingly, it was possible to distinguish fibers with a co-localization of the IgG and the infiltrated cells (Figure 31) and fibers with only IgG deposition.

Loss of the angulated shape was observed in fibers IgG-negative nearby the necrotic and infiltrated areas (Figure 32(A)), and, a comparison with the corresponding section in H&E staining (Figure 32(B)), confirmed an altered cell structure with smooth cytoplasm and boundaries.
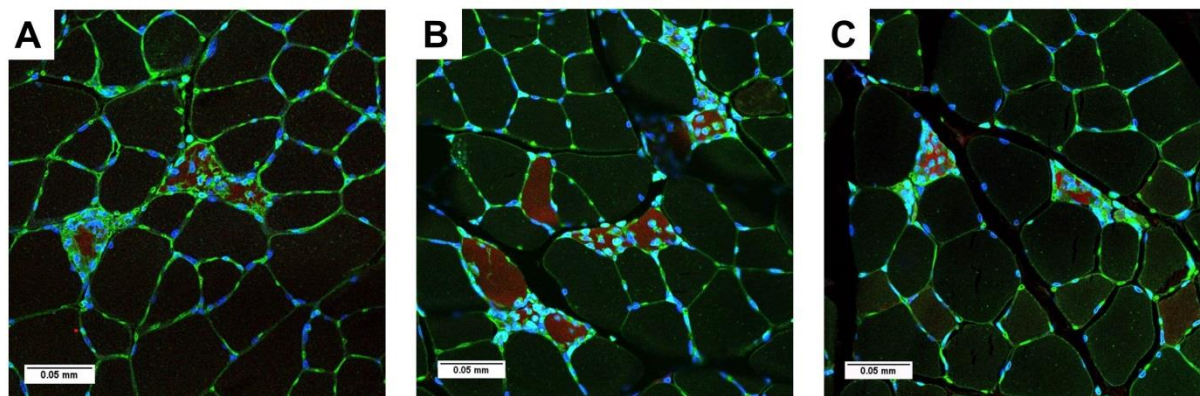
Figure 31: Details of three quadriceps section in IHF staining of mice belonging to Run (A), Run+LEDs (B), Run+CW (C). The cell membranes are labeled in green with the WGA 488-coniugated- The nuclei are stained with the Sytox Orange and displayed in blue. A secondary anti-mouse Alexafluor®647 conjugated is used to stain the immunoglobulins infiltrated into muscle fibers that lost membrane integrity. The IgG signal is co-localized with the infiltrated cells (A) and (B) or is detected alone (B).
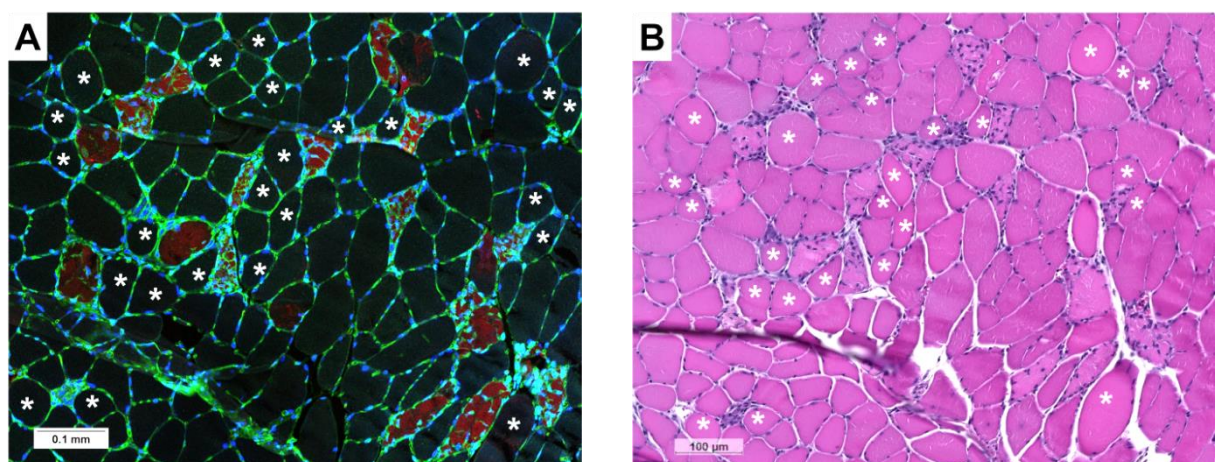
Figure 32: Example of fibers with a round shape nearby the necrotic and infiltrated areas. An area of quadriceps belonging to a Run+LEDs mouse is shown in IHF (A) and H&E (B). White asterisks indicates the fibers that lost the angulated shape and had a smooth cytoplasm without presenting sign of immunoglobulins infiltration (red signal in (A)).

In all the cases, except for the Control group (Figure 33 (A)(B)(E)(F)), swollen fibers and/or hyaline fibers were detected on peripheral areas of the vastii (Figure 33(C)), and at the interface between the vastus and the rectus femoris (Figure 33(D)). The IHF staining of the corresponding sections did not reveal the infiltration of IgG for those fibers (Figure 33(H)(I)).
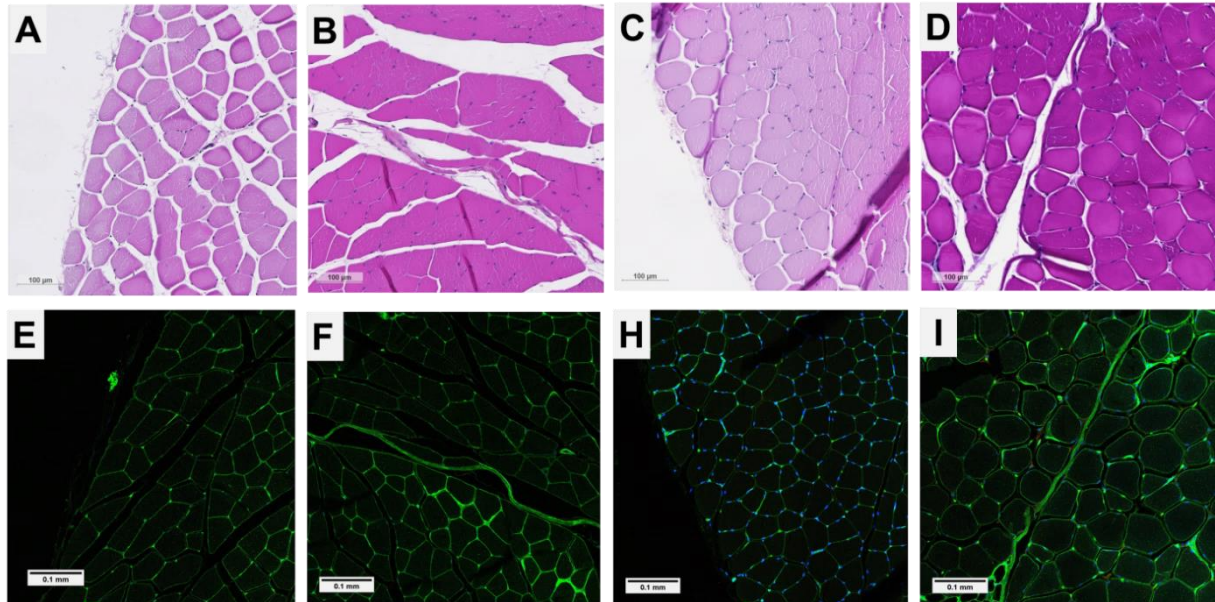
Figure 33: Details of a control mouse section in H&E and IHF at the periphery (A) in H&E and (B) in IHF, and at the interface between the vastus and the rectus femoris (B) (F). Example of swollen and hyaline fibers at the periphery (C) and at the interface between the vastus and the rectus femoris (D). No IgG deposition was detected for the corresponding IHF section (H) (I).

As stated in 2.4.2, the images were post-processed in order to obtain indexes for the quantification of the tissue alteration due to the experimental protocol.

The quantification of the fibers with altered features are reported in terms of means±SD in Table 15 with the distinction between the fibers with IgG deposition, so called red fibers and the muscle cells with no angulated shape (hyaline and swollen) and with negative IgG signal, so called round fibers.

The total amount of altered fibers was obtained by the sum of the red fibers and the round fibers for each experimental group. The total amount of altered fibers was divided on the on the corresponding total fibers number and multiplied per 100 (Figure 34). The 3.4% of the total number of fibers showed alteration in the cell structure for the Run+LEDs. This percentage differed significantly from the 1.3% (p-value≈0.02) of the Run+CW mice. A 2.2% of fibers were affected by the exercise in the Run animals, and this number differed significantly from the mice that receive cryotherapy (p-value≈0.04) and light therapy (p-value≈0.05) post-exercise.

	Mean red fibers ±SD	Mean round fibers ±SD	Mean total altered fibers ±SD
Run	17.4±21.2 (7)	131.5±36.8 (9)	150.8±55.7 (9)
Run + LEDs	106.1±100.5 (4)	132.3±56.9 (9)	243.3±118.4 (9)
Run+ CW	12.5±11.7 (4)	82.8±52.3 (6)	95.3±46.7 (6)

Table 15: Means±SD of total red fibers, total round fibers and the sum of them both (Total altered fibers) for Run, Run+LEDs and Run+CW quadriceps. The red fibres consisted in the numbers of muscular cells with IgG infiltration. The round fibers were meant to be the total amount hyline and swollen fibers.
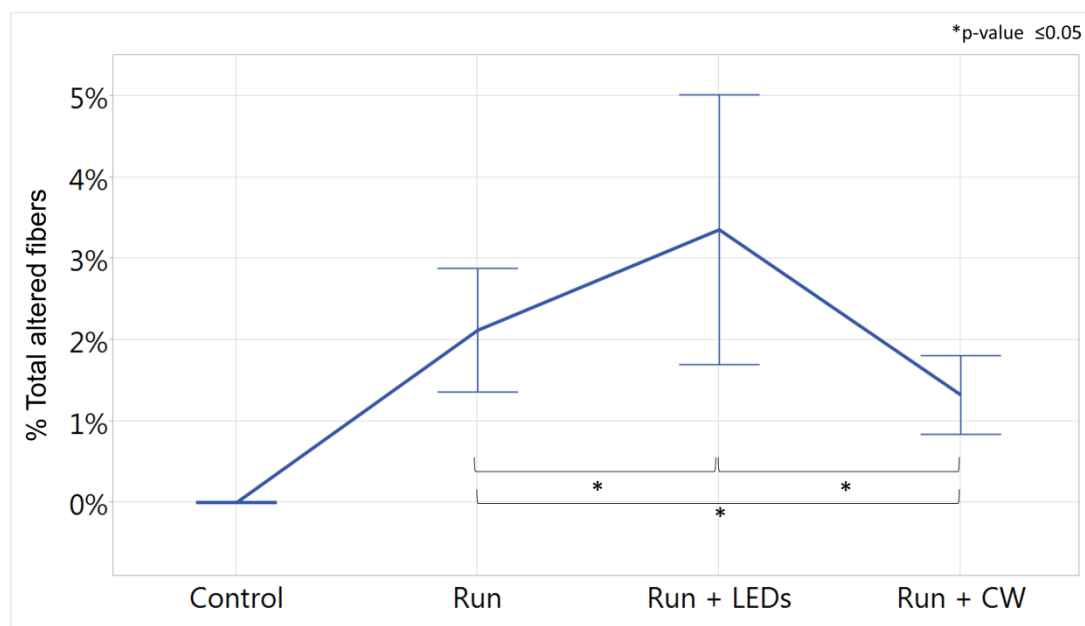
Figure 34: The mean value and the SD of the total altered fibers in percentage is shown for each experimental group. The highest percentage was detected for the Run+LEDs group, with a significant difference in comparison with the 1.3% of the Run+CW (p-value≈0.02) mice and the 2.2% of the Run animals ((p-value≈0.05).

3.6 Independency of muscular damage from the total running time

To demonstrate that the level of damage is independent from the running performance, the total running time (see 3.4.2) was plotted against the markers of damage for each mouse, that are the CK fold change (Figure 35) and the percentage of the altered fibers in the quadriceps (Figure 36).

Referring to Figure 35, at 24h there is a weak linear correlation (R^2=0.52) between the CK fold change and the running time for the animals of the Run group; however, this correlation worsens at 48h (R^2=0.14). For Run+LEDs and Run+CW the linear regression does not describe the correlation at any time point.
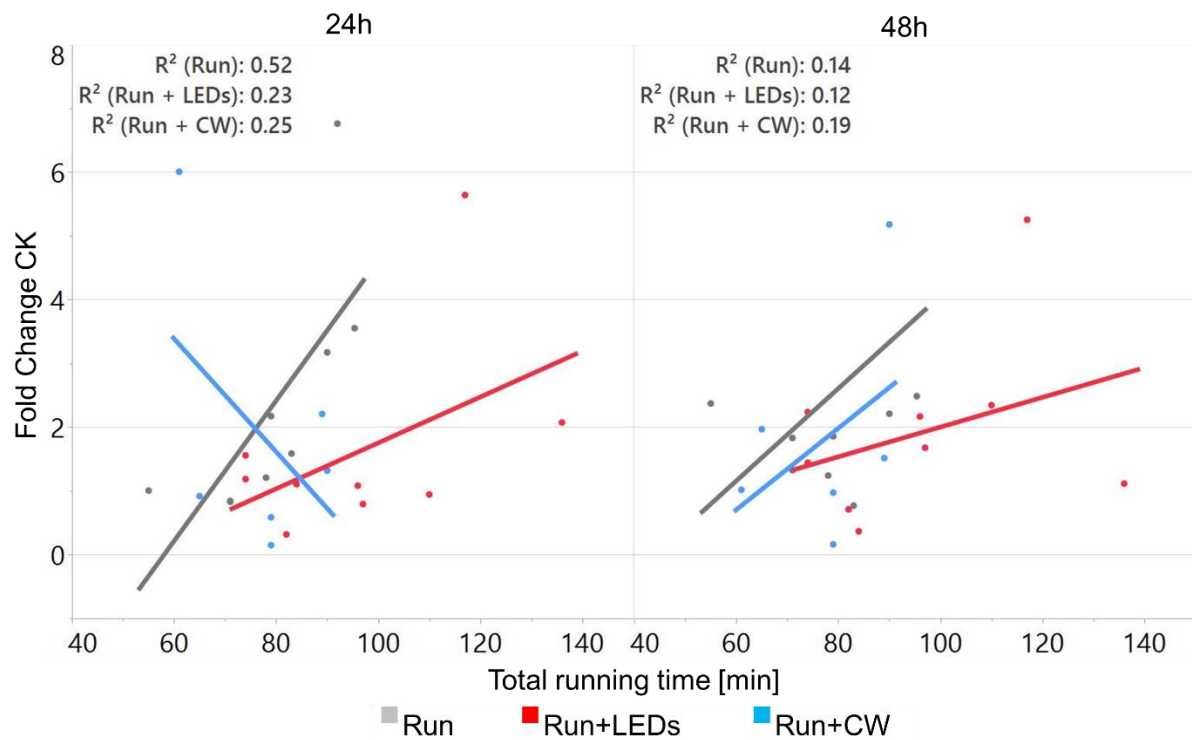
Figure 35: Fold change CK plotted against the total running time at different time point after the running. A dot corresponds to a singular mouse. The lines are the linear regressions created for each points set ant the R² are the coefficient of determination that describe the goodness of the fit. The highest R squared was found for the liner regression of the Run group at 24h. However, the R² fall close to 0 for the 48h time point for all the cases.

The Figure 36 illustrates an upward trend in the percentage of altered fibers with longer running times. In particular, the mouse represented by the highest red point on the right hand side of the graph, was able to run for the longest time and had the highest percentage of altered fibers in the quadriceps at 48h after the exercise. However, considering the other cases, the two variables are not well depicted by a linear correlation, since the R squares are closer to 0 than to 1 for all the experimental groups.
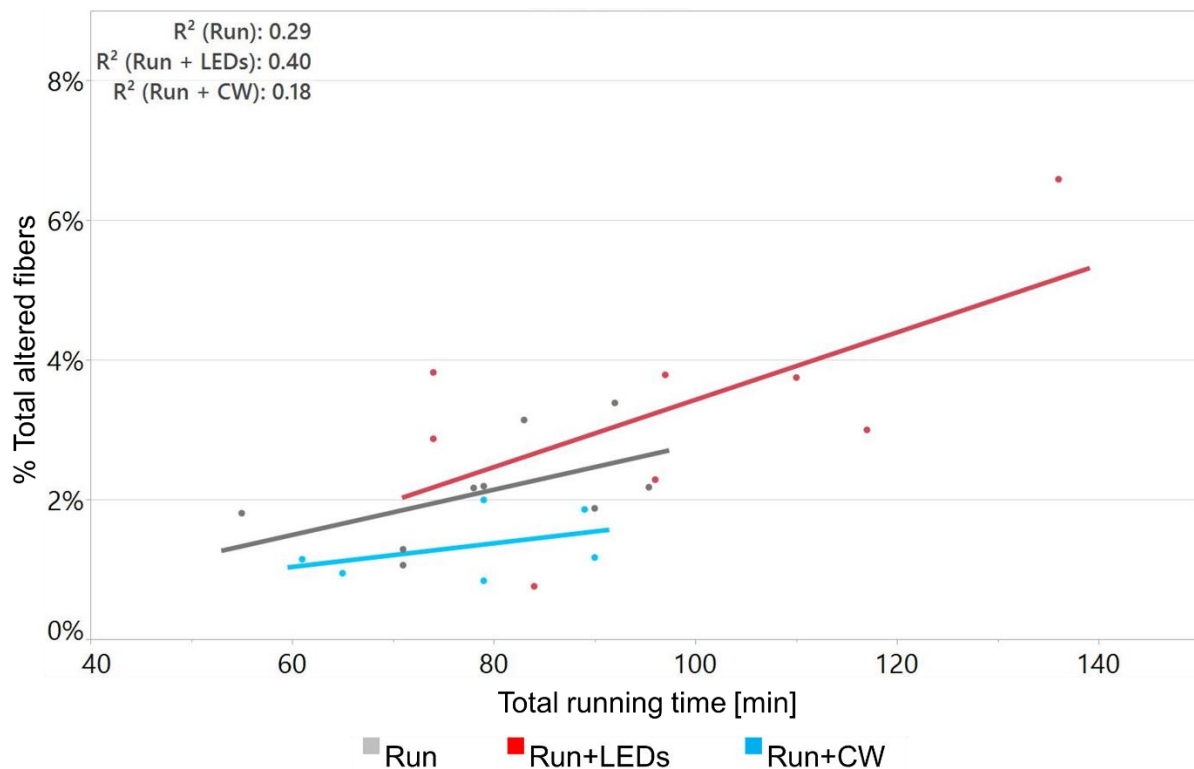
Figure 36: Percentage of total altered fibers plotted against the total running time. A dot corresponds to a singular mouse. The lines are the linear regressions created for each points set ant the R^2 are the coefficient of determination that describe the goodness of the fit. The R squared is closer to 0 than to 1 for all the experimental groups, showing that the linear model does not well describe the correlation between the two variables.

3.7 Gene expression profile changes in response to exercise and the post-exercise therapies

As described in 2.5.2, the RNA extracted from quadriceps biopsies were tested for purity and quality. The samples considered for the gene expression microarray had a 260/280 between 2 and 2.13 and $8.5 \leq RIN \leq 9.3$.

The raw data from the gene chips were analyzed in terms of differential expression compared to a reference. The Control group was considered as reference for all the other experimental groups: Run, Run+LEDs and Run+CW.

3.7.1 Expression of genes related to damage, repair, regeneration and immunity

The analysis at the gene level revealed 2107 genes differentially expressed for the Run group, 2057 for the Run+LEDs and 2302 for the Run+CW, further distinguished in downregulated and upregulated in Table 16.

	Run vs Control	Run+LEDs vs Control	Run+CW vs Control
Significant differentially regulated genes (p-value ≤5%)	2107	2507	2302
Significant upregulated expressed genes (p-value ≤5%)	963	1216	1084
Significant downregulated expressed genes (p-value ≤5%)	1144	1291	1218

Table 16: Number of genes significantly (p-value ≤5%) regulated in each experimental group in comparison to the Control group. The total amount of regulated genes is further distinguished in upregulated and downregulated.

Considering only the upregulated genes, the Venn diagram in Figure 37 shows the significantly regulated genes within the individual experimental group and in common with the other groups. Using the tool of DAVID Bioinformatics Resources 6.7 as described in 2.5.3, the genes were clustered in domains according to the GO annotation, and, those domains were further grouped under customized names that express the location of the genes or the main function. Genes related to membrane and cytoskeleton structures were upregulated in all the groups. Genes that regulate the myogenesis were found upregulated for all the groups and intersections, with the exception of the genes exclusively regulated for the Run group. Up to 50 genes involved in the immune reaction were exclusively upregulated in the quadriceps of the animals that received the infrared/red light, while a number of 5 genes was found significantly in common to the Run and the Run+LEDs. No genes related to the immune system were found upregulated for the cryotherapy group and its intersections with the other groups.

UPREGULATED GENES

Membrane/cytoskeleton: 190
Myogenesis: 4
Immunity: 5

Membrane/cytoskeleton: 148
Myogenesis: 0
Immunity: 0

Membrane/cytoskeleton: 25
Myogenesis: 3
Immunity: 0

Membrane/cytoskeleton: 190
Myogenesis: 4
Immunity: 0

Membrane/cytoskeleton: 255
Myogenesis: 6
Immunity: 50

Membrane/cytoskeleton: 140
Myogenesis: 7
Immunity: 0

Membrane/cytoskeleton: 104
Myogenesis: 4
Immunity: 0

Run vs Control — Run+LEDS vs Control — Run+CW vs Control

393 — 497 — 543 — 604 — 142 — 545 — 540

Figure 37: Venn diagram of the significant regulated genes (p-adjusted≤10%) that were regulated within the individual experimental group and in common with the other groups. The Run+LEDs and Run+CW shares the highest amount (= 27) of regulated pathways in comparison to the control group. 16 pathways are in common to the three groups, 7 pathways in common only to Run and the light group, while the Run and the cryotherapy group do not have any specific pathway in common.

From the membrane/cytoskeleton group, genes coding the proteins of skeletal muscle costameres were selected. As depicted in Figure 38, the structure constituted by integrin, talin, vinculin and desmin, had a similar upregulation trend in all groups, with significance and higher fold change found mostly for the Run+LEDs. Only the expression of the laminin γ1 was affected, while the fold change of the other laminin subunits were at the level of the control. Genes coding for proteins involved in the cell membrane repair were also found significantly upregulated in all groups. In particular, the Figure 39 displays the expression in terms of fold change of myoferlin, caveolin3, dysferlin, annexins, tsugumin-53 and desmoyokin. The dysferlin genes turned out to be the most affected, with a significant regulation exceeding the 2-folds in all the case (except for the Control). The annexin 6 and 11 were overexpressed in all groups, instead, for the Run+CW the annexins 1, 2, 4 and 5 were at the level or under the Control. In all the cases, the cryotherapy group revealed a lower expression of these genes, when compared with the Run and Run+LEDs groups.
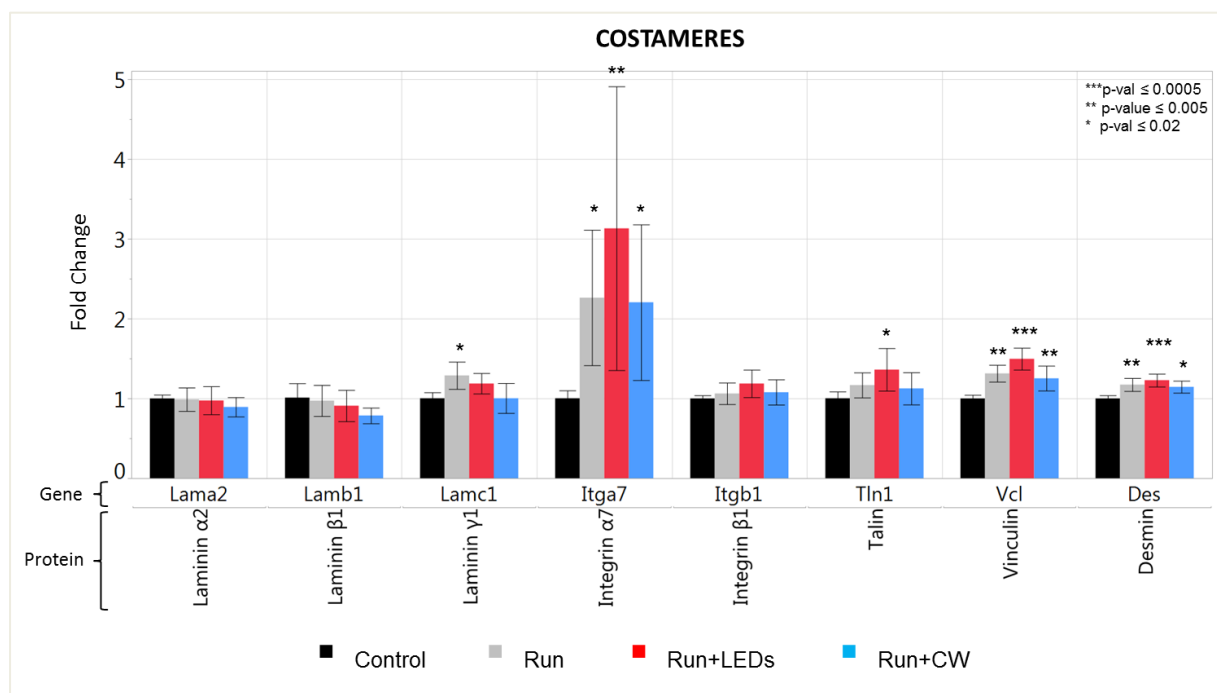
*Figure 38: Bar chart displaying upregulation of genes constituting one of the sarcolemma costameres for all the experimental group. The upregulation is expressed in fold change±SD to the mean expression of the Control group (reference group). The corresponding coding protein is reported on a second axis under the gene name. The * displays the level of significance in comparison to the Control. The fold change = 1 means no change in the expression compared to the reference group.*
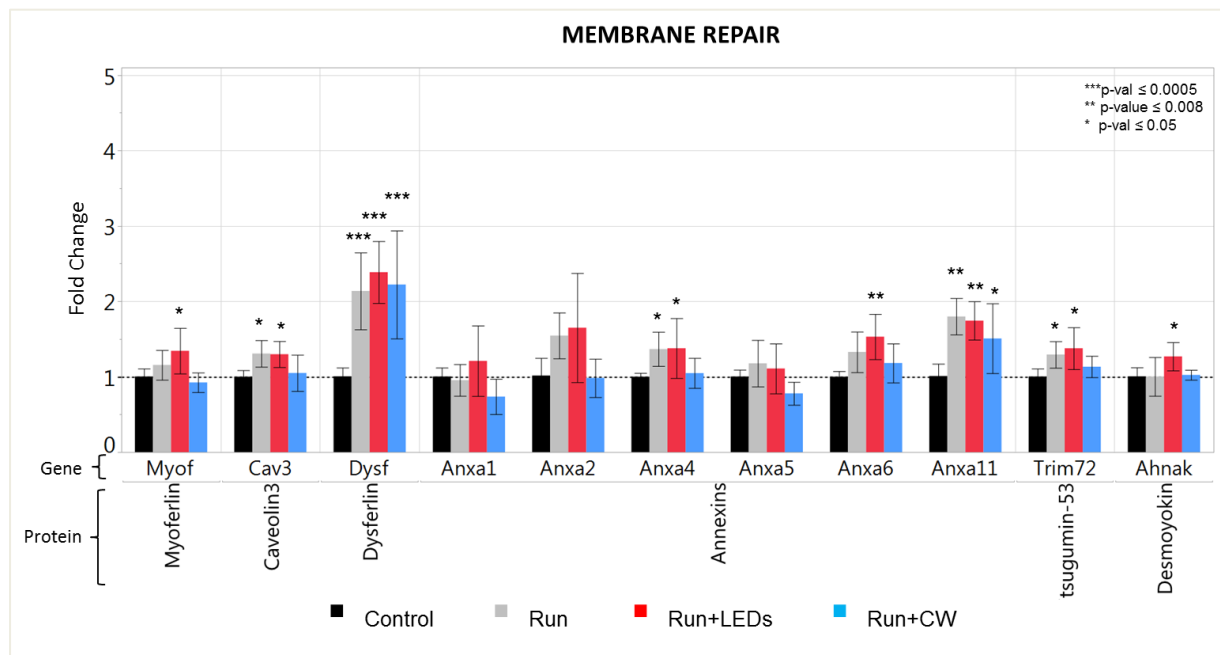
*Figure 39: Bar chart displaying upregulation of genes involved in the cell membrane repair process for all the experimental group. The upregulation is expressed in fold change±SD to the mean expression of the Control group (reference group). The corresponding coding protein is reported on a second axis under the gene name. The * displays the level of significance in comparison to the Control. The fold change = 1 means no change in the expression compared to the reference group.*

The Figure 40 reports the expression of the myogenic regulatory factors (MRFs) genes in terms of fold change to the Control. The expression of Pax3, Pax7, Myf5 did not differ from the control mice. The fold change of the MyoD1 increased to 2 for the light group, to 1.6 for the cold water mice and 1.3 in the case of the running mice without therapy. The gene for myogenin was significantly overexpressed in all groups, with a 2.5 fold change for the Run and Run+LEDs, and 1.7 for the Run+CW. Instead, for the gene coding the herculin protein, the upregulation was found significant only for the Run+LEDs.
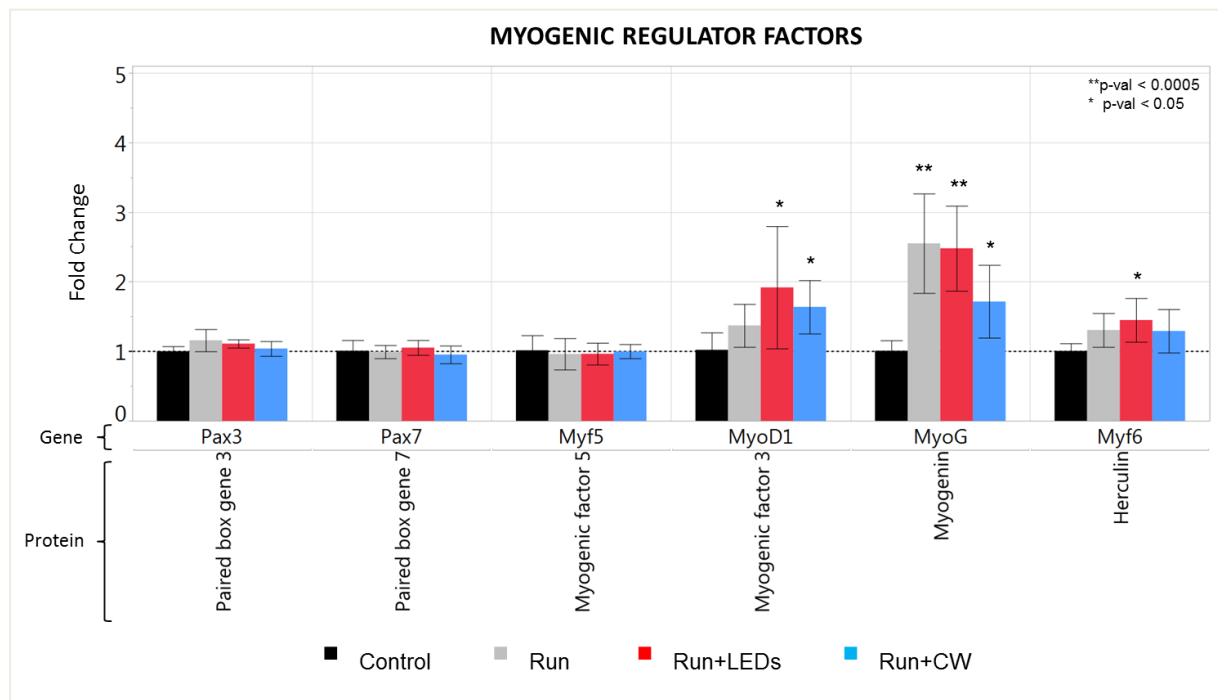
Figure 40: Bar chart displaying the upregulation of genes for all the experimental group. The upregulation is expressed in fold change±SD to the mean expression of the Control group (reference group). The corresponding coding protein is reported on a second axis under the gene name. The * displays the level of significance in comparison to the Control. The fold change = 1 means no change in the expression compared to the reference group.

Among the significant genes involved in the immunity (Figure 37), 10 genes coding markers of immune cells were selected and their expression displayed in the bar chart in Figure 41. The CD68 was over expressed ca. 10-folds for the Run, ca. 6-fold for the Run+LEDs, and only 2-folds for the Run+CW. For F4/80 gene, another macrophage antigen, the expression was much less prominent, and was significant only for the Run+LEDs with a 1.5 fold change. Three genes for monocyte chemokines (ccl2, ccl6 and ccl7) were significantly expressed for the Run+LEDs up to 2.5 fold change. The most pronounced and significant regulation of the other immune markers gene occurred for the infrared/red light group. The lowest regulation of these genes was detected in the case of the cryotherapy post-exercise, was often at the level of the control (i.e. ccl2, Icam1).

These results were in line with the histological evidence of damage to the muscle tissue, involving the costameres structure, but not the basal lamina, and the sarcolemma, with the consequent activation of the immune system and the MRFs for the regeneration of the fibers.
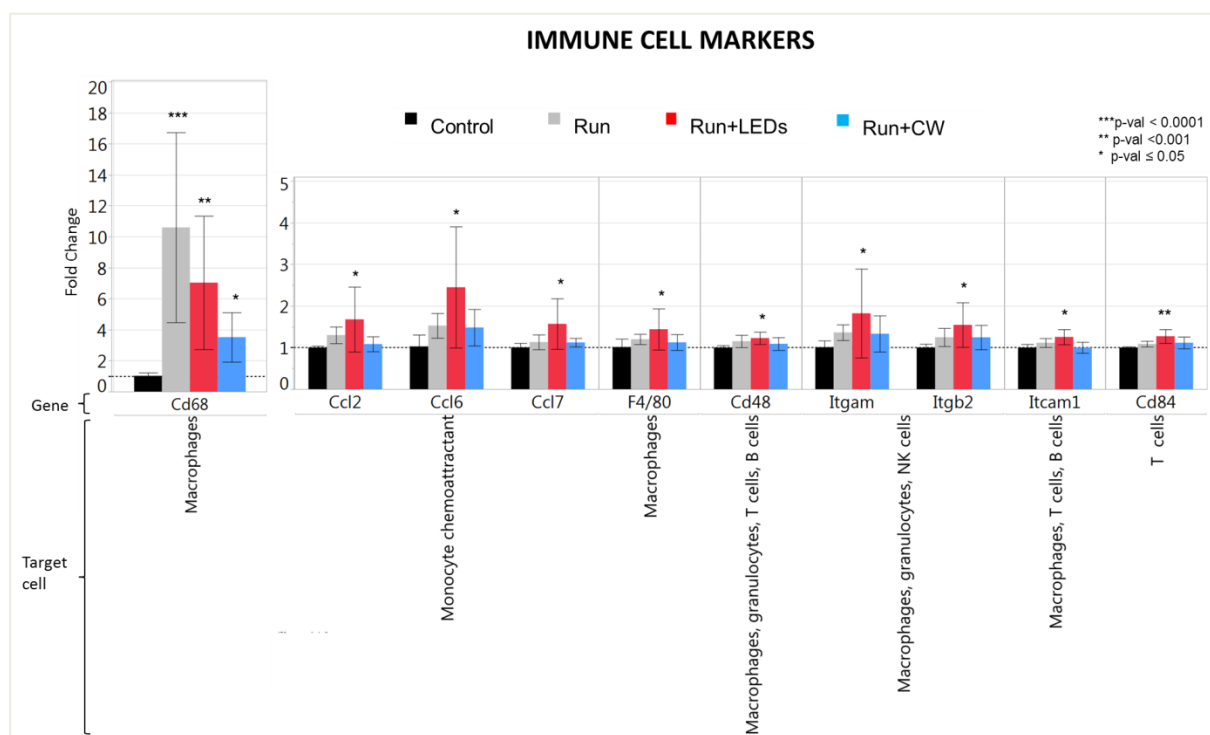
Figure 41: Bar chart displaying the upregulation of genes considered markers for immune cell. The upregulation is reported as fold change±SD on the mean expression of the Control group (reference group). The immune cell type that is correlated to the protein coded by the gene is reported on a second axis under the gene name. The * displays the level of significance in comparison to the Control. The fold change = 1 means no change in the expression compared to the reference group.

3.7.2 Pathways upregulated and downregulated in Run, Run+LEDs, Run+CW in comparison to the Control group

Combining the expression patterns, genes were clustered in pathways according to the KEGG database, as described in 2.5.3.

Table 17 summarizes the amount of KEGG pathways significantly upregulated and downregulated for each experimental group, in comparison to the Control. The number of pathways slightly decreased when more restricted criteria of significance is applied (expressed by the p-adjusted).

	Run Vs Control	Run+LEDs vs Control	Run+CW Vs Control
Significant upregulated pathways (p-adjusted ≤10%)	12	27	10
Significant upregulated pathways (p-value ≤5%)	18	31	12
Significant downregulated pathways (p-adjusted ≤10%)	14	41	50
Significant downregulated pathways (p-value ≤5%)	39	45	56

Table 17: Number of KEGG pathways significantly regulated in each experimental group in comparison to the Control group. The total amount of regulated pathways is further distinguished in upregulated and downregulated. The level of significance is expressed by a p-value ≤5% and a p-adjusted≤10%.

Figure 42 (A) shows a global overview of the distribution of the regulated pathways within the KEGG categories. The majority of the regulated pathways was involved in metabolic processes and were downregulated in all groups. The organismal system was the second category as abundant of the significantly regulated pathways. The Venn diagram in Figure 42 (B) shows that the Run+LEDs and Run+CW shares the highest amount (= 27) of regulated pathways in comparison to the control group. 16 pathways are in common to the three groups, 7 pathways in common only to Run and the light group, while the Run and the cryotherapy group do not have any specific pathways in common.
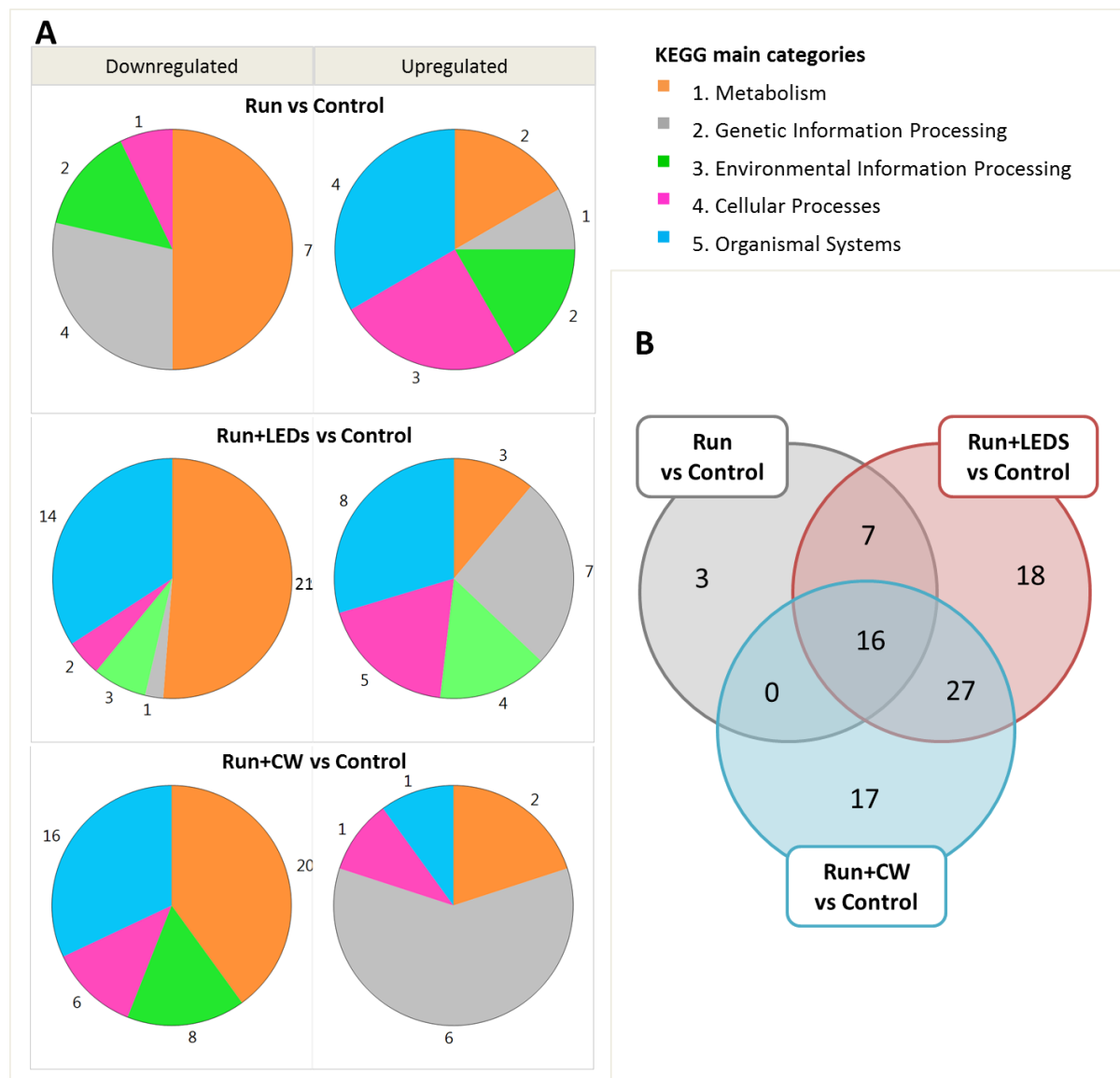
Figure 42: (A) Pie diagrams representing the distribution of significant pathways (p-adjusted≤10%) upregulated and downregulated within the KEGG main categories. The numbers around the pie indicates the amount of pathways for that specific category. The metabolic pathways are strongly downregulated, above all in the Run+LEDs and Run+CW. (B) Venn diagram of the significant pathways (p-adjusted≤10%) that were regulated within the individual experimental group and in common with the other groups. The Run+LEDs and Run+CW shares the highest amount (= 27) of regulated pathways in comparison to the control group. 16 pathways are in common to the three groups, 7 pathways in common only to Run and the light group, while the Run and the cryotherapy group do not have any specific pathway in common.

The Figure 43 reported the 16 pathways in common to the three groups. All the metabolic (category 1.) pathways, like carbohydrate, energy and lipid metabolism, were downregulated in the three experimental groups, except for the N-glycan biosynthesis, that was upregulated, as well as with the lysosome and proteasome pathway. Instead, the PI3K-Akt signaling pathway, ECM-receptor interaction and the focal adhesion were similarly upregulated in Run and Run+LEDs, while they got negatively regulated in the cryotherapy animals.

Figure 43: The 16 KEGG significant regulated pathways (adjusted p-value≤0.1) in common among the Run, Run+LEDs and Run+CW, in comparison to the Control group. The dashed lines are the pathways downregulated in a similar manner. The dashed double lines indicated the similar upregulated pathways. The solid lines are the pathways upregulated for Run and Run+LEDs, and downregulated for Run-CW. NES > 0 are assigned to upregulated pathways, while NES <0 indicates a downregulation of the pathway.

Considering the 7 pathways in common to Run and Run+LEDs (Figure 44), the glycosaminoglycan degradation and pathways related to immune activity, like Fc gamma R-mediated phagocytosis, Intestinal immune network for IgA production and phagosome were upregulated with a similar NES. The osteoclast differentiation was the only pathway downregulated.
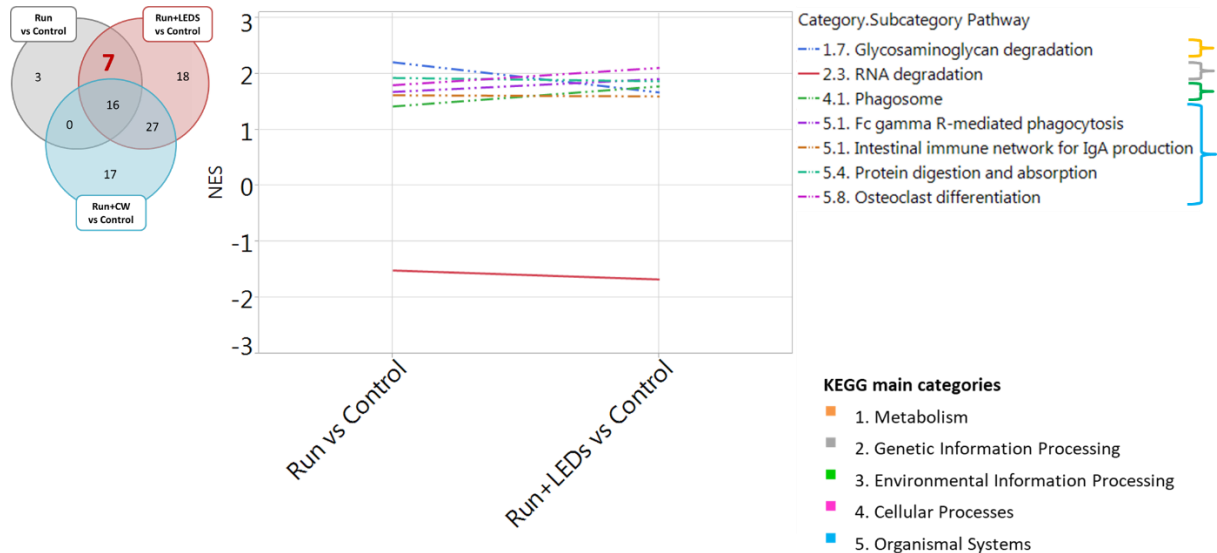
Figure 44: The 7 KEGG significant regulated pathways (adjusted p-value≤0.1) in common between the Run and Run+LEDs and Run+CW, in comparison to the Control group. The dashed double dot lines are the pathways upregulated in a similar manner. The solid line is the only pathway downregulated in common. NES > 0 are assigned to upregulated pathways, while NES <0 indicates a downregulation of the pathway.

The 27 pathways in common to the light and the cryotherapy group had the same regulation pattern (Figure 45). The metabolism of energetic substrates, like pyruvate and butanoate, fatty acids and amino acids, like lysine and tryptophan, were downregulated. Likewise, pathways related to excretory, nervous and sensory system underwent a negative regulation. The only pathways with positive NES were those related to translation of genetic material and protein processing.
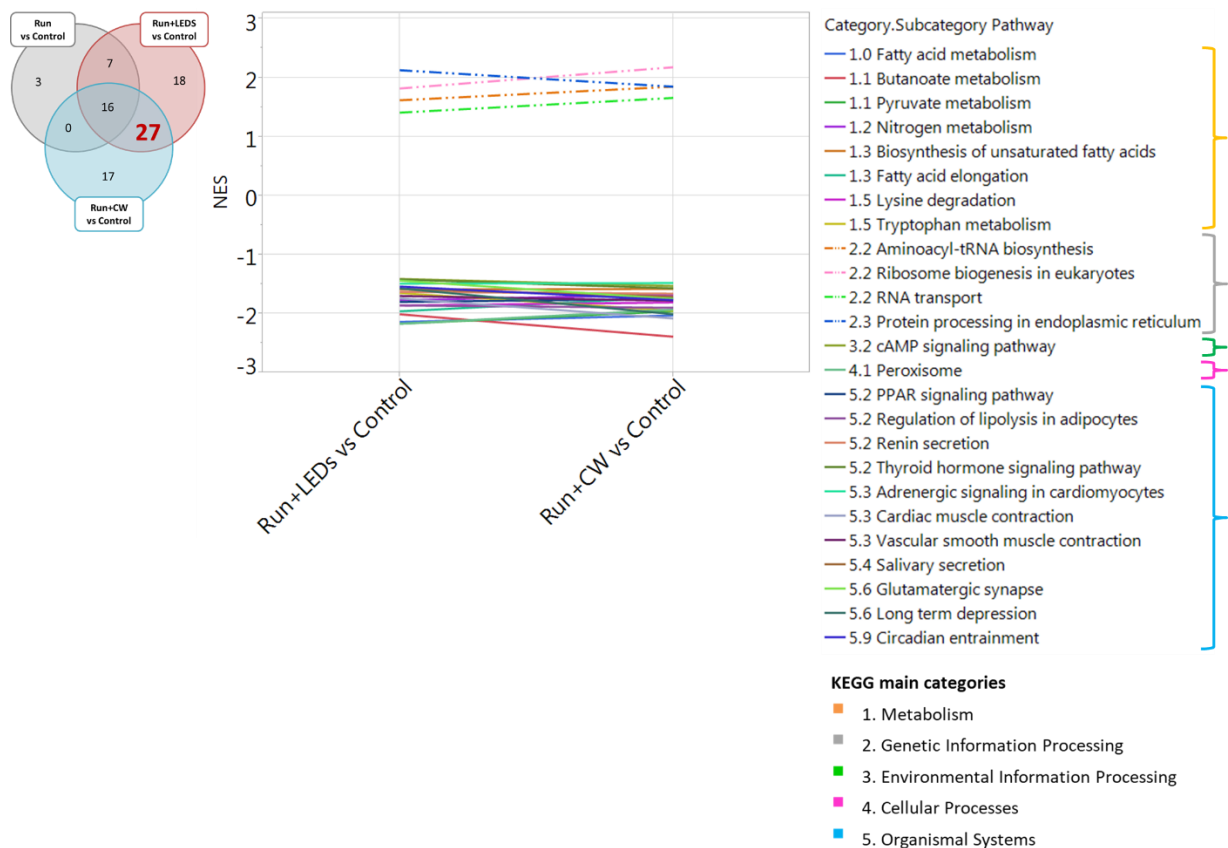
Figure 45: The 27 KEGG significant regulated pathways (adjusted p-value≤0.1) in common between Run+LEDs and Run+CW, in comparison to the Control group. The sol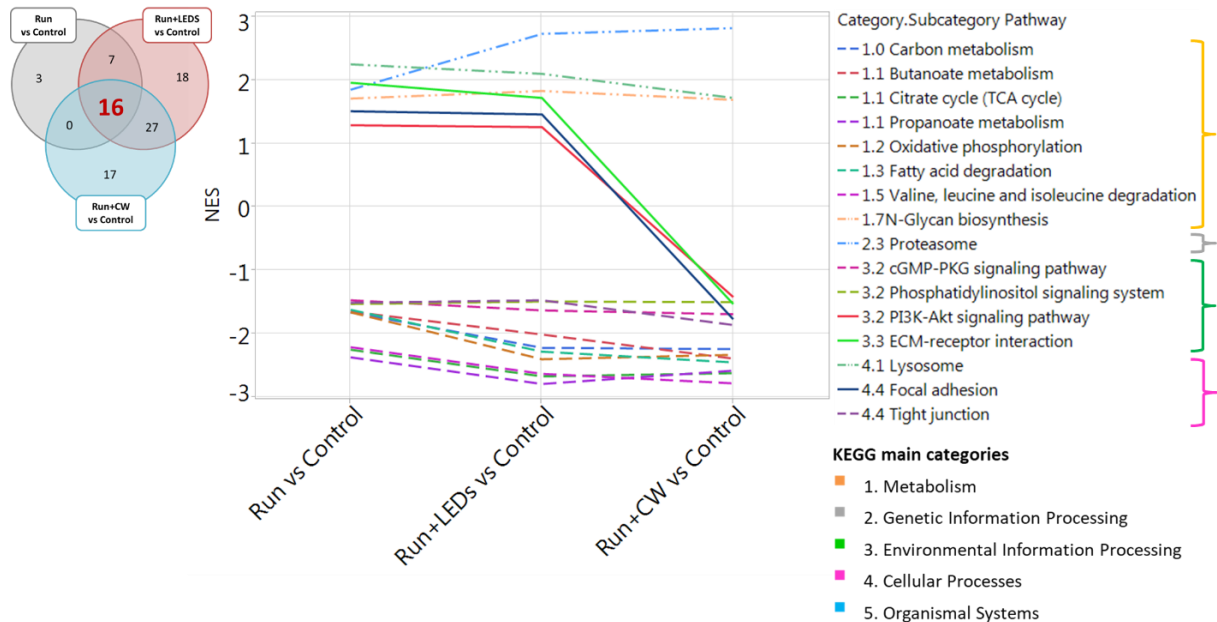id lines are the pathways downregulated in a similar manner. The dashed double dot lines indicated the similar upregulated pathways. NES > 0 are assigned to upregulated pathways, while NES <0 indicates a downregulation of the pathway.

The three pathways significantly expressed only for the Run group (Table 18), are related to a downregulation of genetic information processing, in particular the ubiquitin mediated proteolysis with a NES of -1.82 in comparison to the Control.

Differential gene expression: Run vs Control					
Pathway	Category	Sub-category	NES	Nominal p-value	Adjusted p-value
Spliceosome	5. Organismal Systems	5.1 Immune system	-1.51	0.055	0.062
mRNA surveillance pathway	5. Organismal Systems	5.1 Immune system	-1.5	0.158	0.102
Ubiquitin mediated proteolysis	3. Environmental Information Processing	3.2 Signal transduction	-1.82	0.162	0.006

Table 18: The 3 KEGG pathways were significantly regulated only in the quadriceps of the mice that performed the running without any post-exercise therapy. Every pathway is classified in category and sub-category according to the KEGG database, and is reported with the NES, nominal p-value and adjusted p-value. Positive value of the NES indicates an upregulation of the pathway, while a negative value indicates a downregulation.

A selection of the pathways exclusively expressed in a significant manner for the mice that receive the light therapy, are listed in Table 19. Only for this experimental group, signaling pathways in the sub-category of the immune system (B cell receptor, T cell receptor and Toll-like receptor) turned out to be significantly upregulated. Coherently, other pathways involved into the immune response, like NF-kappa B and TNF signaling were positively regulated.

In Table 20 are selected pathways from the 17 individually regulated in the quadriceps of the cryotherapy mice. The Rap1 and Ras signaling pathways were downregualted, and the actin cytoskeleton as well. The only two pathways related to the immune system were also significantly downregulated.

Differential gene expression: Run+LEDs vs Control

Pathway	Category	Sub-category	NES	Nominal p-value	Adjusted p-value
DNA replication	2. Genetic Information Processing	2.4 Replication and repair	1.63	0.011	0.048
NF-kappa B signaling pathway	3. Environmental Information Processing	3.2 Signal transduction	1.59	0.004	0.025
TNF signaling pathway	3. Environmental Information Processing	3.2 Signal transduction	1.39	0.027	0.094
Endocytosis	4. Cellular Processes	4.1 Transport and catabolism	1.48	0.002	0.012
Apoptosis	4. Cellular Processes	4.3 Cell growth and death	1.66	0.001	0.006
B cell receptor signaling pathway	5. Organismal Systems	5.1 Immune system	1.45	0.021	0.079
T cell receptor signaling pathway	5. Organismal Systems	5.1 Immune system	1.41	0.023	0.085
Toll-like receptor signaling pathway	5. Organismal Systems	5.1 Immune system	1.41	0.024	0.088

Table 19: A selection of the KEGG pathways were significantly regulated only in the quadriceps of the mice underwent the light therapy after the running exercise. Every pathway is classified in category and sub-category according to the KEGG database, and is reported with the NES, nominal p-value and adjusted p-value. Positive value of the NES indicates an upregulation of the pathway, while a negative value indicates a downregulation.

Differential gene expression: Run+CW vs Control

Pathway	Category	Sub-category	NES	Nominal p-value	Adjusted p-value
Rap1 signaling pathway	3. Environmental Information Processing	3.2 Signal transduction	-1.83	0	0.002
Ras signaling pathway	3. Environmental Information Processing	3.2 Signal transduction	-1.88	0	0.002
Regulation of actin cytoskeleton	4. Cellular Processes	4.2 Cell motility	-1.71	0	0.002
Leukocyte transendothelial migration	5. Organismal Systems	5.1 Immune system	-1.67	0.001	0.007
Platelet activation	5. Organismal Systems	5.1 Immune system	-1.54	0.005	0.025

Table 20: A selection of the KEGG pathways were significantly regulated only in the quadriceps of the mice with the cold water application after the running exercise. Every pathway is classified in category and sub-category according to the KEGG database, and is reported with the NES, nominal p-value and adjusted p-value. Positive value of the NES indicates an upregulation of the pathway, while a negative value indicates a downregulation.

3.7.3 KEGG pathways related to the immune response in the Run+LEDs in comparison to the Run group.

The number of genes differentially expressed in the Run+LEDs group in comparison to the Run group, is reported in Table 21.

	Run+LEDs vs Run
Significant differentially regulated genes (p-value ≤5%)	2903
Significant upregulated expressed genes (p-value ≤5%)	1429
Significant downregulated expressed genes (p-value ≤5%)	1474

Table 21: Number of genes significantly (p-value ≤5%) regulated in the Run+LEDs group in comparison to the Run group. The total amount of regulated genes is further distinguished in upregulated and downregulated

The fold change of the markers related to immune cells (reported in 3.7.1) was calculated for all group, keeping the Run group as reference and displayed in Figure 46. The fold change of the light group is above 1 for all the markers, and, for the chemokine Ccl6, Ccl7 and the antigen CD84, were significant.

The fold change of the Run+CW group is in most of the cases at the level of the Control fold change, meaning that the expression of those makers are mitigated to the level of healthy muscle in the cryotherapy animals.

The differential regulation of KEGG pathways in the Run+LEDs group, in comparison to the Run, confirmed the upregulation (positive NES) of the processes related to the immune response Table 22 . However, a level of significance was detected only for the T cell receptor signaling pathway.
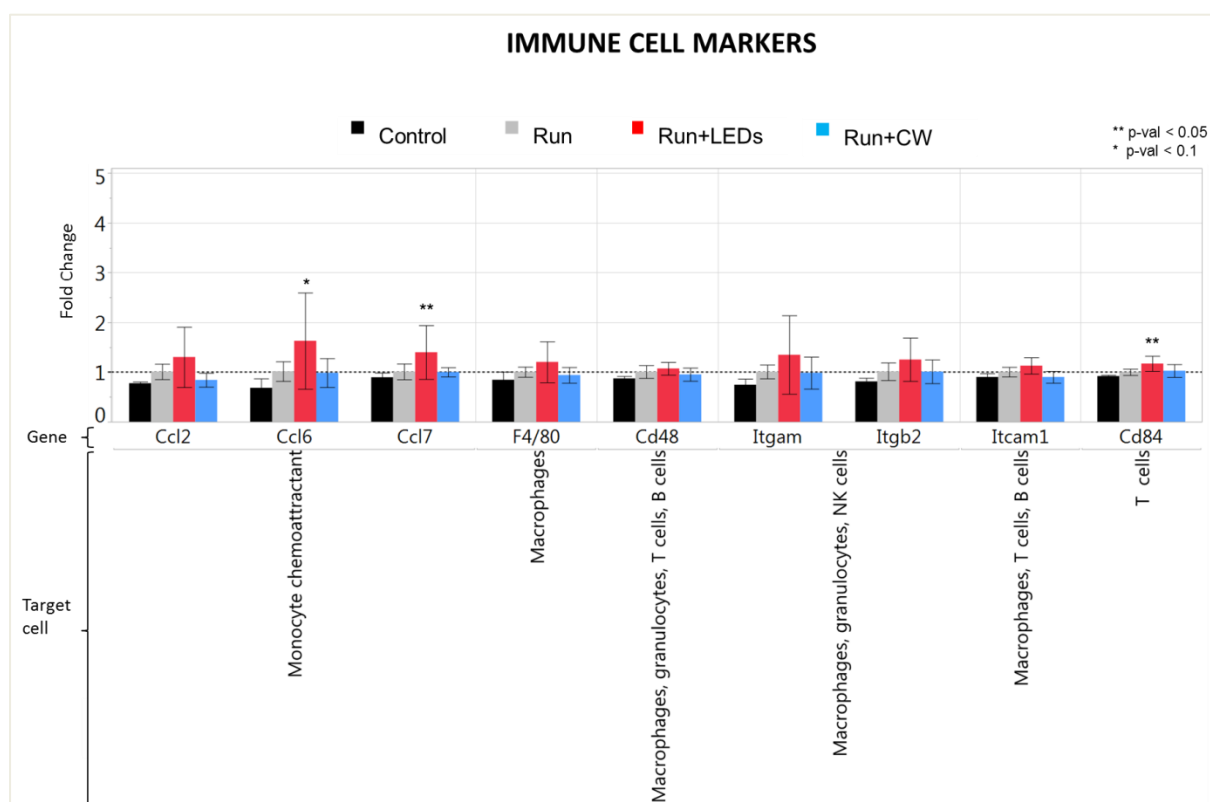
*Figure 46: Bar chart displaying the upregulation of genes considered markers for immune cell. The upregulation is reported as fold change±SD on the mean expression of the Run group (reference group). The immune cell type that is correlated to the protein coded by the gene is reported on a second axis under the gene name. The * displays the level of significance in comparison to the Control. The fold change = 1 means no change in the expression compared to the reference group.*

Differential gene expression: Run+LEDs vs Run

Pathway	Category	Sub-category	NES	Nominal p-value
TGF-beta signaling pathway	3. Environmental Information Processing	3.2 Signal transduction	1.49	0.012
T cell receptor signaling pathway	5. Organismal Systems	5.1 Immune system	1.31	0.055
MAPK signaling pathway	3. Environmental Information Processing	3.2 Signal transduction	1.19	0.088
Fc gamma R-mediated phagocytosis	5. Organismal Systems	5.1 Immune system	1.18	0.158
NF-kappa B signaling pathway	3. Environmental Information Processing	3.2 Signal transduction	1.18	0.162
Chemokine signaling pathway	5. Organismal Systems	5.1 Immune system	1.17	0.128
B cell receptor signaling pathway	5. Organismal Systems	5.1 Immune system	1.11	0.256
TNF signaling pathway	3. Environmental Information Processing	3.2 Signal transduction	1.05	0.344

Table 22: KEGG pathways were upregulated in the quadriceps of the mice which underwent the light therapy after the running exercise in comparison to the Run mice. Every pathway is classified in category and sub-category according to the KEGG database, and is reported with the NES and nominal p-value. Positive value of the NES indicates an upregulation of the pathway.

4   DISCUSSION AND CONCLUSIONS

The literature contains many studies regarding the benefits of the PMB in the red and infrared spectrum on skeletal muscle in vitro and in vivo. In particular, the studies showing the beneficial effect of the visible light on the recovery phase after a damaging exercise have become more frequent.

The first results of this work were achieved applying the infrared light on a culture of muscular cells and measuring the proliferation and production of ATP though colorimetric kits. Additionally, a full gene expression profiling of the cultured cells revealed the stimulation of the pathways involved in the immune system even if the cells were in stress-free condition. The positive results of the *in vitro* experiments functioned as a support for the *in vivo* study. The case study of the *in vivo* experiments was the application of the infra-/red light to the lower limbs of mice which performed a damaging exercise. The first phase of the *in vivo* study consisted in the establishment of an efficient exercise protocol in inducing damage to the muscle. In the second phase, experiments were carried out on with mice that performed the exercise and recover passively afterwards, exercising mice which received the infra-/red light to the legs and exercising mice, the legs of which were treated with cold-water packs. A control group of mice was kept at rest during the experimental period. The changes in the blood parameters, histology and gene expression in the quadriceps of the mice that received the light treatment, revealed the enhanced activity of the immune system, that might speed up the inflammation and the recovery post-exercise. The cold-water application, a common treatment post-exercise, acts in a opposite way, suppressing or delaying the immune response to the muscular damage induced by the exercise.

The results of the in vitro and in vivo study and the potential correlation between the infra-/red light and the immune response will be discussed in the following paragraphs.

4.1   Preliminary study on *in vitro* model of skeletal muscle

At the beginning of this project, the infrared and red light emitted by a LEDs lamp was applied to an *in vitro* model of skeletal muscle in order to confirm the most common response reported in the literature related to cell proliferation and ATP production.

C2C12 is a cell is a cell line originally isolated from dystrophic muscles of C3H male mice[52] and is widely used as *in vitro* model of skeletal muscle tissue[53], since they can be cultured and

differentiated into adult myoblasts, like done in this study (Figure 15). Myoblasts *in vivo*, are the successive state to the activation of muscle satellite cells after a muscle injury. Myoblasts migrate, divide and fuse into myotubes in order to repair the existing muscle fibers.

Several studies evaluated the capability of myoblasts to proliferate[45, 54] and differentiate[43, 44, 55, 56] after the exposure to infra-/red irradiation. Moreover, the effect on mitochondrial activity and energy production induced by the red and infrared light has been widely investigated on different type of cells[57-59], including muscles cells[43, 60]. In these studies, the application of the light occurred during the proliferative phase and the differentiation phase. In our study, the light was applied during the proliferative phase of myoblasts and at the end of the differentiation phase of myotubes.

The experiments of this work started with the application of light at 656nm and 834nm, separately, at three energy densities (1.25 J/cm^2, 2.5 J/cm^2, and 5 J/cm^2) to induce proliferation in C2C12 cells and the effect was checked at 24h after the irradiation. The energy densities were chosen among the most common in the literature concerning the low energy light therapy. The construction features of the lamps allowed a fixed power density at 23mW/cm²; thereby, the different energy densities were obtained adjusting the irradiation time.

The myoblasts irradiated with the 656nm did not increase their proliferation rate, nor the ATP production, at any of the tested dosage (Figure 17). Because of this unsuccessful outcome, the tests with the red wavelength were quitted, and only the 830nm lamp was used.

2.5 J/cm^2 of infrared light induced an increase of 5 to 10% in the XTT signal, and of 5% in the ATP production at 24h. (Figure 18). These two effects disappeared when a dosage <2.5 J/cm^2 or >2.5 J/cm^2 was given to the cells. In this context, one has to keep in mind the biphasic phenomena that characterize any application of the photobiomodulation: insufficient or too much light energy may have an inhibitory effect[48]. As found in the present work, also Wang et al. [49] experienced that 3h after irradiation with 660nm and 830nm light, intracellular ATP increased in hASC cells for dosage ≤10 J/cm^2, while at 30 J/cm^2 the ATP decreased until the background levels.

The effect of the 830nm light on proliferation and ATP production, besides from being dosage-dependent, revealed to be also time-dependent (Figure 19). Indeed, no increase in the XTT signal was detected before the 24h and after the 24h. While, at 12h, the 830nm irradiation stimulated the production of ATP for a mean value of 6% over the control value and the effect on the energy production seemed to be stable until the 24h from the irradiation. However, at

24h also the XTT signal raised, meaning that the richer ATP content might be due to an increase in cell number, and not to an effective improvement of the mitochondrial respiratory chain activity.

The unsuccessful outcome at 656nm and the positive results at 830nm can be explained by the fact that the Cox absorbs the light in a wavelength-dependent manner. Indeed, its absorption spectrum reported by T. Karu[47], has the minimum around 650nm, and one of the four peaks at 830nm. For the last two decades, the Cox has been proposed as primary photoacceptor for infra-/red light in mammalian cells[47]. The light acts in a way that increases the Cox activity and leading to a higher mitochondrial membrane potential, and consequently, to higher performance of the ATP synthase[48]. At 656nm, Cox has a reduced photo energy absorption, inducing an activity comparable to a no light situation. Instead, at 830nm, the photoacceptor capability is maximized, leading to a maximum activity of the Cox that was evident with an increased ATP production at 12h after the irradiation. However, the effect seems to disappear at 24h, where the higher ATP content can be attributed to a higher number of myoblasts in comparison to the no-light control. Cox has a role also in the cell proliferation. Indeed, Karu at al. reported that the absorption spectrum of Cox exhibits the same trend of the action spectrum for the stimulation of DNA synthesis at cellular level[61], with one of the peaks at 830nm.

GSEA analysis executed on myoblasts at 12h and 24h from the 2.5 J/cm^2 of infrared irradiation, revealed opposite trend in the activation of genetic pathways. At 12h, some metabolic pathways were significantly downregulated (Table 9). In particular, the downregulation of the glycolysis/gluconeogenesis might be due to a negative feedback given by the over production of ATP induced by the infrared light. Indeed, in proliferative cells under aerobic conditions and with an overflow of ATP, the glycolysis is the first step that gets inhibited in order to stop the energetic production at the level of the mitochondrial respiratory chain[62]. At 24h after the irradiation, the myoblasts showed an upregulation of metabolism, and, at the gene level at 24h, cyclin D1, cyclin D2, cyclin D3, protein kinase B (Akt) and the heat shock protein 90 (Hsp90) were significantly upregulated. Hence, it can hypothesized that the increased XTT and ATP signal at 24h after the irradiation, might be due to an increased proliferative and metabolic activity.

As described before, the infra-/red light stimulates directly the production of ATP, which has been correlated indirectly to the increase of the proliferation rate of cells by Schroeder et al.[63] The authors proposed the existence of a retrograde signaling from the mitochondria to the

cell nucleus activated by the infrared light. The mechanism involved primarily the reactive oxygen species (ROS) generated by the infrared stimulation of the Cox[60, 61]. The enhanced activity of Cox increases the mitochondrial membrane potential, causing an increase in ATP synthesis and changes in the concentration of ROS[60], which occurred at 12h from the irradiation in this case. ROS stimulates the activation of the nuclear factor kappa B[64] (NF-kappa B), a transcription factor that translocates from the cytosol to the nucleus and starts the transcription of genes related to antioxidation and cell proliferation. Hence, at 24h from irradiation, the proliferative effect was reflected by the increase in XTT and ATP signal and expression of cell cycle genes. However, to confirm this mechanism, further investigations should be executed in order to detect NF-kappa B factors between the 12h and 24h, since at this time points the corresponding pathways were not significantly regulated anymore.

For what concerns the application of the infrared light to differentiated myotubes, the only effect observed was a 2.5% in the fold change of the ATP signal at 6h after the irradiation. The XTT signal was also measured, and the signal was stable at the level of the control for any time point: probably because the myotubes are differentiated cells and do not proliferate anymore. The outcome on ATP production in this study was disappointing if compared to the literature. Indeed, Ferraresi et al.[43] exposed differentiated C2C12 myotubes to a cluster of red and infrared LEDs with an energy density of 2.5 J/cm^2, and they detected an ATP content three times higher than the control values at 3h and 6h from the irradiation.

GSEA was performed for 6h, 12h and 24h after the infrared irradiation. At 12h after the irradiation, the light activated pathways related to the immune system, even if the cells were under stress-free conditions (Table 10). The activation of cytokine-cytokine receptor interaction pathway was mainly due to the upregulation of genes coding for CC family chemokines (i.e. ccl7 with 2.11 fold change and ccl2 with 2.63 fold change), TNF family cytokines, interleukins and the corresponding receptors. Coherently, the TNF and chemokine signaling pathways were significantly upregulated. Already two decades ago, Young at al.[65] demonstrated that 12h after the exposure to light at 660nm, 820nm and 870nm, the macrophages were stimulated to release important wound repair mediators that encouraged the proliferation of fibroblasts. Recent evidence has identified the skeletal muscle as a secretory organ[66], able to release chemokines[67], earlier associated only to immune cells. Moreover, it has been demonstrated that chemokines are promoting the proliferation and fusion of myoblasts[68], in addition to the traditional chemoattactant function.

4.2 Assessment of exercise-induced damage muscle model

There exist several *in vivo* models of muscular damage to which the phototherapy was applied in order to evaluate the beneficial effect. For instance, models where the damage was externally provoked through an impact trauma with a metal mass falling through a metal guide[25, 69, 70], or with a cryoinjury generated by the direct contact of the muscle with a metal rod cooled in liquid nitrogen[27, 71]. Other authors chose to anesthetize the animal and connect the distal part of a selected muscle to an isometric transductor and to a bipolar electrode, in order to induce contractions leading to fatigue of the muscle[28]. The advantage of these methods is the control of the damage inflicted to the tissue; however, they are far from a realistic situation where the damage is provoked, for instance, by physical activity. Hence, even if there are more variables in play, thus a muscular damage model induced by exercise has been preferred in this study.

Several protocols are proposed in literature where mice and rats are forced to physical activity, like climbing[31], running[72] and swimming[73]. In this study, the run on treadmills was chosen as modality of exercise. The usage of a treadmill allows the control of some training parameters, like the load, the distance and the speed.

CD-1 male mouse was the strain selected for this study, since it well performs in spatial learning tasks[74]. Moreover, CD-1 mice are Swiss strain derived, and the Swiss Webster mice showed elevated performance on voluntary wheel and treadmill running[75]. In this study, it has been shown that three bouts of exhaustive running at -25° slope executed by untrained mice, succeeded in inducing a damage in muscular tissue, visible at 48h after the exercising day. Indeed, forcing a muscle to work until exhaustion is one of the well described ways to increase the muscular strength and power[76, 77].

48h after the exhaustive run, quadriceps were characterized by necrotic areas, with infiltration of inflammatory cells, swollen and hyaline fibers (Figure 23). None of these features was present in the muscles of the control mice (Figure 22). Running downhill predisposes the extensor (and antigravity) muscles to injury because the exercise is biased toward the performance of eccentric contractions, which are the most damaging work for skeletal muscles[35-37, 78-80]. Quadriceps, gastrocnemius and soleus undergo eccentric contraction because of their role to slow down the body against the gravity on a negative slope. In this study, only quadriceps were morphologically affected. It was reported that the downhill running for rats induce a certain degree of injury in soleus and gastrocnemius[35, 37, 81, 82].

However, in other studies, the degree of injury sustained by the soleus muscle in mice has been null or minimal[83, 84]. A plausible explanation for the lesser damage to the soleus compared to rats, might be due to a lower body mass. Indeed, it has been demonstrated that the injury sustained by the soleus muscle is related to the animal's size[85].

The time points for the tissue harvesting at 48h, 72h and 168h were chosen taking into account the possible time course of the degradation, inflammation and regeneration phase. The duration of each phase following muscle injury, depends on the mode, duration and intensity of the exercise, hence on the entity of the injury. Immediately after the exercise, the damaged fibers undergoes necrosis and internal proteins, like creatine kinase, are noted in the blood stream. Neutrophils appear in muscles already within 1h after the damaging exercise[16]. After 12h, macrophages start to accumulate[37, 86]. Macrophages have a double role: in the first days they remove cellular debris and release pro-inflammatory cytokines, and after 48h a phenotypic switch occurs, promoting an anti-inflammatory and repairing phase[87].

The degeneration of the quadriceps at 48h after the damaging exercise involved the presence of necrotic fibers, neutrophils and macrophages and the increase of the CK, like shown previously in the literature[35, 88]. At 72h, it was expected to see more foci of infiltrated cells and and even a higher fold change of the CK[15, 34, 89]. Instead, only hypereosinophilic round fibers and swollen fibers were observed (Figure 24). Swollen fibers (Figure 24(B)) are a sign of stress due to increased inner pressure (i.e. for an accumulation of electrolytes), hypereosinophilic fibers (also called hyaline fibers) represent an early stage of cell necrosis. It might be supposed that the damage induced by exercise was not so severe to be still manifested at 72h, or, the 2 mice used for the 72h time point were an unlucky case.

168h after muscular injury was chosen as a checkpoint for the regeneration process, meaning the presence of fibers with central nuclei where the cell necrosis had taken place. Nevertheless, the exercised quadriceps seemed healthy like one of the control mice. A possible explanation might be that the injury was not severe like in other models where the damage was inflicted, for instance, by trauma[69], cardiotoxin[90] or ischemia[26]. For the model proposed in this work, 7 days were too far from the injury; hence, the time window of the regeneration was missed because it occurred before the 168h.

The histology of muscle at the end of the long-term uphill and downhill run did not show any evident sign of damage. The unsuccessful protocols might be due to the low value of maximum speed or to the adaptation of the muscles to the training all over the two weeks. The maximum running velocity at 30cm/s was chosen from the literature data[10, 38, 91]. However, in this study,

the subjects were C57BL/6 mice, which are bad performers in running[29]. At the beginning, it was not considered that the performance variability is related to the strain, therefore, the initial load of the run was much less than what CD-1 mice could tolerate.

4.3 The impact of the photobiomodulation and cryotherapy on the recovery

The main aim of the *in vivo* experiment was to evaluate the infra-/red light therapy on the 48h post-exercise events in comparison to a passive recovery and to an active treatment commonly used in the sport environment.

In this work, the phototherapy was delivered to the trained muscle through an array of LEDs at 830nm and 656nm. The LEDs were preferred to the most common laser technology. The LED array allows a wider and an uniform area of irradiation, is cheaper, safer and a more versatile technology. Furthermore, the LEDs technology is suitable for the design of flexible and wearable systems that would be convenient for the sport environment. The irradiation parameters where adapted, as much as it was permitted by the owned system, to the most used in the literature[28, 30, 92-94]. The power density was set to the maximum for both wavelengths; the dosage released to the muscle was adjusted with an irradiation time of 3 minutes, resulting in 5.8 J/cm^2 for the infrared and 2.5 J/cm^2 for the red light.

Among the most common practice to speed up the post-exercise recovery is the cryotherapy, consisting in the application of coolants to the exercised muscles. The first application method tried in this study, was 5min of half body immersion of three mice into water at 4 ±1 °C (see 2.3.3). This choice was made on the basis of a study where Wistar rats were placed in 10°C water for 10min after swimming[30, 42]. However, the plasma analysis revealed the C-RP significantly increased: 15% at 24h and 33% at 48h post-exercise. Instead, no remarkable changes were detected for the CK. Despite of the rapid C-RP increment, the H&E histology of the all harvested muscles (quadriceps, triceps surae and tibialis) had a normal morphology, comparable to a control muscle. Hence, the C-RP change was caused by another factor not related to the exhaustive exercise protocol. A possible explanation was that 5min in hypothermia were sufficient to induce a modest tissue ischemia in the testes or in the gut, activating signaling pathways related to inflammation[95] and increasing the plasma level of C-RP. Indeed, the LDH, a marker for tissue hypoxia, was found of 1-fold higher than the control value. The H&E histology of the three mice testes was checked, revealing no tissue injury. Unfortunately, no part of the intestine had been harvested. There are studies where the

cryotherapy consisted in the immersion of half body of rodents in cold water, without the consequences described[30, 42]. However, in these experiments, the temperature of the water was around 10°C, that means a lesser thermal shock, and, the subjects were rats, that means a higher body mass than mice and so, a slower cooling down. In the light of this hypothesis, the modality of the cryotherapy was modified and the remaining mice of the same group received the treatment by ice-cold water packs applied only to the exercised limbs. Indeed, the comparison in Figure 25 displayed that the modality of application influenced the trend of C-RP and LDH: when the application was restricted only to the inferior limbs, the two parameters remained at the level of the control.

The mice were grouped in the active experimental groups (control excluded) like shown in Table 11. The fact that the total running time was higher in mice in the light treatment group, was purely fortuitous. Indeed, the treatments were applied post-exercise and could not have influenced the performance on the treadmills.

In this study, the light therapy did not avoid that the increase of the plasma CK caused by the exercise (Figure 27). Indeed, the CK at 48h for the Run+LEDs was found at the same level of the Run group, which was about 1-fold higher than the control. Several studies reported the capability of the infra-/red light to decrease the CK activity when the treatment was applied before the muscular performance[72, 73, 92, 96], suggesting a protective effect of the phototherapy. In the present work, instead, the irradiation was performed after the induction of the damage by three sets of exhaustive runs, hence, it is reasonable not to expect that the therapy prevented the injury to the fibers structures, and the consequent leakage of CK into the blood stream. A study conducted on soccer players, showed a reduction of CK values in plasma immediately after the application of a cluster of infra-/red LEDs after the exercise[92]. However, in this case, no measurements of the CK were performed in long-term, like at 24h and 48h. Indeed, in another clinical study, where the infrared light is applied to the muscles of trained volunteers after the execution of 5 blocks of run at different inclinations, the CK levels at 24h and 48h from the exercise did not significantly differ between the light treated runners and the passive recovery group[97]. The CK raised also for the Run+CW, but the range of values was wider than the other groups, probably due to the lower number of animals (6 instead of 9) or for reasons related to the cooling of the tissue that will be discussed later in this paragraphs.

Since the CK is a marker commonly correlated to the muscular damage, the same increase of plasma CK for the Run and Run+LEDs animals at 48h ensured, a comparable level of muscular

damage, in despite of the total running time that was on average higher for the mice in the light group (Table 11). Indeed, the exercise, with or without treatment, leads to rearrangement of the cytoskeleton and membrane (Figure 37), meaning activities related to cell signaling, division, mobility and, in this specific case, muscle contraction. Indeed, the contraction and the transmission of the force among the adjacent fibers occurs through the cytoskeleton and membrane proteins, which are weak points that get injured and had to be repaired[98-100]. This is the reason why proteins constituting some costameres were upregulated. In particular, the subunit α7 of the membrane integrin was the most affected, with 3-folds for the LEDs group and 2.2-folds for the other two. The talin and the vinculin proteins, the genes of which were slightly upregulated as well, perform the connection to the actin cytoskeleton. The deepest expressed protein of the cytoskeleton was the desmin. The laminin gene, coding for the protein that functions as connector of the cell membrane to the ECM, did not turned out to be regulated. These results suggest that the exercising protocol applied in this model affected only the portion at the interface between the internal and external compartments of the muscle cells. Instead, costameres like dystrophin-associated glycoproteins (i.e. dystroglycan and sarcoglycan), turned out to be more resistant and the expression of the corresponding genes were at the level of the control. The Figure 47 depicts a simplified model of costameres.

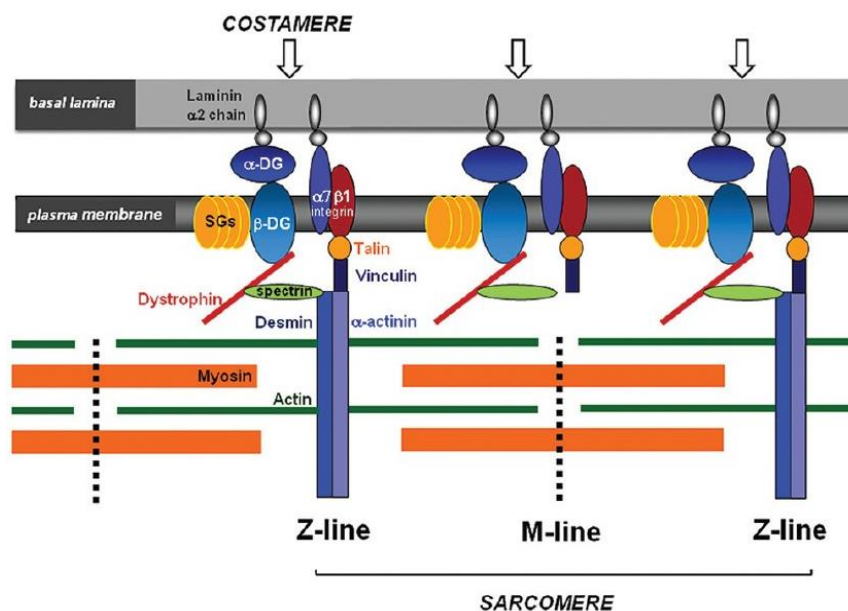*Figure 47: Simplified model of the costameres. The costameres are structures, which lie at the sarcolemma over the Z and M lines of nearby myofibrils. This model depicts the relationship of costameres with basal lamina, plasma membrane and cytoskeleton proteins. The contractive apparatus connect to the sarcolemma and the basal lamina through two ways: via the dystroglycan complex (α-DG and β-DG) and the other via the integrins[6].*

The upregulation of genes coding for proteins involved in the membrane repair is a further confirmation of the damage induced by the downhill run. The gene coding the dysferlin, a well-known protein recruited during the repair process was 2-fold higher for all the groups at 48h after the exhaustive run. Caveolin3 is the membrane protein that interacts with dysferlin for membrane resealing[101-103] and was slightly upregulated only in the Run and Run+LEDs group. There are other proteins, the cytoplasmic concentration of which increase in conjunction with membrane tears. These proteins are annexins and mitsugumin 53[101-105], and the corresponding genes were upregulated in all groups (control excluded). During skeletal muscle regeneration, dysferlin also acts together with desmoyokin[101], which was upregulated only in the BPM group.

In response to muscle injury, even in a modest case, the satellite stem cells become active and start to proliferate towards the injured site in order to regenerate the damaged area. The muscular stem cells, after the activation, undergo different fates characterized by a hierarchic expression of myogenic regulator factors (MRFs). According to the hierarchy of transcription factors regulating myogenic lineage (Figure 48), the regenerative process in the damaged quadriceps of all experimental groups, appeared to be at the terminal phase of early differentiation[106, 107] (Figure 41). Indeed, the Pax3 and Pax7, markers for quiescent satellite cells, were expressed at the level of the control for all the active groups, meaning that the satellite pool was already restored. The same was for the Myf5 expression, meaning that the activation and proliferative phase was over. MyoD1 (MyoD in Figure 48) and the Myf6 (Mrf4 in Figure 48) were upregulated but under the level of the MyoG expression. Moreover, the irradiated muscles of the Run+LEDs group, appeared to be slightly further in the differentiation process, since the Myf6 was significantly upregulated only for this group of mice. MyoD1 regulates several phase of the myogenic process, and its expression is attenuated during the cell fusion phase. Myogenin and herculin, coded by the MyoG and Myf6 gene respectively, have a master regulatory role by controlling differentiation. According to the scheme proposed in Figure 48, the recovery period at 48h from the exercise, reached the phase of early differentiation of newly myocytes, more pronounced in the Run and Run+LEDs than in the quadriceps treated with ice cold package.
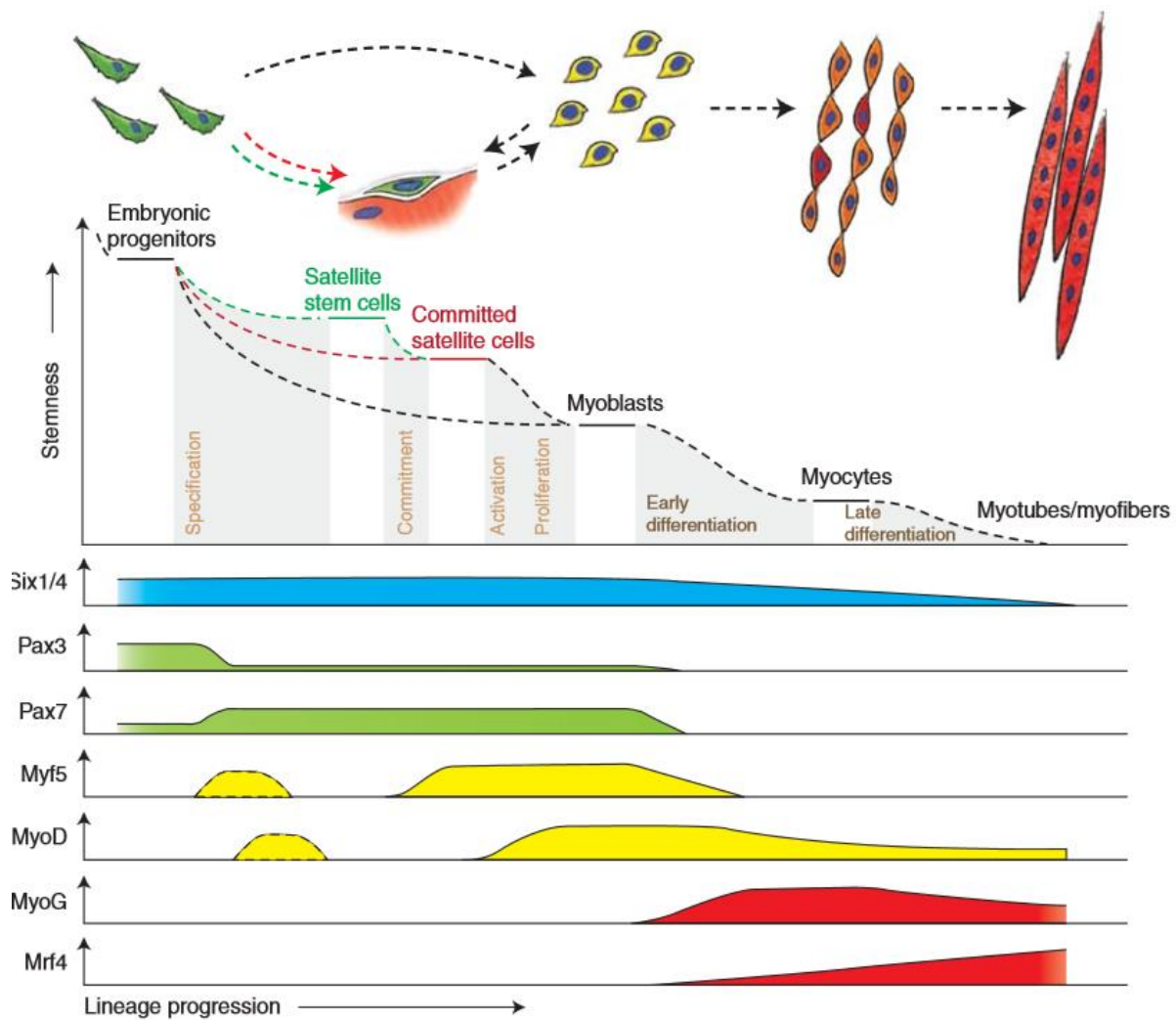
Figure 48: Hierarchy of transcription factors regulating the progression of the myogenic lineage of cells during skeletal muscle genesis or regeneration[107].

Exercise affects the metabolism and this is evident in the high number of metabolic pathways appeared as significantly regulated in the entire experimental group (Figure 42) at 48h after the exhaustive run. The metabolism of substrates that fuel the muscles during the exercise, like carbon, fatty acids and amino acids, and processes for energy production like TCA cycle and oxidative phosphorylation, were downregulated (Figure 43). Several biosynthesis processes contribute to the restoration of the homeostasis of substrates consumed during the physical activity, like ATP, phosphocreatine glycogen, through lipid oxidation for instance. Amino acids like valine are irreversibly catabolized during the activity, and needed to be restored after the exercise. All these pathways get upregulated immediately after the exercise in order to restore the metabolic homeostasis[108]. However, at 48h from the exercise performed in this study, the pathway analyses suggest that the metabolic recovery period had been over and the same pathways had been suppressed. Even more metabolic pathways were downregulated by the Run+LEDs and the Run+CW groups (Figure 45), probably because of the

downregulation of the PPARs, which function as regulatory transcription factors of metabolic processes involving carbohydrate, lipids and proteins. The ubiquitin-mediated proteolysis pathway is one of the major mechanism to degrade unneeded or damaged proteins, and was upregulated only in the Run group (Table 18). While, both the light therapy and the cryotherapy, promoted pathways related to protein synthesis, like Aminoacyl-tRNA biosynthesis, ribosome biogenesis, RNA transport and protein processing.

A similar level of CK, and response in the gene expression of pathways and genes related to metabolism, repair and regeneration, brought us to the conclusion that the damage occurred for the three active groups in a similar manner, slightly attenuated in the Run+CW group.

However, a significant difference turned out among the experimental groups, when the damage was quantified by counting the affected fibers on the histological section of quadriceps (Figure 34). Indeed, the irradiated quadriceps had 1.6 times and 2.6 times more of altered fibers in comparison to the Run and Run+CW group, respectively. One might think that the CK leaked from other muscles for the Run and Run+CW, but the sections of the other harvested muscles were similar to a healthy control tissue. It can be noticed that the number of the immunoglobulin-infiltrated fibers in the Run+LEDs muscles was close to the amount of round fibers in the Run group (Table 15). The red fibers are co-localized with infiltrated immune cells and one can assume that the round fibers surrounding the red ones were swollen because of the inflammation in progress. One might consider the round fibers of the Run quadriceps as predominantly hyaline fibers (an early stage of necrosis) and only few of them affected by the immune cells activity. Hence, a reasonable speculation is that the level of damage in the two groups is similar, but the light treated muscles were in an advanced inflammation status at 48h. Indeed, the inflammation is visibly more pronounced in the Run+LEDs, as it is depicted in Figure 29 and Figure 30. Moreover, the C-RP raised already at 24h for the phototherapy group, while for the Run group it increased the control level only at 48h (Figure 28). This fact further reinforced the hypothesis that the inflammation response started in advance in the muscles of the mice that received the infra-/red therapy. Consequentially, the higher number of red fibers in the exercised muscles of the LEDs group might be due to the infiltration of immunoglobulins through secondary injuries to the membrane caused by the activity of immune cells.

One of the most interesting points of this work, was the finding that the immune system was highly stimulated by the infra-/red light also at the gene level. In the comparison between the Run+LEDs and the control group (Table 19), the two important signaling pathways of NF-kappa

B and TNF signaling were significantly upregulated with a NES of 1.59 and 1.39, respectively. Moreover, the receptors signaling pathway of T cells and Toll-like receptor were upregulated, as well. Looking at the details of the listed pathways (Appendix B, Appendix C, Appendix D), the NF-kappa B factors and genes of the MAPK cascade are upregulated and play a role in the regulation of the TNF (Appendix B), T cell receptor (Appendix C,) and Toll-like receptor (Appendix D) signaling pathways. The NF-kappa B pathway (Appendix A) appears to be mostly activated by the interaction of cytokines, ROS and hypoxic conditions, due to the transcription of genes related to inflammation, cell proliferation and lymphocytes adhesion. The NF-kappa B pathways is already stimulated by an intensive exercise, peaking at 2-4h after the activity[109,110]. In the case of the Run+LED mice of this study, in addition to the exercise, the infra-/red light irradiation kept the NF-kappa B pathway active until 48h from the exercise through a ROS-dependent mechanism, as discussed before (see paragraph 4.1). Moreover, the infra-/red light had probably increased the level of NO, acting as a dissociation agent of the NO from Cox and other intracellular stores. NO is a well-known signaling factor for immune cells[18]. In literature, the results regarding the action of the light on the NF-kappa B factors are in contrast. A study on embryonic mouse fibroblasts depicted the activation of the NF-kappa B until 24h by 810nm laser beam[64], while a report on injured rat muscles showed a reduction of IkBα expression after 7 and 14 days of irradiation[70]. An explanation for opposite results could be that the initial response to cell stress typical of NF-kappa B activation induces a productive response that includes lower activation of this pathway when measured at a later time point when the light has had a therapeutic effect. Another possibility regards the biphasic response to light: a prolonged irradiation period gives an opposite biological reaction[48].

The clusters of significant genes in Figure 37 revealed that 50 genes related to the immune response were upregulated exclusively in the irradiated quadriceps, against the 5 in common with the passive recovery mice. Among these genes, several markers for immune cells were found (Figure 41). The Cd68 marker was the highest and significant upregulated for all the groups in comparison to the control: 10 folds for the Run group, 6.5 folds for the Run+LEDs and 2.5 folds for the Run+CW. Ccl2, ccl6, ccl7, important chemokines, and epitopes related to macrophages and T cells and were found significantly over-expressed only in the irradiated quadriceps. The Cd68 is a well know marker of macrophages M1[111] that regulate the inflammatory and proliferative phase post-injury. In a recent study[112] a cryoinjury on the tibialis anterior of male rats was treated with red and infrared light, once a day for up to 7 days. At day 2 the Cd68 macrophages were 50% reduced by the light in comparison to the

injured muscle without the therapy. At day 7, the amount of M2, the anti-inflammatory phenotype of macrophages, was 4 to 5 folds higher than the injuried tibialis. The authors hypothesized that the light modulates the inflammatory response in favor of the regenerative process.

For the present work, a further analysis was run in order to isolate the effect of the light therapy from the effect of the exercise. Hence, a selected differential pathway analysis between the Run+LEDs and the Run was performed, which meant to keep the Run group as reference instead of the control (Table 22). In this case, among the first significantly upregulated were the T cell receptor, TGF-β and MAPK signaling pathways. The NF-kappa B, TNF, B cell receptor and chemokine signaling pathway were still stimulated but not matching the criteria of significance, meaning that their significant upregulation was due to a combined effect of the exercise and the light therapy.

T cells are a population appearing in the tissue around the third day after the damage[113], in a second wave of immune cell infiltration. There is evidence that T cells can secrete growth factors and cytokines able to modulate the microenvironment of the injured site, crucial for muscle regeneration. Indeed, T-cell-deficient mice displayed a delay of early growth in skeletal muscle[114]. Moreover, adult mice lacking T cells, showed impaired muscle regeneration abilities that was fully recovered after injections of cytokines secreted by T-cell[115]. Up to now, no studies have reported the response of T cells to infra-/red light. However, based on the results reported in this study, it can be hypothesized that the stimulation of T cells is a consequence of the upregulation of the NF-kappa B signaling pathway.

TGF-β is a multifunctional cytokine that has been mainly studied for its role in stimulation of the production of ECM components, like collagen and fibronectin[116]. Besides of this "classical" action, the TGF-β factor has a further double role in muscles: initially it acts a potent chemoattractant for neutrophils and monocytes; later, it suppresses the inflammatory response in order to have a favorable environment for the healing[117]. Anyhow, the beneficial role of TGF-β is controversial. Several studies have reported that blocking the TGF-β activity improves muscle regeneration accompanied by an increase in myoblast differentiation and reduction of fibrosis[118, 119]. On the other hand, a study reported that the inhibition of TGF-β action in muscles damaged by eccentric contractions, led to a rapid recovery in short-term, but also to an incomplete structural muscle regeneration, reducing the muscle strength in the long-term[120]. The action of infrared or red light at low dosage (from 0.1 J/cm^2 up to 6 J/cm^2) on the expression or release of TGF-β factor has been demonstrated in humans and animals

in the context of wound healing: for instance in diabetes subjects[121, 122] or in healthy patients undergoing gingival surgery[123]. Mitochondrial ROS might have a role also in the activation of TGF-β, as a correlation between those two factors in normal human lung fibroblasts has been found[124]. Even if no studies are available on skeletal muscles, the mechanism that activates the TGF-β signaling pathways might be the same for damaged muscle fibers and in situ fibroblasts and endothelial cells. Moreover, the TGF-β signaling pathway has been positively correlated in recent studies to the shift in macrophage polarization from M1 to M2[125]. At any time point following injury, the inflammatory infiltrate consists of a mix of macrophage phenotypes and diverse states of activation, however, the predominance of M2 macrophages over the M1 indicates the predominance of the regeneration process over the inflammation. Usually M2 macrophages are identified in the tissue approximately around the third day after the damage, and persist for seven days[126]. They secrete anti-inflammatory cytokines, like the TGF-β itself, to repress the local inflammatory response and promote the differentiation of myoblasts into myotubes, in order to repair the injured site. The expressions of genes displayed in Figure 41 and the upregulation of T cells and TGF-β signaling pathways suggest that the infiltration is a mix of immune cells that usually appear in the tissue later than the M1 macrophages.

At last, it is well documented that the MAPK signaling pathway is activated right after the exercise, probably induced by ROS[127]. However, in this case, its activation at 48h after the run and 24h after the last light therapy session, seems to be due specifically to the infra-/red light. In a study, the authors suggest that the red light in muscle cells does not act via a stress signal to stimulate the MAPK signaling; probably the light acts via other signal transduction pathways, but they do not propose any mechanism[128]. Here, it can be supposed that the MAPK cascade could have been activated by the interaction between the TGF-β factor and the corresponding receptor[129, 130]. Anyhow, in previous studies, the MAPK signaling appeared to be involved in the metabolic and mitogenic plasticity of skeletal muscle in response to exercise[131-133], and the phototherapy might enhance its activity.

The cryotherapy seems to mitigate the signs of damage induced by exercise, in terms of structural deterioration and inflammation. Indeed, the increase of CK was less pronounced than the other two groups (Figure 27). The C-RP remained at the level of the control for any time point (Figure 28), similar to what was reported in a previous study on humans, where a full body cryotherapy kept at the control level several inflammatory markers[134]. The outcome of the blood analysis is in line with what was observed on the muscle histology: the Run+CW

mice had the lowest amount of damaged fibers (Figure 34) and infiltrated areas (Figure 30). Besides the histological appearance and plasma analysis, the muscles were anyway affected by the exercise. This is reflected by the upregulation of genes related to costameres (Figure 38), membrane repair (Figure 39) and myogenesis (Figure 40), even if at a more attenuated level. The signs of the secondary injury mainly due to the activity of immune cells was almost absent.

The downregulation of the Rap1 and Ras signaling pathways in quadriceps of Run+CW mice, in comparison to the control (Table 20), are coherent with the downregulation of the pathways shown in Figure 43. Indeed, the downregulation of the RAS affects the Rap1 signaling pathway. The Rap1 signaling pathways was downreagulated, affecting the regulation of the ECM receptor interaction and focal adhesion. Both Rap1 and Ras contribute to the downregulation of the actin cytoskeleton and PI3-Akt signaling pathway. The leukocytes transendothelian migration was suppressed, explaining the low infiltrated area and the lowest expression of Cd68 in comparison to the other groups (Figure 41). The reason may lie in the fact that the tissues shrank and the vessels contracted because of the low temperature, reducing the blood flow and cell swelling, and making the membranes less permeable to proteins and immune cells. Indeed, it has been demonstrated that local hypothermia reduced the recruitment and adhesion of leukocytes in the striated muscles of hamsters due to the reduced microvascular perfusion[135]. Inflammatory processes were decreased because of a reduction in macrophages infiltration in the tibialis anterior of rats, which underwent cryotherapy post-injury[136]. Moreover, the cooling of the tissue, slows down the local metabolism of the cells, which demand a lower amount of energy and suffer less external stress[137, 138]. All these effects related to the lowering of the temperature are prolonged for hours after the cryo-treatment. Indeed, studies demonstrates that the intramuscular blood flow remain depressed[139] or continue to decrease during the post-cooling period[138, 140], likely because the intramuscular temperature remain below the baseline for hours following the cooling. Taken together, these results suggest that the cryotherapy slowed down processes like cell proliferation, migration and cell to cell or to matrix interactions, ruled by Rap1, Ras and PI3-Akr signaling pathways, and, for which cytoskeleton and ECM structures are involved. Moreover, leukocytes infiltration is significantly reduced, even if mechanisms related to the repairing of the muscular damage were in process. Hence, what it is suppressed is the inflammation response. However, previous studies suggest that cryotherapy, despite decreasing inflammation, might delay the muscle regeneration process[141], as the immune cells, like macrophages and T cells, are

fundamental for the healing process. On the other hand, a chronic inflammation negatively affects the regeneration and mass gain after exercise[142]. Hence, inflammation must not be seen always as something to suppress in the case of exercise-induced muscle damage, but it has to be kept under control in order not to reach dangerous levels.

The infra-/red light and the cold water applied after the exercise, have some mechanisms of action in common, as observed by the pathways significantly regulated by both therapies (Figure 45) and discussed before. However, a part from that, the outcome of the experiments of this work leads to the assertion that the two treatments affect the muscles in a very different manner, opposite from the point of view of the immune response: the infra-/red light application enhance the inflammation response, while the cryotherapy suppresses it. In literature there are some comparative studies aiming to choose the best post-exercise treatment between the photo- and cryotherapy[30, 42, 92]. The authors selected the light treatment as best recovery therapy, able to reduce plasma CK, number of necrotic fibers and infiltration of immune cells; while, the cryotherapy exacerbate the condition of the muscles with more inflammation and necrosis. These results are in contrast with what is reported in other studies aiming exclusively to evaluate the effects of cryotherapy. The most of them display the capability of the hypothermia in attenuating the inflammatory reaction to a muscular injury[134-136]. Instead, as discussed before, the outcome of experiments only with the infra-/red light, show the capability of the phototherapy to stimulate the recruitment of M2 macrophages[112, 125]. Given these controversial results available in literature, it is very difficult to understand the mechanisms of action and the benefits of each treatment.

An important concept regarding the action of the photobiomodulation is that the response from the tissue strongly depends on a combination of parameters, such as dose, wavelength, power density, energy density, frequency of irradiation and interval between consecutive irradiations. Hence, the contrasting evidences in literature can be explained with the difference of these parameters.

To conclude, in Table 23 the events that occurred and were detected at 0h, 24h and 48h after the damaging exercise are summarized. Figure 49 depicts a possible relationship between the immune response and the light therapy applied to the quadriceps that was damaged by the eccentric exercise, based on the knowledge gained from previous studies in literature and the results achieved in this work.

	Events at 0h	Events at 24h	Events at 48h		
		Plasma	Plasma	Histology	Gene expression
Run group	Exercice-induced damage	CK ↑	CK ↑↑ C-RP ↑↑	Damaged fibers ↑↑ Infiltrated area ↑↑	Metabolism ↓ Proteolysis ↑↑ Costameres ↑↑ Membran repair ↑↑ MRFs ↑↑ Immune cell antigens ↑
Run + LEDs group	Exercice-induced damage Infra-/red light	CK ↑ C-RP ↑	CK ↑↑ C-RP ↑↑ Infra-/red light	Damaged fibers ↑↑↑ Infiltrated area ↑↑↑	Metabolism ↓↓ Protein synthesis ↑↑ Costameres ↑↑ Membran repair ↑↑ MRFs ↑↑ Immune cell antigens ↑↑ Inflammatory pathways ↑↑
Run + CW group	Exercice-induced damage Ice-cold water	Ice-cold water	CK ↑	Damaged fibers ↑ Infiltrated area ↑	Metabolism ↓↓ Protein synthesis ↑↑ Costameres ↑↑ Membran repair ↑ MRFs ↑ Immune cell antigens ↑

Table 23: Summary of the events that occurred and were detected in this study at different time points from the damaging exercise for the three experimental groups. The number of arrows correlates the intensity of the event.

PROPOSED RELATIONSHIP BETWEEN THE IMMUNE RESPONSE AND THE INFRA-/RED LIGHT APPLIED TO MUSCLES DAMAGED BY EXERCISE
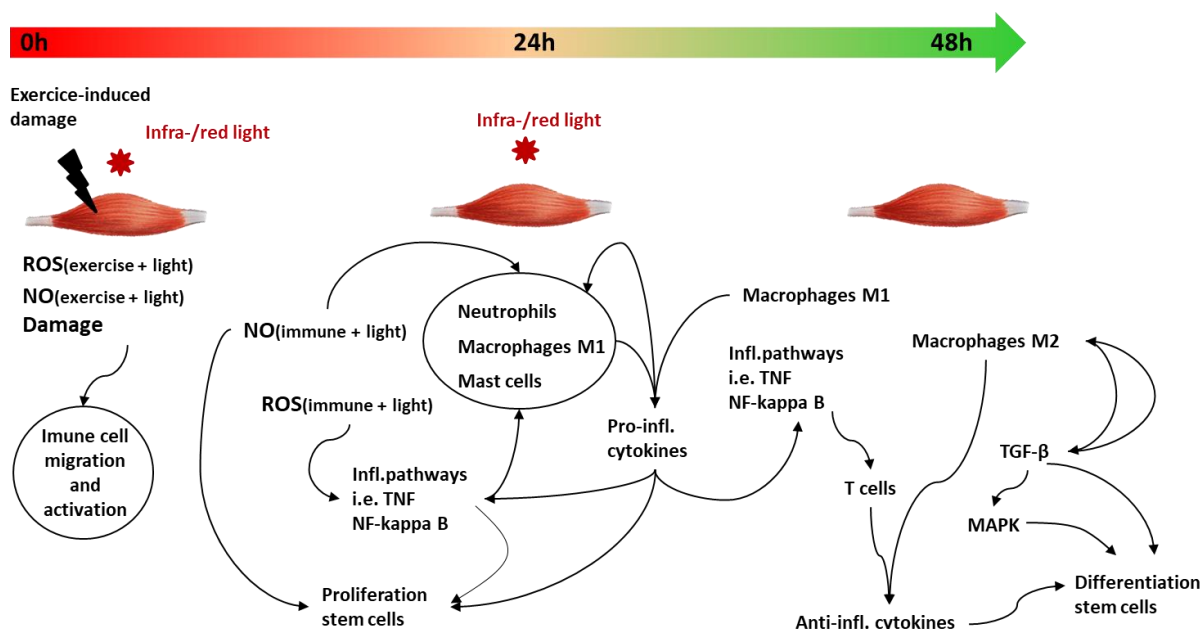
Figure 49: The suggested relationship in the immune response and the light therapy applied to quadriceps damaged by exercise. 0h is the time point when the animals performed the downhill running, that provoked structural damage, the release of NO from the dying fibers and increase ROS. In addition, the levels of NO and ROS were increased by the action of the infra-/red light. These events induced the recruitment of a mixed population of cells (neutrophils, macrophages M1 and mast cells) for debris clearance. At 24h, the concentration of ROS and NO are kept over the physiological levels because of the second application of light therapy and the action of the immune cells. NO promotes the activation of stem cells, while ROS enhances the activity of immune cells and activate inflammatory pathways that recruit more immune cells and promote the stem cell

86

proliferation. Pro-inflammatory cytokines trigger the activation of inflammatory pathways, recruit stem cells and more immune cells at the injured site. The inflammation response turned out to be more intense, some signs of the anti-inflammation phase appeared already at 48h. T cell migration and adhesion was stimulated by NF-kappa B. The signaling pathways of TGF-β promote the differentiation of stem cells and the shift of macrophages from M1 to M2 phenotype, which release the TGF-β factor as well. TGF-β activated the MAPK cascade that is involved in muscle plasticity and promote the differentiation of satellite cells. Macrophages M2 and T cells release anti-inflammatory cytokines leading to the resolution of the inflammation response in advantage of the regeneration phase. Hence, at 48h the muscles underwent the light therapy were in between the end of the pro-inflammation phase and the beginning of the anti-regeneration phase.

4.4 Conclusion

The outcome of this work provide interesting and new hints on the mechanisms of biophotomodulation in the infra-/red spectrum on muscular recovery after a damaging exercise.

Starting from an *in vitro* model of skeletal muscle, it has been possible to identify the potential of phototherapy in the context of healing after muscle injury: it promotes the chemotaxis in myotubes and proliferation of myoblasts. The proliferative response is seen as a benefit in healthy cells in the case of wound healing, but it has to be carefully considered in the case of cancer cells. In myotubes, in stress-free condition, the activation of pro-inflammatory pathways by infra-/red light is an interesting event if contextualized to the case of muscle injury, where the tissue has to be cleaned from debris before being repaired. Indeed, the additional promotion of inflammatory pathways might be helpful to speed up the initial inflammatory phase and promote the repair process by proliferative myoblasts.

The exercising protocol of the *in vivo* study succeeded in inducing a moderate damage and stress in the quadriceps muscles, evident in the histological and/or genetic changes. Probably a higher number of animals per group would reduce the statistical variability.

The infra-/red light seems to enhance the immune response in the muscles which underwent a damaging exercise and PBM afterwards. The probable key of this outcome is the overproduction of ROS, as a consequence of the stress induced by exercise and of enhanced mitochondrial activity induced by the infra-/red light. Another possible mechanism is the release of NO by the action of the light as a dissociation agent between the NO and the Cox or other intracellular storage. NO attracts and increase the activity of the immune cells during the pro-inflammation phase. The ROS and cytokines activate the NF-kappa B signaling pathways that plays an important role in enhancing the inflammation response. The upregulation of NF-kappa B, TNF, TGF-β and T cells signaling pathway and the upregulation of different type of antigens, lead to the assumption that the cell infiltration detected on the histology of irradiated muscles, is a mix of cells that belong to the pro- and anti-inflammation

phase, which usually starts in injured muscles later than 2 days. The speculation here is that the infra-/red light is speeding up the pro-inflammation phase anticipating the time course of T cells infiltration and the polarization of M2 macrophages; promoting the shift from the pro- to the anti-inflammation phase already at the second day after the damage.

The cryotherapy shows clear signs of mitigation of muscular damage affected by exercise. The lowering temperature is probably the main mechanism of action that lead to reduction of blood flow, suppression metabolism, cell migration and immune response.

The two post exercise treatments, showed some mechanisms of action in common involving processes for protein production, but, a part from that, they affected the exercised muscles in a very different manner: the cryotherapy suppressed the post-exercise inflammation, the infra/-red light instead, enhanced the immune response. The reduction of inflammation prevents the DOMS and allows the restart of the physical activity after a shorter resting period. However, it is not clear if the cryotherapy prevented the damage and the secondary injury or slowed down the repairing process, delaying the regeneration. Indeed, pro- and anti-inflammation phase are both needed to build up functional and stronger muscular tissue. On the other hand, a chronic inflammation hinders the tissue healing.

At the time point where the experiments were ended, it was not possible to observe the fate of the quadriceps at 48h after the exercise, neither to verify what occurred before the 48h. The only proven evidence in this work is that the immune response is pushed up and signals involved in the regeneration phase are activated in advance in the muscles treated twice with the phototherapy after the exercise. Further investigations in short-term would help to understand the causes, and, long-term studies would be useful to better understand the following point: is the infra-/red light speeding up the recovery, enhancing the pro-inflammation response and promoting the anti-inflammation phase, or induces an unbalanced stimulation that will prolong the recovery period? For what concerns the present work, these remain open questions.

In conclusion, this work provides additional information on the mechanism of action of the infra-/red light therapy, not reported previously in literature. The enrichment regards mainly the genetic response induced by the light on muscles, which underwent a damaging exercise. The pathways, however, were not fully regulated, and a higher number of animals per experimental group might give to the results more statistical relevance.

5   SUMMARY

Skeletal muscle is the most abundant tissue in the body, comprising circa 40% of the total body weight. The main function is the generation of force through contraction to produce movements or maintain the posture[1]. Eccentric contractions performed during an uncustomized action, induce a certain level of damage[10, 11], which is manifested in the subject with symptoms of DOMS[9]. DOMS is the physical manifestation of what happens at the micro tissue environment in the days following the injury: pro-inflammatory immune cells are recruited in order to remove tissue debris, damaged structures are digested through proteolysis, and muscle stem cells expand and migrate towards the injured area. After the third day, the inflammation response is attenuated and cytokines and growth factors are released in order to promote the regeneration processes.

The availability of a treatment that improves the muscle status after the exercise would be convenient to shorten the recovery period. Cryotherapy is the most commonly applied to muscles after exercise modulating the DOMS as a consequence of a reduced inflammatory response[50, 51]. In the last decades, photobiomodulation (PBM) in the red and infrared spectrum has been identified as a possible post-exercise intervention. Indeed, clinical studies reported its protective effect when applied before or during exercise, reducing pain, damage, and increasing the performance of the subjects[39, 40]. Additionally, in animals, BPM depicted a decreased of myonecrosis and oxidative stress[31, 42]. In *in vitro* studies, PBM promoted the energy production in myocytes, the proliferation of myoblasts[43] and their differentiation into myotubes[44], the cell cycle entry of satellite cells[45].

In this study, the application of 2.5 J/cm^2 infrared light to an *in vitro* model of skeletal muscle modulated the proliferation and energy production. Additionally, the gene expression profiling, revealed the activation of pathways related to the inflammatory reaction.

There results led to *in vivo* experiments. The physical exercise was chosen to cause damage. The protocol consisted in forcing 10 weeks old CD-1 male mice to run until exhaustion on a downhill treadmill for three times in a single day. The application of infra-/red light or ice-cold water packs occurred immediately after the exercise and at 24h. Independently from the type of recovery (with or without therapy), the quadriceps displayed signs of damage at 48h after exercise: increase of CK levels; necrosis of fibers detected in the histology; upregulation of genes coding for costameres, membrane repair proteins, and MFRs.

The immune system was stimulated by the infra-/red therapy: pathways related to both pro-inflammation (TNF and NF-kappa B signaling pathway) and anti-inflammation phase (T cell receptor and TGF-β signaling pathway) were significantly upregulated. The upregulation of the NF-kappa B led to cell survival, inflammation and leucocytes adhesion. The latter may explain the upregulation of the T cell signaling pathway. T cells belong to the second wave of immune cells and have a crucial role in creating a favorable environment for muscle regeneration[113-115]. Moreover, the infra-/red light stimulates the TGF-β signaling pathway in exercised muscles, as already demonstrated for other type of tissues[121-123]. TGF-β is correlated to the shift of the macrophages from the pro-inflammation to the anti-inflammation phenotype, which promotes the regeneration of the tissue[125]. Moreover, chemokines and markers for different phenotypes of macrophages and T cells were significantly upregulated only by the infra-/red light. These results suggested that the signaling cascades related to the regeneration phase had begun earlier in the PMB group. A possible explanation is the mechanism of action of the PMB in the infra-/red spectrum. In particular the overproduction of NO and ROS due to the enhanced activity of mitochondria and the NOS release[39], in addition to the ones induced by the damaging exercise. ROS and NO trigger signals related to the recruitment of immune cells, stem cells activation and activate processes like the NF-kappa B signaling pathway[18].

Infra-/red light and cryotherapy affected the exercised muscles in a very different manner. The cryotherapy seems to mitigate structural deterioration and inflammation. Genes coding for proteins of costameres, membrane repair process and myogenesis were upregulated. At the pathways level, the leukocyte transendothelian migration was suppressed, explaining the C-RP at the level of the control, the low infiltrated area and the lowest expression of Cd68. Moreover, the cryotherapy slowed down processes like cell proliferation, migration and cell to cell or to matrix interactions, ruled by Rap1, Ras and PI3-Akr signaling pathways. All these effect are probably consequences of the low temperature that reduces the local cell metabolism[136], blood flow, cell swelling, recruitment and adhesion of leukocytes[135].

The main finding is explained by the stimulation of the immune response from the infra-/red light applied twice after the damaging exercise, while, the cryotherapy attenuates the damage and the inflammation. Which of the therapies is the best one for the recovery post-exercise, is still an open issue. It is a matter of clarifying if the light therapy speeds up the inflammatory process in advance of the regeneration or prolonging it, and if the cryotherapy protects from the damage or suppresses the inflammation delaying regeneration process.

6 REFERENCES

1. Frontera, WR, Ochala, J: Skeletal muscle: a brief review of structure and function. *Calcif Tissue Int,* 96**:** 183-195, 2015.

2. Fu, X, Wang, H, Hu, P: Stem cell activation in skeletal muscle regeneration. *Cell Mol Life Sci,* 72**:** 1663-1677, 2015.

3. Pollack, GH: The cross-bridge theory. *Physiol Rev,* 63**:** 1049-1113, 1983.

4. Sciorati, C, Rigamonti, E, Manfredi, AA, Rovere-Querini, P: Cell death, clearance and immunity in the skeletal muscle. *Cell Death Differ,* 23**:** 927-937, 2016.

5. Richfield, D: Medical gallery of David Richfield. *WikiJournal of Medicine*, 2014.

6. Sabatelli, P, Pellegrini, C, Faldini, C, Merlini, L: Cytoskeletal and extracellular matrix alterations in limb girdle muscular dystrophy 2I muscle fibers. *Neurol India,* 60**:** 510-511, 2012.

7. Ramaswamy, KS, Palmer, ML, van der Meulen, JH, Renoux, A, Kostrominova, TY, Michele, DE, Faulkner, JA: Lateral transmission of force is impaired in skeletal muscles of dystrophic mice and very old rats. *J Physiol,* 589**:** 1195-1208, 2011.

8. Tiidus, PM: *Skeletal Muscle Damage and Repair*, 2008.

9. Asmussen, E: Observations on Experimental Muscular Soreness. *ActaRheumScand,* 2**:** 109-116, 1956.

10. Hody, S, Lacrosse, Z, Leprince, P, Collodoro, M, Croisier, JL, Rogister, B: Effects of eccentrically and concentrically biased training on mouse muscle phenotype. *Med Sci Sports Exerc,* 45**:** 1460-1468, 2013.

11. Lieber, RL: Biomechanical response of skeletal muscle to eccentric contractions. *J Sport Health Sci,* 7**:** 294-309, 2018.

12. Hyldahl, RD, Chen, TC, Nosaka, K: Mechanisms and Mediators of the Skeletal Muscle Repeated Bout Effect. *Exerc Sport Sci Rev,* 45**:** 24-33, 2017.

13. Morgan, DL, Talbot, JA: The Addition of Sarcomeres in Series Is the Main Protective Mechanism Following Eccentric Exercise. *Journal of Mechanics in Medicine and Biology,* 2**:** 421-431, 2002.

14. Morgan, DL: New insights into the behavior of muscle during active lengthening. *Biophys J,* 57**:** 209-221, 1990.

15. Hyldahl, RD, Hubal, MJ: Lengthening our perspective: morphological, cellular, and molecular responses to eccentric exercise. *Muscle Nerve,* 49**:** 155-170, 2014.

16. Fielding, RA, Manfredi, TJ, Ding, W, Fiatarone, MA, Evans, WJ, Cannon, JG: Acute phase response in exercise. III. Neutrophil and IL-1 beta accumulation in skeletal muscle. *Am J Physiol,* 265**:** 166-172, 1993.

17. Malm, C, Nyberg, P, Engstrom, M, Sjodin, B, Lenkei, R, Ekblom, B, Lundberg, I: Immunological changes in human skeletal muscle and blood after eccentric exercise and multiple biopsies. *J Physiol,* 529**:** 243-262, 2000.

18. Yang, W, Hu, P: Skeletal muscle regeneration is modulated by inflammation. *J Orthop Translat,* 13**:** 25-32, 2018.

19. Schiaffino, S, Pereira, MG, Ciciliot, S, Rovere-Querini, P: Regulatory T cells and skeletal muscle regeneration. *FEBS J,* 284**:** 517-524, 2017.

20. Arnold, L, Henry, A, Poron, F, Baba-Amer, Y, van Rooijen, N, Plonquet, A, Gherardi, RK, Chazaud, B: Inflammatory monocytes recruited after skeletal muscle injury switch into antiinflammatory macrophages to support myogenesis. *J Exp Med,* 204: 1057-1069, 2007.

21. Baumert, P, Lake, MJ, Stewart, CE, Drust, B, Erskine, RM: Genetic variation and exercise-induced muscle damage: implications for athletic performance, injury and ageing. *Eur J Appl Physiol,* 116**:** 1595-1625, 2016.

22. de Almeida, P, Lopes-Martins, RA, De Marchi, T, Tomazoni, SS, Albertini, R, Correa, JC, Rossi, RP, Machado, GP, da Silva, DP, Bjordal, JM, Leal Junior, EC: Red (660 nm) and infrared (830 nm) low-level laser therapy in skeletal muscle fatigue in humans: what is better? *Lasers Med Sci,* 27**:** 453-458, 2012.

23. Ferraresi, C, Bertucci, D, Schiavinato, J, Reiff, R, Araujo, A, Panepucci, R, Matheucci, E, Jr., Cunha, AF, Arakelian, VM, Hamblin, MR, Parizotto, N, Bagnato, V: Effects of Light-Emitting Diode Therapy on Muscle Hypertrophy, Gene Expression, Performance, Damage, and Delayed-Onset Muscle Soreness: Case-control Study with a Pair of Identical Twins. *Am J Phys Med Rehabil,* 95**:** 746-757, 2016.

24. Park, KS, Lee, MG: Effects of unaccustomed downhill running on muscle damage, oxidative stress, and leukocyte apoptosis. *J Exerc Nutrition Biochem,* 19**:** 55-63, 2015.

25. Silveira, PC, da Silva, LA, Pinho, CA, De Souza, PS, Ronsani, MM, Scheffer Dda, L, Pinho, RA: Effects of low-level laser therapy (GaAs) in an animal model of muscular damage induced by trauma. *Lasers Med Sci,* 28**:** 431-436, 2013.

26. Paoni, NF, Peale, F, Wang, F, Errett-Baroncini, C, Steinmetz, H, Toy, K, Bai, W, Williams, PM, Bunting, S, Gerritsen, ME, Powell-Braxton, L: Time course of skeletal muscle repair and gene expression following acute hind limb ischemia in mice. *Physiol Genomics,* 11**:** 263-272, 2002.

27. Fernandes, KP, Alves, AN, Nunes, FD, Souza, NH, Silva, JA, Jr., Bussadori, SK, Ferrari, RA: Effect of photobiomodulation on expression of IL-1beta in skeletal muscle following acute injury. *Lasers Med Sci,* 28**:** 1043-1046, 2013.

28. de Almeida, P, Lopes-Martins, RA, Tomazoni, SS, Silva, JA, Jr., de Carvalho Pde, T, Bjordal, JM, Leal Junior, EC: Low-level laser therapy improves skeletal muscle performance, decreases skeletal muscle damage and modulates mRNA expression of COX-1 and COX-2 in a dose-dependent manner. *Photochem Photobiol,* 87**:** 1159-1163, 2011.

29. Massett, MP, Berk, BC: Strain-dependent differences in responses to exercise training in inbred and hybrid mice. *Am J Physiol Regul Integr Comp Physiol,* 288**:** 1006-1113, 2005.

30. da Costa Santos, VB, de Paula Ramos, S, Milanez, VF, Correa, JC, de Andrade Alves, RI, Dias, IF, Nakamura, FY: LED therapy or cryotherapy between exercise intervals in Wistar rats: anti-inflammatory and ergogenic effects. *Lasers Med Sci,* 29**:** 599-605, 2014.

31. Ferraresi, C, Parizotto, NA, Pires de Sousa, MV, Kaippert, B, Huang, YY, Koiso, T, Bagnato, VS, Hamblin, MR: Light-emitting diode therapy in exercise-trained mice increases muscle performance, cytochrome c oxidase activity, ATP and cell proliferation. *J Biophotonics,* 8**:** 740-754, 2015.

32. Brancaccio, P, Lippi, G, Maffulli, N: Biochemical markers of muscular damage. *Clin Chem Lab Med,* 48**:** 757-767, 2010.

33. Germolec, DR, Frawley, RP, Evans, E: Markers of inflammation. *Methods Mol Biol,* 598**:** 53-73, 2010.

34. Tomiya, A, Aizawa, T, Nagatomi, R, Sensui, H, Kokubun, S: Myofibers express IL-6 after eccentric exercise. *Am J Sports Med,* 32**:** 503-508, 2004.

35. Smith, HK, Plyley, MJ, Rodgers, CD, McKee, NH: Skeletal muscle damage in the rat hindlimb following single or repeated daily bouts of downhill exercise. *Int J Sports Med,* 18**:** 94-100, 1997.

36. Armstrong, RB, Ogilvie, RW, Schwane, JA: Eccentric exercise-induced injury to rat skeletal muscle. *J Appl Physiol Respir Environ Exerc Physiol,* 54**:** 80-93, 1983.

37. Zuo, Q, Wang, SC, Yu, XK, Chao, WW: Response of macrophages in rat skeletal muscle after eccentric exercise. *Chin J Traumatol,* 21**:** 88-95, 2018.

38. Kawanishi, N, Mizokami, T, Niihara, H, Yada, K, Suzuki, K: Neutrophil Depletion Attenuates Muscle Injury after Exhaustive Exercise. *Med Sci Sports Exerc,* 48**:** 1917-1924, 2016.

39. Huang, YY, Chen, AC, Carroll, JD, Hamblin, MR: Biphasic dose response in low level light therapy. *Dose Response,* 7**:** 358-383, 2009.

40. Leal-Junior, EC, Vanin, AA, Miranda, EF, de Carvalho Pde, T, Dal Corso, S, Bjordal, JM: Effect of phototherapy (low-level laser therapy and light-emitting diode therapy) on exercise performance and markers of exercise recovery: a systematic review with meta-analysis. *Lasers Med Sci,* 30**:** 925-939, 2015.

41. Nampo, FK, Cavalheri, V, Ramos Sde, P, Camargo, EA: Effect of low-level phototherapy on delayed onset muscle soreness: a systematic review and meta-analysis. *Lasers Med Sci,* 31**:** 165-177, 2016.

42. Camargo, MZ, Siqueira, CP, Preti, MC, Nakamura, FY, de Lima, FM, Dias, IF, Toginho Filho Dde, O, Ramos Sde, P: Effects of light emitting diode (LED) therapy and cold water immersion therapy on exercise-induced muscle damage in rats. *Lasers Med Sci,* 27**:** 1051-1058, 2012.

43. Ferraresi, C, Kaippert, B, Avci, P, Huang, YY, de Sousa, MV, Bagnato, VS, Parizotto, NA, Hamblin, MR: Low-level laser (light) therapy increases mitochondrial membrane potential and ATP synthesis in C2C12 myotubes with a peak response at 3-6 h. *Photochem Photobiol,* 91**:** 411-416, 2015.

44. Zhang, CP, Li, SD, Wang, XY, Chen, P, Wang, CZ, Fu, XB, Kang, HX, Shen, BJ, Liang, J: Effect of Low Power Laser Irradiation on the Ability of Cell Growth and Myogenic Differentiation of Myoblasts Cultured In Vitro. *Int J Photoenergy,* 2014**:** 1-8, 2014.

45. Shefer, G, Partridge, TA, Heslop, L, Gross, JG, Oron, U, Halevy, O: Low-energy laser irradiation promotes the survival and cell cycle entry of skeletal muscle satellite cells. *J Cell Sci,* 115**:** 1461-1469, 2002.

46. De Marchi, T, Leal Junior, EC, Bortoli, C, Tomazoni, SS, Lopes-Martins, RA, Salvador, M: Low-level laser therapy (LLLT) in human progressive-intensity running: effects on exercise performance, skeletal muscle status, and oxidative stress. *Lasers Med Sci,* 27**:** 231-236, 2012.

47. Karu, T: Primary and secondary mechanisms of action of visible to near-IR radiation on cells. *J Photochem Photobiol B,* 49**:** 1-17, 1999.

48. Huang, YY, Sharma, SK, Carroll, J, Hamblin, MR: Biphasic dose response in low level light therapy - an update. *Dose Response,* 9**:** 602-618, 2011.

49. Wang, Y, Huang, YY, Wang, Y, Lyu, P, Hamblin, MR: Red (660 nm) or near-infrared (810 nm) photobiomodulation stimulates, while blue (415 nm), green (540 nm) light inhibits proliferation in human adipose-derived stem cells. *Sci Rep,* 7**:** 1-10, 2017.

50. White, GE, Wells, GD: Cold-water immersion and other forms of cryotherapy: physiological changes potentially affecting recovery from high-intensity exercise. *Extrem Physiol Med,* 2**:** 16-26, 2013.

51. Leeder, J, Gissane, C, van Someren, K, Gregson, W, Howatson, G: Cold water immersion and recovery from strenuous exercise: a meta-analysis. *Br J Sports Med,* 46**:** 233-240, 2012.

52. Yaffe, D, Saxel, O: Serial passaging and differentiation of myogenic cells isolated from dystrophic mouse muscle. *Nature,* 270**:** 725-727, 1977.

53. Burattini, S, Ferri, P, Battistelli, M, Curci, R, Luchetti, F, Falcieri, E: C2C12 murine myoblasts as a model of skeletal muscle development: morpho-functional characterization. *Eur J Histochem,* 48**:** 223-233, 2004.

REFERENCES

54. Monici, M, Cialdai, F, Ranaldi, F, Paoli, P, Boscaro, F, Moneti, G, Caselli, A: Effect of IR laser on myoblasts: a proteomic study. *Mol Biosyst,* 9**:** 1147-1161, 2013.

55. Silva, LM, Silva, CA, Silva, A, Vieira, RP, Mesquita-Ferrari, RA, Cogo, JC, Zamuner, SR: Photobiomodulation Protects and Promotes Differentiation of C2C12 Myoblast Cells Exposed to Snake Venom. *PLoS One,* 11**:** 1-16, 2016.

56. Mesquita-Ferrari, RA, Alves, AN, de Oliveira Cardoso, V, Artilheiro, PP, Bussadori, SK, Rocha, LA, Nunes, FD, Fernandes, KP: Low-level laser irradiation modulates cell viability and creatine kinase activity in C2C12 muscle cells during the differentiation process. *Lasers Med Sci,* 30**:** 2209-2213, 2015.

57. Avci, P, Gupta, A, Sadasivam, M, Vecchio, D, Pam, Z, Pam, N, Hamblin, MR: Low-level laser (light) therapy (LLLT) in skin: stimulating, healing, restoring. *Semin Cutan Med Surg,* 32**:** 41-52, 2013.

58. Karu, T, Pyatibrat, L, Kalendo, G: Irradiation with He-Ne laser increases ATP level in cells cultivated in vitro. *J Photochem Photobiol B,* 27**:** 219-223, 1995.

59. Giuliani, A, Lorenzini, L, Gallamini, M, Massella, A, Giardino, L, Calza, L: Low infra red laser light irradiation on cultured neural cells: effects on mitochondria and cell viability after oxidative stress. *BMC Complement Altern Med,* 9**:** 1-10, 2009.

60. Nguyen, LM, Malamo, AG, Larkin-Kaiser, KA, Borsa, PA, Adhihetty, PJ: Effect of near-infrared light exposure on mitochondrial signaling in C2C12 muscle cells. *Mitochondrion,* 14**:** 42-48, 2014.

61. Karu, TI: Multiple roles of cytochrome c oxidase in mammalian cells under action of red and IR-A radiation. *IUBMB Life,* 62**:** 607-610, 2010.

62. Berg JM, TJ, Stryer L.: Section 16.2, The Glycolytic Pathway Is Tightly Controlled. In: *Biochemistry 5th edition.* 5th ed. New York, W H Freeman and Company, 2002.

63. Schroeder, P, Pohl, C, Calles, C, Marks, C, Wild, S, Krutmann, J: Cellular response to infrared radiation involves retrograde mitochondrial signaling. *Free Radic Biol Med,* 43**:** 128-135, 2007.

64. Chen, AC, Arany, PR, Huang, YY, Tomkinson, EM, Sharma, SK, Kharkwal, GB, Saleem, T, Mooney, D, Yull, FE, Blackwell, TS, Hamblin, MR: Low-level laser therapy activates NF-kB via generation of reactive oxygen species in mouse embryonic fibroblasts. *PLoS One,* 6**:** 1-8, 2011.

65. Young, S, Bolton, P, Dyson, M, Harvey, W, Diamantopoulos, C: Macrophage responsiveness to light therapy. *Lasers Surg Med,* 9**:** 497-505, 1989.

66. Pedersen, BK: Muscle as a secretory organ. *Compr Physiol,* 3**:** 1337-1362, 2013.

67. Peake, JM, Della Gatta, P, Suzuki, K, Nieman, DC: Cytokine expression and secretion by skeletal muscle cells: regulatory mechanisms and exercise effects. *Exerc Immunol Rev,* 21**:** 8-25, 2015.

68. Griffin, CA, Apponi, LH, Long, KK, Pavlath, GK: Chemokine expression and control of muscle cell migration during myogenesis. *J Cell Sci,* 123**:** 3052-3060, 2010.

69. Luo, L, Sun, Z, Zhang, L, Li, X, Dong, Y, Liu, TC: Effects of low-level laser therapy on ROS homeostasis and expression of IGF-1 and TGF-beta1 in skeletal muscle during the repair process. *Lasers Med Sci,* 28**:** 725-734, 2013.

70. Rizzi, CF, Mauriz, JL, Freitas Correa, DS, Moreira, AJ, Zettler, CG, Filippin, LI, Marroni, NP, Gonzalez-Gallego, J: Effects of low-level laser therapy (LLLT) on the nuclear factor (NF)-kappaB signaling pathway in traumatized muscle. *Lasers Surg Med,* 38**:** 704-713, 2006.

71. Ribeiro, BG, Alves, AN, Dos Santos, LA, Cantero, TM, Fernandes, KP, Dias Dda, S, Bernardes, N, De Angelis, K, Mesquita-Ferrari, RA: Red and Infrared Low-Level Laser Therapy Prior to Injury with or without

Administration after Injury Modulate Oxidative Stress during the Muscle Repair Process. *PLoS One,* 11**:** 1-13, 2016.

72. Silva, AA, Leal-Junior, EC, D'Avila Kde, A, Serra, AJ, Albertini, R, Franca, CM, Nishida, JA, de Carvalho Pde, T: Pre-exercise low-level laser therapy improves performance and levels of oxidative stress markers in mdx mice subjected to muscle fatigue by high-intensity exercise. *Lasers Med Sci,* 30**:** 1719-1727, 2015.

73. Sussai, DA, Carvalho Pde, T, Dourado, DM, Belchior, AC, dos Reis, FA, Pereira, DM: Low-level laser therapy attenuates creatine kinase levels and apoptosis during forced swimming in rats. *Lasers Med Sci,* 25**:** 115-120, 2010.

74. Aujnarain, AB, Luo, OD, Taylor, N, Lai, JKY, Foster, JA: Effects of exercise and enrichment on behaviour in CD-1 mice. *Behav Brain Res,* 342**:** 43-50, 2018.

75. Lerman, I, Harrison, BC, Freeman, K, Hewett, TE, Allen, DL, Robbins, J, Leinwand, LA: Genetic variability in forced and voluntary endurance exercise performance in seven inbred mouse strains. *J Appl Physiol,* 92**:** 2245-2255, 2002.

76. Drinkwater, EJ, Lawton, TW, Lindsell, RP, Pyne, DB, Hunt, PH, McKenna, MJ: Training leading to repetition failure enhances bench press strength gains in elite junior athletes. *J Strength Cond Res,* 19**:** 382-388, 2005.

77. Mitchell, CJ, Churchward-Venne, TA, West, DW, Burd, NA, Breen, L, Baker, SK, Phillips, SM: Resistance exercise load does not determine training-mediated hypertrophic gains in young men. *J Appl Physiol,* 113**:** 71-77, 2012.

78. Kasperek, GJ, Snider, RD: Increased protein degradation after eccentric exercise. *Eur J Appl Physiol Occup Physiol,* 54**:** 30-34, 1985.

79. Proske, U, Morgan, DL: Muscle damage from eccentric exercise: mechanism, mechanical signs, adaptation and clinical applications. *J Physiol,* 537**:** 333-345, 2001.

80. Eston, RG, Mickleborough, J, Baltzopoulos, V: Eccentric activation and muscle damage: biomechanical and physiological considerations during downhill running. *Br J Sports Med,* 29**:** 89-94, 1995.

81. Ogilvie, RW, Armstrong, RB, Baird, KE, Bottoms, CL: Lesions in the rat soleus muscle following eccentrically biased exercise. *Am J Anat,* 182**:** 335-346, 1988.

82. Liu, XG, Zhou, YJ, Liu, TC, Yuan, JQ: Effects of low-level laser irradiation on rat skeletal muscle injury after eccentric exercise. *Photomed Laser Surg,* 27**:** 863-869, 2009.

83. Carter, GT, Kikuchi, N, Abresch, RT, Walsh, SA, Horasek, SJ, Fowler, WM, Jr.: Effects of exhaustive concentric and eccentric exercise on murine skeletal muscle. *Arch Phys Med Rehabil,* 75**:** 555-559, 1994.

84. Lynch, GS, Fary, CJ, Williams, DA: Quantitative measurement of resting skeletal muscle [Ca2+]i following acute and long-term downhill running exercise in mice. *Cell Calcium,* 22**:** 373-383, 1997.

85. Kasperek, GJ, Snider, RD: The susceptibility to exercise-induced muscle damage increases as rats grow larger. *Experientia,* 41**:** 616-617, 1985.

86. Tsivitse, SK, McLoughlin, TJ, Peterson, JM, Mylona, E, McGregor, SJ, Pizza, FX: Downhill running in rats: influence on neutrophils, macrophages, and MyoD+ cells in skeletal muscle. *Eur J Appl Physiol,* 90**:** 633-638, 2003.

87. Tidball, JG, Villalta, SA: Regulatory interactions between muscle and the immune system during muscle regeneration. *Am J Physiol Regul Integr Comp Physiol,* 298**:** R1173-1187, 2010.

88. Komulainen, J, Kytola, J, Vihko, V: Running-induced muscle injury and myocellular enzyme release in rats. *J Appl Physiol,* 77**:** 2299-2304, 1994.

89. McLoughlin, TJ, Mylona, E, Hornberger, TA, Esser, KA, Pizza, FX: Inflammatory cells in rat skeletal muscle are elevated after electrically stimulated contractions. *J Appl Physiol,* 94**:** 876-882, 2003.

90. Wagner, KR, Liu, X, Chang, X, Allen, RE: Muscle regeneration in the prolonged absence of myostatin. *Proc Natl Acad Sci U S A,* 102**:** 2519-2524, 2005.

91. Kawanishi, N, Kato, K, Takahashi, M, Mizokami, T, Otsuka, Y, Imaizumi, A, Shiva, D, Yano, H, Suzuki, K: Curcumin attenuates oxidative stress following downhill running-induced muscle damage. *Biochem Biophys Res Commun,* 441**:** 573-578, 2013.

92. Leal Junior, EC, de Godoi, V, Mancalossi, JL, Rossi, RP, De Marchi, T, Parente, M, Grosselli, D, Generosi, RA, Basso, M, Frigo, L, Tomazoni, SS, Bjordal, JM, Lopes-Martins, RA: Comparison between cold water immersion therapy (CWIT) and light emitting diode therapy (LEDT) in short-term skeletal muscle recovery after high-intensity exercise in athletes--preliminary results. *Lasers Med Sci,* 26**:** 493-501, 2011.

93. De Marchi, T, Schmitt, VM, Machado, GP, de Sene, JS, de Col, CD, Tairova, O, Salvador, M, Leal-Junior, EC: Does photobiomodulation therapy is better than cryotherapy in muscle recovery after a high-intensity exercise? A randomized, double-blind, placebo-controlled clinical trial. *Lasers Med Sci,* 32**:** 429-437, 2017.

94. de Paiva, PR, Tomazoni, SS, Johnson, DS, Vanin, AA, Albuquerque-Pontes, GM, Machado, CD, Casalechi, HL, de Carvalho, PT, Leal-Junior, EC: Photobiomodulation therapy (PBMT) and/or cryotherapy in skeletal muscle restitution, what is better? A randomized, double-blinded, placebo-controlled clinical trial. *Lasers Med Sci,* 31**:** 1925-1933, 2016.

95. Carey, HV, Mangino, MJ, Southard, JH: Changes in gut function during hibernation: implications for bowel transplantation and surgery. *Gut,* 49**:** 459-461, 2001.

96. Assis, L, Yamashita, F, Magri, AM, Fernandes, KR, Yamauchi, L, Renno, AC: Effect of low-level laser therapy (808 nm) on skeletal muscle after endurance exercise training in rats. *Braz J Phys Ther,* 19**:** 457-465, 2015.

97. Hausswirth, C, Louis, J, Bieuzen, F, Pournot, H, Fournier, J, Filliard, JR, Brisswalter, J: Effects of whole-body cryotherapy vs. far-infrared vs. passive modalities on recovery from exercise-induced muscle damage in highly-trained runners. *PLoS One,* 6**:** 1-7, 2011.

98. Monti, RJ, Roy, RR, Hodgson, JA, Edgerton, VR: Transmission of forces within mammalian skeletal muscles. *J Biomech,* 32**:** 371-380, 1999.

99. Lehti, TM, Kalliokoski, R, Komulainen, J: Repeated bout effect on the cytoskeletal proteins titin, desmin, and dystrophin in rat skeletal muscle. *J Muscle Res Cell Motil,* 28**:** 39-47, 2007.

100. Estrella, NL, Naya, FJ: Transcriptional networks regulating the costamere, sarcomere, and other cytoskeletal structures in striated muscle. *Cell Mol Life Sci,* 71**:** 1641-1656, 2014.

101. Blazek, AD, Paleo, BJ, Weisleder, N: Plasma Membrane Repair: A Central Process for Maintaining Cellular Homeostasis. *Physiology (Bethesda),* 30**:** 438-448, 2015.

102. Roostalu, U, Strahle, U: In vivo imaging of molecular interactions at damaged sarcolemma. *Dev Cell,* 22**:** 515-529, 2012.

103. Cai, C, Weisleder, N, Ko, JK, Komazaki, S, Sunada, Y, Nishi, M, Takeshima, H, Ma, J: Membrane repair defects in muscular dystrophy are linked to altered interaction between MG53, caveolin-3, and dysferlin. *J Biol Chem,* 284**:** 15894-15902, 2009.

104. Cai, C, Masumiya, H, Weisleder, N, Matsuda, N, Nishi, M, Hwang, M, Ko, JK, Lin, P, Thornton, A, Zhao, X, Pan, Z, Komazaki, S, Brotto, M, Takeshima, H, Ma, J: MG53 nucleates assembly of cell membrane repair machinery. *Nat Cell Biol,* 11**:** 56-64, 2009.
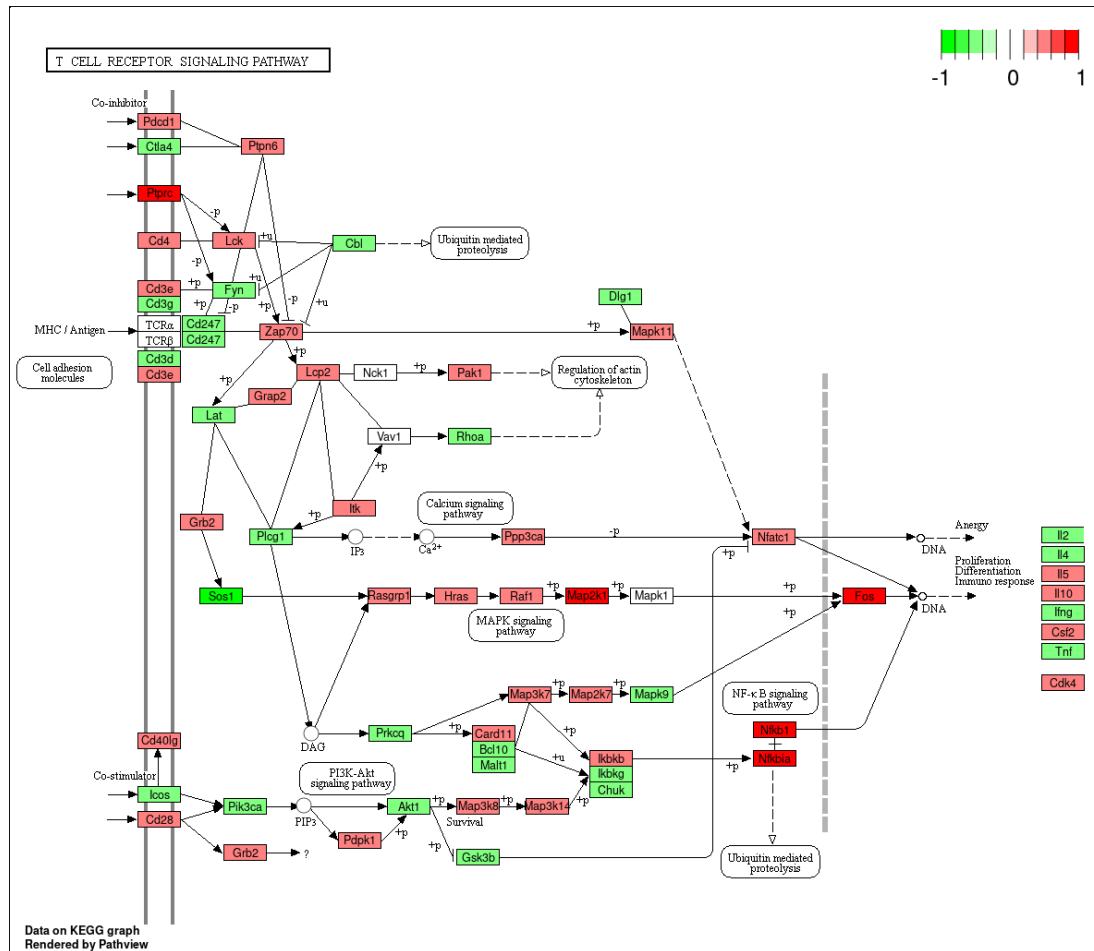
105. Boye, TL, Maeda, K, Pezeshkian, W, Sonder, SL, Haeger, SC, Gerke, V, Simonsen, AC, Nylandsted, J: Annexin A4 and A6 induce membrane curvature and constriction during cell membrane repair. *Nat Commun,* 8**:** 1-11, 2017.

106. Yin, H, Price, F, Rudnicki, MA: Satellite cells and the muscle stem cell niche. *Physiol Rev,* 93**:** 23-67, 2013.

107. Bentzinger, CF, Wang, YX, Rudnicki, MA: Building muscle: molecular regulation of myogenesis. *Cold Spring Harb Perspect Biol,* 4**:** 1-16, 2012.

108. Egan, B, Zierath, JR: Exercise metabolism and the molecular regulation of skeletal muscle adaptation. *Cell Metab,* 17**:** 162-184, 2013.

109. Ji, LL, Gomez-Cabrera, MC, Steinhafel, N, Vina, J: Acute exercise activates nuclear factor (NF)-kappaB signaling pathway in rat skeletal muscle. *FASEB J,* 18**:** 1499-1506, 2004.

110. Vella, L, Caldow, MK, Larsen, AE, Tassoni, D, Della Gatta, PA, Gran, P, Russell, AP, Cameron-Smith, D: Resistance exercise increases NF-kappaB activity in human skeletal muscle. *Am J Physiol Regul Integr Comp Physiol,* 302**:** 667-673, 2012.

111. Mantovani, A, Biswas, SK, Galdiero, MR, Sica, A, Locati, M: Macrophage plasticity and polarization in tissue repair and remodelling. *J Pathol,* 229**:** 176-185, 2013.

112. Souza, NHC, Mesquita-Ferrari, RA, Rodrigues, M, da Silva, DFT, Ribeiro, BG, Alves, AN, Garcia, MP, Nunes, FD, da Silva Junior, EM, Franca, CM, Bussadori, SK, Fernandes, KPS: Photobiomodulation and different macrophages phenotypes during muscle tissue repair. *J Cell Mol Med,* 22**:** 4922-4934, 2018.

113. Cheng, M, Nguyen, MH, Fantuzzi, G, Koh, TJ: Endogenous interferon-gamma is required for efficient skeletal muscle regeneration. *Am J Physiol Cell Physiol,* 294**:** 1183-1191, 2008.

114. Morrison, J, Palmer, DB, Cobbold, S, Partridge, T, Bou-Gharios, G: Effects of T-lymphocyte depletion on muscle fibrosis in the mdx mouse. *Am J Pathol,* 166**:** 1701-1710, 2005.

115. Fu, X, Xiao, J, Wei, Y, Li, S, Liu, Y, Yin, J, Sun, K, Sun, H, Wang, H, Zhang, Z, Zhang, BT, Sheng, C, Wang, H, Hu, P: Combination of inflammation-related cytokines promotes long-term muscle stem cell expansion. *Cell Res,* 25**:** 655-673, 2015.

116. Ignotz, RA, Massague, J: Transforming growth factor-beta stimulates the expression of fibronectin and collagen and their incorporation into the extracellular matrix. *J Biol Chem,* 261**:** 4337-4345, 1986.

117. Sanjabi, S, Zenewicz, LA, Kamanaka, M, Flavell, RA: Anti-inflammatory and pro-inflammatory roles of TGF-beta, IL-10, and IL-22 in immunity and autoimmunity. *Curr Opin Pharmacol,* 9**:** 447-453, 2009.

118. Zimowska, M, Duchesnay, A, Dragun, P, Oberbek, A, Moraczewski, J, Martelly, I: Immunoneutralization of TGFbeta1 Improves Skeletal Muscle Regeneration: Effects on Myoblast Differentiation and Glycosaminoglycan Content. *Int J Cell Biol,* 2009**:** 1-16, 2009.

119. Taniguti, AP, Pertille, A, Matsumura, CY, Santo Neto, H, Marques, MJ: Prevention of muscle fibrosis and myonecrosis in mdx mice by suramin, a TGF-beta1 blocker. *Muscle Nerve,* 43**:** 82-87, 2011.

120. Gumucio, JP, Flood, MD, Phan, AC, Brooks, SV, Mendias, CL: Targeted inhibition of TGF-beta results in an initial improvement but long-term deficit in force production after contraction-induced skeletal muscle injury. *J Appl Physiol,* 115**:** 539-545, 2013.

121. Ruh, AC, Frigo, L, Cavalcanti, M, Svidnicki, P, Vicari, VN, Lopes-Martins, RAB, Leal Junior, ECP, De Isla, N, Diomede, F, Trubiani, O, Favero, GM: Laser photobiomodulation in pressure ulcer healing of human diabetic patients: gene expression analysis of inflammatory biochemical markers. *Lasers Med Sci,* 33**:** 165-171, 2018.

122. Fekrazad, R, Sarrafzadeh, A, Kalhori, KAM, Khan, I, Arany, PR, Giubellino, A: Improved Wound Remodeling Correlates with Modulated TGF-beta Expression in Skin Diabetic Wounds Following Combined Red and Infrared Photobiomodulation Treatments. *Photochem Photobiol,* 94**:** 775-779, 2018.

123. Keskiner, I, Lutfioglu, M, Aydogdu, A, Saygun, NI, Serdar, MA: Effect of Photobiomodulation on Transforming Growth Factor-beta1, Platelet-Derived Growth Factor-BB, and Interleukin-8 Release in Palatal Wounds After Free Gingival Graft Harvesting: A Randomized Clinical Study. *Photomed Laser Surg,* 34**:** 263-271, 2016.

124. Jain, M, Rivera, S, Monclus, EA, Synenki, L, Zirk, A, Eisenbart, J, Feghali-Bostwick, C, Mutlu, GM, Budinger, GR, Chandel, NS: Mitochondrial reactive oxygen species regulate transforming growth factor-beta signaling. *J Biol Chem,* 288**:** 770-777, 2013.

125. Zhang, F, Wang, H, Wang, X, Jiang, G, Liu, H, Zhang, G, Wang, H, Fang, R, Bu, X, Cai, S, Du, J: TGF-beta induces M2-like macrophage polarization via SNAIL-mediated suppression of a pro-inflammatory phenotype. *Oncotarget,* 7**:** 52294-52306, 2016.

126. Tidball, JG: Regulation of muscle growth and regeneration by the immune system. *Nat Rev Immunol,* 17**:** 165-178, 2017.

127. Kramer, HF, Goodyear, LJ: Exercise, MAPK, and NF-kappaB signaling in skeletal muscle. *J Appl Physiol,* 103**:** 388-395, 2007.

128. Shefer, G, Oron, U, Irintchev, A, Wernig, A, Halevy, O: Skeletal muscle cell activation by low-energy laser irradiation: a role for the MAPK/ERK pathway. *J Cell Physiol,* 187**:** 73-80, 2001.

129. Zhang, YE: Non-Smad pathways in TGF-beta signaling. *Cell Res,* 19**:** 128-139, 2009.

130. Chapnick, DA, Warner, L, Bernet, J, Rao, T, Liu, X: Partners in crime: the TGFbeta and MAPK pathways in cancer progression. *Cell Biosci,* 1**:** 35-42, 2011.

131. Yu, M, Stepto, NK, Chibalin, AV, Fryer, LG, Carling, D, Krook, A, Hawley, JA, Zierath, JR: Metabolic and mitogenic signal transduction in human skeletal muscle after intense cycling exercise. *J Physiol,* 546**:** 327-335, 2003.

132. Coffey, VG, Zhong, Z, Shield, A, Canny, BJ, Chibalin, AV, Zierath, JR, Hawley, JA: Early signaling responses to divergent exercise stimuli in skeletal muscle from well-trained humans. *FASEB J,* 20**:** 190-192, 2006.

133. Yu, M, Blomstrand, E, Chibalin, AV, Krook, A, Zierath, JR: Marathon running increases ERK1/2 and p38 MAP kinase signalling to downstream targets in human skeletal muscle. *J Physiol,* 536**:** 273-282, 2001.

134. Pournot, H, Bieuzen, F, Louis, J, Mounier, R, Fillard, JR, Barbiche, E, Hausswirth, C: Time-course of changes in inflammatory response after whole-body cryotherapy multi exposures following severe exercise. *PLoS One,* 6**:** 1-8, 2011.

135. Thorlacius, H, Vollmar, B, Westermann, S, Torkvist, L, Menger, MD: Effects of local cooling on microvascular hemodynamics and leukocyte adhesion in the striated muscle of hamsters. *J Trauma,* 45**:** 715-719, 1998.

136. Vieira Ramos, G, Pinheiro, CM, Messa, SP, Delfino, GB, Marqueti Rde, C, Salvini Tde, F, Durigan, JL: Cryotherapy Reduces Inflammatory Response Without Altering Muscle Regeneration Process and Extracellular Matrix Remodeling of Rat Muscle. *Sci Rep,* 6**:** 1-12, 2016.

137. Carvalho, N, Puntel, G, Correa, P, Gubert, P, Amaral, G, Morais, J, Royes, L, da Rocha, J, Soares, F: Protective effects of therapeutic cold and heat against the oxidative damage induced by a muscle strain injury in rats. *J Sports Sci,* 28**:** 923-935, 2010.

138. Ihsan, M, Watson, G, Lipski, M, Abbiss, CR: Influence of postexercise cooling on muscle oxygenation and blood volume changes. *Med Sci Sports Exerc,* 45**:** 876-882, 2013.

139. Yanagisawa, O, Homma, T, Okuwaki, T, Shimao, D, Takahashi, H: Effects of cooling on human skin and skeletal muscle. *Eur J Appl Physiol,* 100**:** 737-745, 2007.

140. Yanagisawa, O, Kudo, H, Takahashi, N, Yoshioka, H: Magnetic resonance imaging evaluation of cooling on blood flow and oedema in skeletal muscles after exercise. *Eur J Appl Physiol,* 91**:** 737-740, 2004.

141. Takagi, R, Fujita, N, Arakawa, T, Kawada, S, Ishii, N, Miki, A: Influence of icing on muscle regeneration after crush injury to skeletal muscles in rats. *J Appl Physiol,* 110**:** 382-388, 2011.

142. Norheim, KL, Cullum, CK, Andersen, JL, Kjaer, M, Karlsen, A: Inflammation Relates to Resistance Training-induced Hypertrophy in Elderly Patients. *Med Sci Sports Exerc,* 49**:** 1079-1085, 2017.

7 APPENDIX

Appendix A: NF-Kappa B signaling pathway from KEGG database. The color code is only qualitative, indicating the magnitude of upregulation (in green) or downregulation (in red) of a gene according to the intensity of the color.

Appendix B: TNF signaling pathway from KEGG database. The color code is only qualitative, indicating the magnitude of upregulation (in green) or downregulation (in red) of a gene according to the intensity of the color.

101

Appendix C: T cell receptor signaling pathway from KEGG database. The color code is only qualitative, indicating the magnitude of upregulation (in green) or downregulation (in red) of a gene according to the intensity of the color.
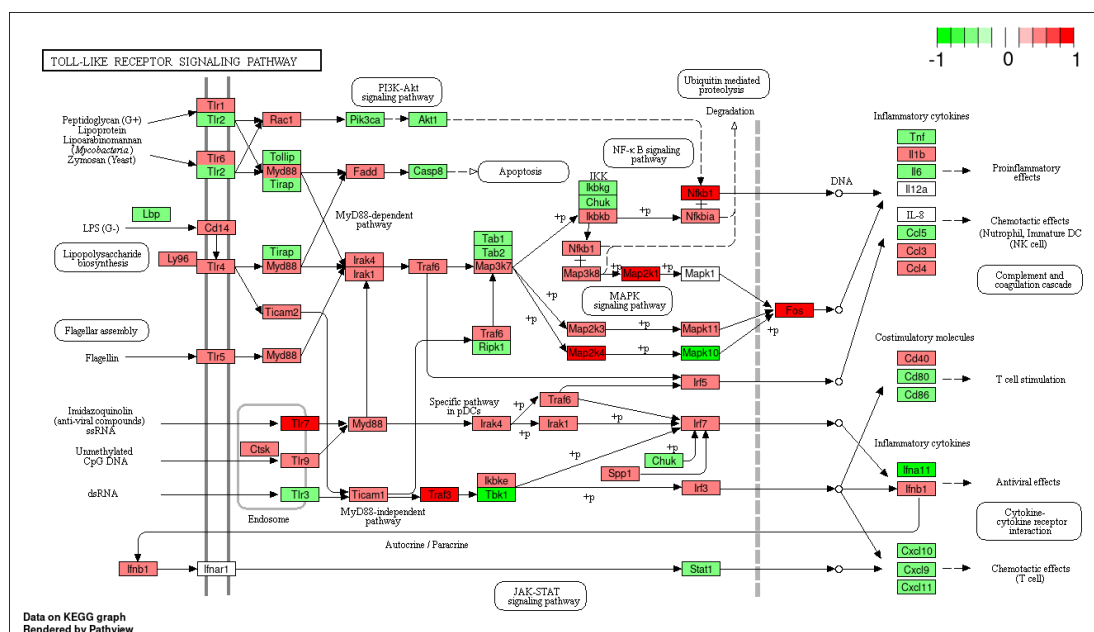
Appendix D: Toll-like receptor signaling pathway from KEGG database. The color code is only qualitative, indicating the magnitude of upregulation (in green) or downregulation (in red) of a gene according to the intensity of the color.

8 CURRICULUM VITAE AND PUBLICATIONS

PERSONAL INFORMATION

Name und Vorname:	Fabiola Arpino
Geburtsdatum:	27.09.1987
Geburtsort:	Mesagne, Italy
Familienstand:	Unmarried
Vater:	Donato Arpino
Mutter:	Amelia Assunta Cavaliere

SCHOOLING

2001 – 2006	Liceo Scientifico Leonardo Da Vinci, San Vito dei Normanni, Italy

UNIVERSITIES

Start:1st June 2014 End: Present	**PhD student**, Medical Research Center, University of Heidelberg, Germany. **Thesis title**: Photobiomodulation of the response to exercise-induced damage in murine skeletal muscle Supervisor: Prof. Norbert Gretz.
Start: 1st March 2010 End: 20th December 2012	**MSc** Biomedical Engineering, Politecnico di Milano, Italy **Thesis title**: Analisi computazionale del moto di una particella in un condotto di piccolo diametro. Supervisor: Prof. Gabriele A. Dubini.

Start:1st September 2006 End: 22nd February 2010	**BSc** Biomedical Engineering, Politecnico di Milano, Italy **Thesis title**: Design and construction of a de-oxygenator for human blood circulating in an extracorporeal hydraulic circuit.

JOBS

Start: 1st July 2013 End: 31st October 2013	**Internship** at BASF, Germany **Task:** Design and optimization of a bioreactor for bacterial fermentation through computational fluid dynamics modeling
Start:1st March 2009 End: 31st May 2009	**Internship** at Università degli Studi di Milano **Task:** Recording and elaborating data by stereophotogrammetric and laser-scanning imaging systems for facial morphology.

PUBLICATIONS

Becker, A, Distler, E, Klapczynski, A, Arpino, F, Kuch, N, Simon-Keller, K, Sticht, C, van Abeelen, FA, Gretz, N, Oversluizen, G: Blue light inhibits proliferation of melanoma cells. In: SPIE (Ed.) *SPIE BiOS.* San Francisco, International Society for Optics and Photonics, 2016 pp 969503-969513.

Becker, A, Klapczynski, A, Kuch, N, Arpino, F, Simon-Keller, K, De La Torre, C, Sticht, C, van Abeelen, FA, Oversluizen, G, Gretz, N: Gene expression profiling reveals aryl hydrocarbon receptor as a possible target for photobiomodulation when using blue light. *Sci Rep,* 6**:** 33847, 2016.

PATENTS

Patent in collaboration with URGO (Dijon, FR) regarding the pro-proliferative effect of 7.5min blue light found in human keratinocytes and human fibroblasts: "Flexible device for the irradiation of chronic wounds inducing wound healing by accelerated proliferation of fibroblasts and keratinocytes (LEDs (wavelength 450-490nm))", EP16181721.8 (EU), PCT/EP2017/068951 (USA).

9   ACKNOWLEDGEMENTS

I would like to thank Prof. Norbert Gretz for giving me the opportunity to work in his group, for his support and all the knowledge that I have gained during this period through the tools that he has provided.

I thank Prof. Dr. Rüdiger Rudolf, for sharing his knowledge and for the consulting, he provided during the project.

I thank Dr. Carsten Sticht, Dr. Carolina De La Torre and Dr. Khan Arif ul Maula for their work, knowledge and support.

I thank Viktoria Skude for the help, support and tips provided during the animal experimentation.

I thank Sina Schwalm and Edda Eustachi for their valuable work, all the good conversations and encouragements.

I thank all the colleagues at the ZMF and TASCDT for sharing knowledge, frustrations and successes. Thanks for the collaboration and mental support. In particular thanks to Anna Klapczynski, Cristina Daniele, Matteo Rigon, Natalia Kuch and Stefania Palumbo. A special thanks to Anja Becker, an ex-colleague and a friend of mine that introduced me to the cell culture and followed me at the beginning, when I had no background in this field.